Simulating the climatic response of Hardangerjøkulen in southern Norway since the Little Ice Age

Master's thesis in Earth Science

HENNING ÅKESSON

Department of Earth Science
Faculty of Mathematics and Natural Sciences
UNIVERSITY OF BERGEN

MASTER'S THESIS IN EARTH SCIENCE

Simulating the climatic response of Hardangerjøkulen in southern Norway since the Little Ice Age

HENNING ÅKESSON

Department of Earth Science
Faculty of Mathematics and Natural Sciences
UNIVERSITY OF BERGEN

Bergen, Norway 2014

Simulating the climatic response of
Hardangerjøkulen in southern Norway
since the Little Ice Age

HENNING ÅKESSON

Master's thesis
Department of Earth Science
Faculty of Mathematics and Natural Sciences
University of Bergen
Bergen
Norway

Cover:
Hardangerjøkulen seen from southeast on September 9, 2010. Photo: Petter Bjørstad

Bergen, Norway 2014

Abstract

Glacier and ice cap volume changes currently amount to half of the total contribution from the cryosphere to sea-level rise. Ice caps and their outlet glaciers are dynamically different from the Greenland and Antarctic ice sheets, and respond considerably faster to climate change.

We use a shallow-ice version of the Ice Sheet System Model (ISSM) to model the dynamics and evolution of the maritime-continental Hardangerjøkulen ice cap in southern Norway from the Little Ice Age (LIA) until today. We force the ice flow model with a dynamically calibrated mass balance history based on moraine evidence from the Little Ice Age maximum in 1750, as well as later outlet glacier front positions from moraines and direct measurements. Glaciological mass balance measurements force the model from the 1960s onwards, and we validate the model using a surface digital elevation model from 1995 and aerial photographs.

The model successfully reproduces most of the LIA extent of the ice cap. Outlet glaciers retreat too far in the model for the early 1900s, while observed ice extent after 1960 is accurately represented. This coincides with the period where direct mass balance data is used as forcing, indicating its key role. A comparison with a digital elevation model from 1995 reveals a very good agreement of surface topography, except for a too thick eastern ice cap.

We find a non-linear relationship between mass balance perturbations and ice volume response, where Hardangerjøkulen is more sensitive to negative than positive mass balance changes. We discuss these findings in light of reconstructed past changes and future predictions.

Keywords: ice cap, Norway, climate, numerical modelling, ice dynamics, mass balance, sliding

Preface

As a first year bachelor student, I started off thinking I would one day work with poverty and environmental issues in rural Africa. However, during my second semester, one very dedicated lecturer (who later became my master co-supervisor) lit a spark in me, which by now has grown into a full-blown wildfire. Thank you Jostein Bakke for introducing me to the world of glaciers.

Most Africans will never get the chance to stare in awe upon blue glacier ice. They will likely never hear the rumble of a large chunk of ice breaking off the front of a glacier dipping its toes into water. And hardly will these people ever get an opportunity to listen to the roar of water rushing from the surface into the heart of a glacier.

Ironically, perhaps, these and other people living in the 'third-world' are those facing the worst consequences of the ice broken off and the meltwater rushing away. They depend on the water downstream of the mountains; some live in low-lying areas, without the infrastructure to tackle rising seas. Since I didn't become (well, it's never to late...?) an environmental worker in rural Africa, I hope instead the following pages can make a tiny piece in the big climate puzzle, and eventually benefit the people least responsible yet most vulnerable to a changing climate.

Acknowledgements

A number of people have helped me along the occasionally bumpy road leading to this final thesis. My supervisors Kerim Nisancioglu, Jostein Bakke and Rianne Giesen deserve a round of applause for giving me ideas, guiding me during the project and encouraging me through the final stretch of write-up. Rianne Giesen is worthy a special thanks for hosting me at the Institute for Marine and Atmospheric research Utrecht (IMAU), for providing invaluable knowledge and data of Hardangerjøkulen ice cap and for answering my sometimes very long puzzled emails. I am also indebted to the ISSM team at University California Irvine and NASA Jet Propulsion Laboratory, whose open-source ice model I set out to learn. This would have been impossible without Mathieu Morlighem, who invested many hours helping me with the technicalities and possibilities of ISSM and ice modelling.

In addition, several other people gave me valuable scientific input; thank you Michiel Helsen, Atle Nesje, Benedict Reinardy and Petra Langebroek. Hallgeir Elvehøy and Solveig Winswold at NVE also deserve attention for providing data and in-depth insights of Hardangerjøkulen. I also wish to acknowledge Petter Bjørstad, who let me use his (I think) stunning photo as the front page of my thesis.

I am very thankful to the renewable energy company BKK for supporting me with a generous scholarship, opening up possibilities to attend several conferences as well as enabling a month-long stay at IMAU.

Thomas Shaw and Mikkel Arne Kristiansen did considerable efforts trying to improve my writings - I owe you both! In addition, I wish to thank Mikkel for being a generally psyched person and a partner in crime over many years in Bergen and elsewhere.

My friends at the Centre for Climate Dynamics at the Bjerknes Centre; thank you for making my study environment a less boring place. In fact, my days sitting (and

standing) here working have been quite enjoyable. And thank you fellow master students Susanne Meidell and Tine Sørbye, for good company and inviting me to numerous 'cake-Thursdays' at Department for Earth Science.

Lastly, thank you Ida, Olof and Anna for being who you are.

I wish you happy reading.

Henning Åkesson,
Bergen, May 2014

List of Figures

List of Tables

"If not us, who? If not now, when?"
– Hillel the Elder

Contents

1 Introduction

1.1 Background and motivation

The interplay between snow and ice and Earth's other subsystems occurs on a range of spatial and temporal scales through direct interactions and feedback mechanisms (Hock 2005). Compared with Greenland (7.36 m Sea Level Equivalent (SLE)) and Antarctica (58.3 m SLE), glaciers and small ice caps (GICs) comprise a small part (0.41 m SLE) of the total global ice volume (Vaughan et al. 2013). Still, GICs respond considerably faster to climate change, mainly due to their small size and the ice temperature being closer to or at the melting point (Vaughan et al. 2013; Oerlemans 1997; Nesje and Matthews 2012). Recent global decline in glacier ice across all continents (Gardner et al. 2013) is viewed as one of the clearest signs of the impacts of a warming climate (Vaughan et al. 2013). Further projected accelerated mass loss (Radic et al. 2013; Giesen and Oerlemans 2013) is predicted to have considerable impact on 21st century sea level rise (Marzeion et al. 2012; Church et al. 2013; see Fig.1.1) and beyond (Levermann et al. 2013). Given the inertia of the ice sheets, assessments of the response of glaciers and small ice caps to climate are essential. Although the 170 000 GICs in the world constitute a small part of *potential* sea level rise, they currently amount to about half of the contribution from the cryosphere (Shepherd et al. 2012; Vaughan et al. 2013).

From a hydrological viewpoint, glaciers have a significant impact on catchment hydrology (Hock 2005), where water is stored as snow and ice on a range of timescales (Jansson et al. 2003). Future glacier mass loss is also predicted to alter runoff patterns worldwide (Bliss et al. 2014). Being dependent on the climatic regime, 21^{st} century predictions for most regions (including Scandinavia) show significant decreases in glacial runoff, whereas some regions show initial increases followed by decreases (Svalbard and Iceland) or even increases (Canadian and Russian Arctic).

In a socioeconomic sense, knowledge about mountain glaciers is imperative, not least to provide an informative base for policy makers and stakeholders. For example. fresh water is emerging as an increasingly important asset. In Norway, hydro-electric power production generates 98 % of the country's electricity, of which 15 % come from glaciated catchments (Andreassen et al. 2005). Future changes in runoff magnitudes and patterns will undoubtedly affect hydropower operations.

Also, activities like glacier hiking and skiing crucially depend on future glacier behaviour and pace of projected retreat. Some may even argue that glaciers as a part of our landscape have some value in itself, as a part of our cultural (or rather, natural) heritage.

Given these changes, it should be clear that there is a need to quantify links between future climate and glaciers with associated sea level rise and socioeconomic impacts. Such understanding is dependent on detailed knowledge of past and present behaviour of different glacier types and their relationship to local weather and climate on different timescales (Giesen and Oerlemans 2010).

From a more scientific angle, there is a need for further interaction between empiricists

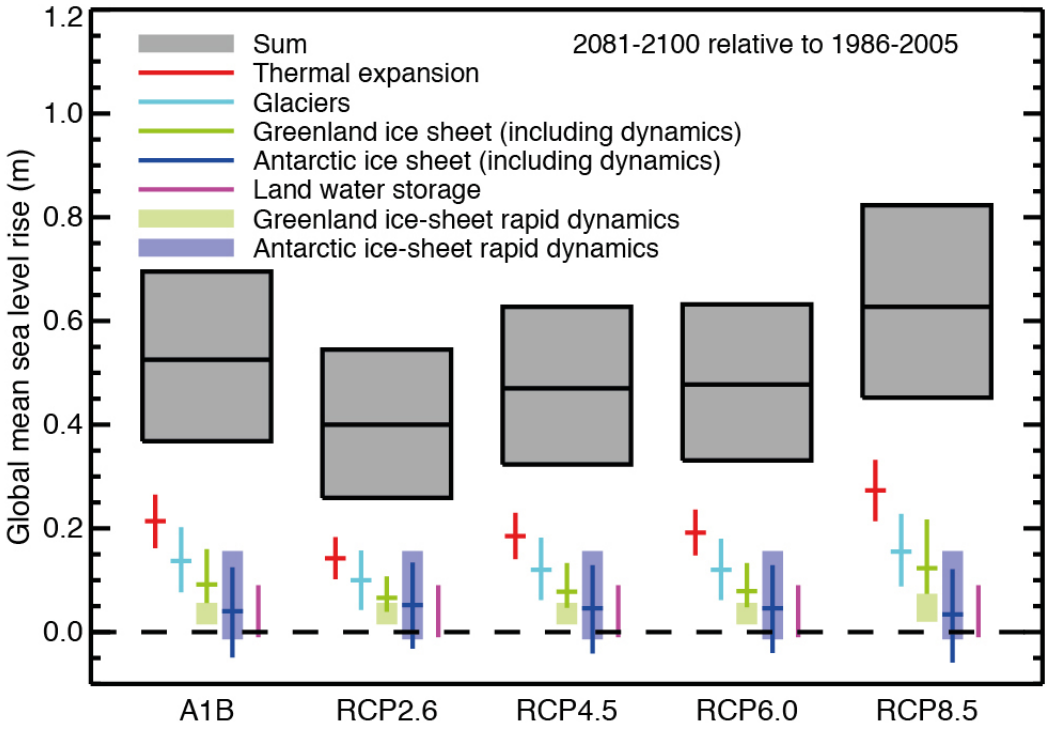

Figure 1.1: Likely ranges and median values for global mean sea level rise and its contributions from individual sources in 2081-2100 relative to 1986-2005, as predicted by process-based models for the Representative Concentration Pathways (RCPs) used in IPCC (2013) and the SRES A1B scenario used in IPCC (2007). Note that the contribution from glaciers and ice caps (here termed "glaciers") are roughly that of Greenland and Antarctica combined. Figure from Church et al. 2013.

and modellers, both within the paleocommunity and workers focused on the present and future. For example, using ice models in combination with independent glacier proxy reconstructions has potential to deepen our understanding of past glacier-climate interactions. In Norway (and elsewhere), numerous studies of past glacier activity exist (e.g. Nesje et al. 1991; Dahl and Nesje 1994; Bakke et al. 2005), using physical, chemical and biological proxies in sediment cores from distal glacier-fed lakes. However, there is sometimes a lack of quantitative considerations of glaciologic processes in such studies. Models could potentially provide an independent check and further guidance to how such reconstructions can be interpreted or improved. Regarding present-day studies, it should be beyond doubt that models and observations are mutually dependent, not least illustrated by the recent rise of interest in data assimilation methods within glaciology.

1.2 Glaciers in Norway

Norway is covered by 2692 km^2 of glaciers, of which 43% is located in southern Norway (Fig 1.2; Andreassen et al. 2012a). The general trend during the 20th century has been a decrease in glacier area, with monitored continental glaciers showing a near continuous retreat since the 1960s. The maritime glaciers in mainland Norway advanced during the 1990s (Fig. 1.3), mainly in response to winters with heavy snowfall during the period 1989-95 (Andreassen et al. 2005; Nesje et al. 2008). This event has been linked to a coinciding period of positive North Atlantic Oscillation. Since the year 2000, all monitored glaciers have retreated in response to net mass losses (Kjøllmoen et al. 2011).

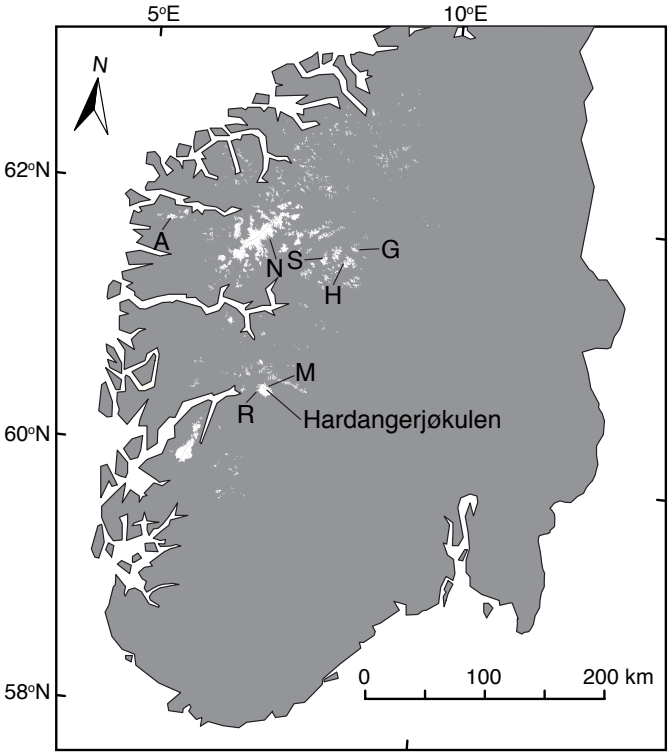

Figure 1.2: Glaciers in southern Norway (white), including Hardangerjøkulen's two outlet glaciers Rembesdalskåka (R) and Midtdalsbreen (M). The others are Ålfotbreen (A), Nigardsbreen (N), Storbreen (S), Hellstugubreen (H) and Gråsubreen (G). Figure modified from Giesen et al. 2009.

Most glaciers in mainland Norway are considered temperate (Andreassen et al. 2012a), meaning their bed are at the pressure melting point. If the winter cold wave is not eliminated during the following summer, a glacier is defined as cold-based and frozen to its bed (Cuffey and Paterson 2010). Observations on thermal regime only exist for a few Norwegian glaciers. Given that the continental glaciers of the eastern parts of southern Norway have thin snow cover and glacier termini above the mountain permafrost altitude,

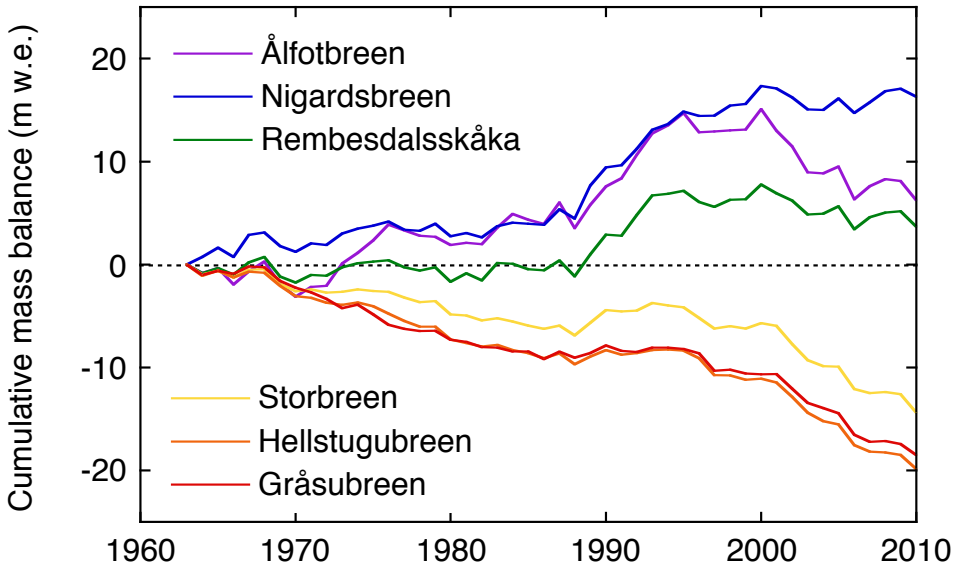

Figure 1.3: Cumulative mass balance 1963-2010 for selected Norwegian glaciers along an west-east transect, from the most maritime glacier Ålfotbreen to the most continental, Gråsubreen. Data from NVE.

it could well be that these glaciers have cold zones in their frontal parts (Etzelmüller and Hagen 2005).

The sensitivity of a glacier to climate is in part controlled by its hypsometry (the distribution of area with altitude) of the glacier (Cuffey and Paterson 2010). Ice caps (plateau glaciers) are especially sensitive to climate change due to their large and flat distribution of the ice mass. Small changes in the equlibrium-line altitude (ELA) can have large effects on ice caps, since comparatively large parts of the accumulation will change to ablation area, or vice versa (Nesje et al. 2008). In southern Norway, all large ice masses (> 25 km^2) are flat ice caps, with steeper outlet glaciers, located in a maritime to transitional climate within 150 km from the coast.

1.3 Modelling glaciers and climate

In order to understand interactions between glaciers and climate, observations and modelling efforts should go hand in hand (Van Der Veen 2013). Observations are crucial to calibrate and evaluate model performance. Conversely, ice sheet and glacier models give us opportunities to test theories and to progress further in our understanding of the underlying processes and their relative importance. However, many processes in glaciology are still poorly understood and all models therefore rely on assumptions and parameterizations. Further, the relative importance of individual processes depend on spatial and temporal scales in question. Complex (which does not always imply more realistic) models need more computational resources. It is therefore integrative to determine which processes that are crucial to the problem at hand, and which process that are regarded less important and therefore can be simplified or ignored at the

temporal and spatial scale of interest. Moreover, insufficient data or the need to keep computation time down may also be the cause of simplification.

Ice sheet models are generally constructed to model ice flow over large spatial scales. The characteristics of an ice sheet differ in several ways from those of mountain glaciers and ice caps. Ice sheets spread under their own weight and their large-scale flow can transgress topographical boundaries at their beds. They are several kilometres thick and have typical lengths scales of thousands of kilometres. In contrast, glaciers move down a sloping bed due to gravity and is affected by local topography at much smaller spatial scales. These differences affect the ability to model ice flow for ice sheets compared to glaciers. Processes present and simplifications valid in an ice sheet model may or may not be valid at the glacier or ice cap scale, and ice sheets models may therefore not be used ad hoc to model glacier response to climate. Given that the predicted contribution from GICs to 21st century sea level rise is roughly the same as that of Greenland and Antarctica added together, it should be clear that our understanding of and ability to model glaciers and climate need further attention. Along these lines, it would be required to understand and be able to model individual glaciers accurately, before we can upscale to regional or global estimates.

To save computation time and facilitate accurate interpretation of model results, it can be desirable to use a simple model, as long as it captures a glacier's response to climate[1].

Of specific interest is in what way we need to adapt ice sheet models in order to model smaller ice masses like glaciers and ice caps. In this study, the performance of a numerical ice sheet model is tested on Hardangerjøkulen, an ice cap in southern Norway, from the Little Ice Age until today. Until glaciological mass balance records are available in the 1960s, the mass balance history is dynamically calibrated by using moraine evidence, aerial and satellite imagery as well as from direct length measurements of outlet glaciers. Results are compared with past ice cap extents and available digital elevation models (DEMs), as well as with existing model studyies (Giesen 2009; Giesen and Oerlemans 2010). Similarities and differences to other studies on ice cap - climate interactions are also highlighted.

This study can be seen as one step towards understanding glacier-climate interactions and our ability to model them, by means of an integrated model-data approach. Hardangerjøkulen was chosen as a test case because of the abundance of glaciological data available and the existence of previous model studies (Giesen 2009; Giesen and Oerlemans 2010). The potential to apply this methodology to other well studied Norwegian ice caps and glaciers (e.g. Folgefonna and Jostedalsbreen ice caps in western Norway) and compare with Hardangerjøkulen provide further motivation for this thesis.

[1]Here, a quote commonly attributed to Albert Einstein is appropriate: 'Make everything as simple as possible, but not simpler'. This may seem similar to Occam's Razor, which endorse a simple solution without too many uncertain assumptions. However, Einstein's quote has been termed Einstein's razor, and is normally interpreted as a warning for over-simplification, when too much simplification along the lines of Occam's Razor will lead to wrong conclusions. Einstein's quote is probably paraphrased from what he said in a lecture in Oxford, 1933 ("On the Method of Theoretical Physics" The Herbert Spencer Lecture, delivered at Oxford (10 June 1933); also published in *Philosophy of Science*, Vol. 1, No. 2 (April 1934), pp. 163-169., p. 165.)

1.4 Aim and objectives

Aim
Investigate the glaciological response of Hardangerjøkulen ice cap from the "Little Ice Age" until present-day using an ice sheet model.

Research questions

1. Can the Ice Sheet System Model (ISSM) accurately simulate the evolution of Hardangerjøkulen from the Little Ice Age maximum until today?

2. How sensitive is Hardangerjøkulen to changes in mass balance?

3. How sensitive is the model to choice of sliding parameterization?

To answer questions above, data for model boundary conditions, forcing and calibration are compiled. This include past and present ice cap geometries, outlet glacier front positions and surface mass balance records.

1.5 Scope

This study focuses on climate-glacier links on annual to multi-centennial time scales. Therefore, seasonal behaviour is not of primary interest. This does not mean that seasonally varying variables such as accumulation and ablation are ignored, but simply that these are not accounted for explicitly in the model. Implicitly, these variations are included by using yearly averaged values of mass balance.

No attempts are made in this study to model the evolution of Hardangerjøkulen during early and mid-Holocene. Instead, the period studied is the last few centuries, starting some 150 years before the Little Ice Age maximum.

1.6 Outline

This thesis is organized as follows. First, a general overview of ice dynamics and glacier interactions with the atmosphere and climate, along with an introduction to ice sheet modelling, is included in Chapter 2. The Hardangerjøkulen ice cap is then described in Chapter 3, as well a summary of past and present glacier activity relevant to this thesis. In Chapter 4, the ice sheet model employed is described, as well as the treatment of input data. Chapter 5 gives the findings of this study. These results are discussed in Chapter 6, along with comparisons with previous studies. Conclusions and some suggested future directions are included in Chapter 7 and 8.

2 Theoretical basis

This chapter gives an overview of concepts of ice dynamics and mass balance relevant to this thesis. The intention is not to give an exhaustive review of the full glaciological literature, but to provide enough background to understand the physics of the ice model used.

To fully appreciate the contents of this chapter, especially Sect. 2.1 on ice dynamics, some background in mathematics and physics is advantageous. Readers wishing a descriptive introduction to ice modelling can skip to the final Section 2.3.

For readers in need of a more in-depth understanding, this is given in existing excellent textbooks, such as on glacier physics (Cuffey and Paterson 2010), mechanics (Hooke 2005), dynamics (Greve and Blatter 2009; Van Der Veen 2013) and mass balance (Bamber and Payne 2004).

2.1 Ice dynamics

2.1.1 Stress and strain

Stress

Much of the description of glacier flow is based on concepts of continuum mechanics. This includes the notion of a continuous material with its physical quantities, such as mass and momentum, distributed uniformly over a small volume part of that material (Batchelor 2000, p.5; Van Der Veen 2013, p.8). When we apply principles of continuum mechanics to glacier ice, we seek to describe how ice deforms in response to a force. Since ice is regarded a continuum material, we can use a single constitutive relation to model glacier flow, with the goal of linking stress to deformation. The constitutive relation for ice is called Glen's flow law (Glen 1955) and is described in Sect. 2.1.2.

Stress is a force per unit area, with dimensions N m^{-1} or Pa. Two types of stresses exist; normal and shear stress. A normal stress acts normal to a surface, while a shear stress acts along (parallel to) a surface. We can use a unit cube around a point to illustrate these concepts in three dimensions (Fig. 2.1).

The cube can be seen as an infinitesimal volume, for example representing a point in the glacier (Hooke 2005, p.10). For three perpendicular surfaces going through that point, there are one normal stress and two shear stresses. Altogether this makes nine stress components acting on a specific point. In the Cartesian coordinate system, stress components are denoted σ_{ij}, where i,j = x,y,z. The first subscript, i, shows the direction perpendicular to the surface on which the stress is acting, whereas the second subscript, j, indicates in which direction the stress is acting. For example, σ_{xy} acts in the y-axis direction, along the plane normal to the the x-axis (i.e. the xz-plane; Van Der Veen 2013).

The nine stress components σ_{ij} shown in Fig. 2.1 can be expressed symbolically in a

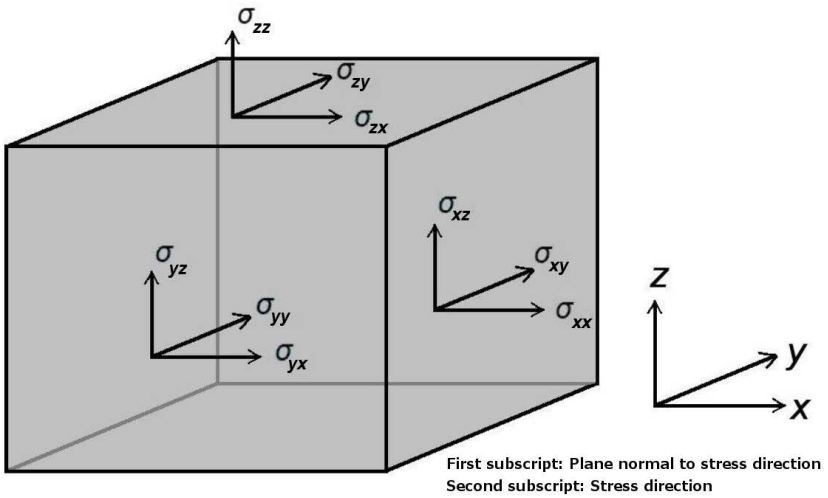

Figure 2.1: Components of the stress tensor on the perpendicular faces of a unit cube (Figure from van der Veen (2013), p.8).

matrix:

$$\sigma_{ij} = \begin{bmatrix} \sigma_{xx} & \sigma_{yx} & \sigma_{zx} \\ \sigma_{xy} & \sigma_{yy} & \sigma_{zy} \\ \sigma_{xz} & \sigma_{yz} & \sigma_{zz} \end{bmatrix} \tag{2.1}$$

The collection of stress vectors above are known as full (or Cauchy) stress tensors $\boldsymbol{\sigma}$. The Cauchy stress tensor can be divided into a volumetric stress (or hydrostatic pressure) $\sigma_v = P$ and deviatoric stresses τ_{ij}. Deviatoric stresses can be viewed as the difference between a specific normal stress at a point and the average normal stress conditions for that point. Taking the average of the sum of the three normal stresses (that is, the average of the trace $Tr(\boldsymbol{\sigma})$) we get the hydrostatic (or cryostatic) pressure:

$$P = \frac{1}{3}Tr(\sigma) = \frac{1}{3}(\sigma_{xx} + \sigma_{yy} + \sigma_{zz}) \tag{2.2}$$

Since P only affects the normal stresses, deviatoric shear stresses are the same as corresponding non-deviatoric or total shear stresses. Only non-hydrostatic stresses affect the deformation in response to a stress field (Hooke 2005, p.257; Van Der Veen 2013, p.11). The deviatoric stresses τ_{ij} is then

$$\tau_{ij} = \sigma_{ij} - \frac{1}{3}\delta_{ij}(\sigma_{xx} + \sigma_{yy} + \sigma_{zz}), \tag{2.3}$$

where δ is the Kronecker delta, with $\delta_{ij} = 1$ if $i = j$, and $\delta_{ij} = 0$ if $i \neq j$. This means that for $i = j$ (that is, a normal stress), the deviatoric normal stress is the full normal stress minus the hydrostatic pressure. For example, the deviatoric normal stress in in x-direction is

$$\sigma'_{xx} = \sigma_{xx} - \frac{1}{3}(\sigma_{xx} + \sigma_{yy} + \sigma_{zz}) \tag{2.4}$$

When $i \neq j$ (that is, for a shear stress), we see that the second term in Eq. (2.3) vanishes, and the deviatoric stress equals the non-deviatoric, as justified above.

We need the nine stress components to describe the state of stress, but only six of these are independent. The stress tensor is symmetric along its main diagonal, implying that $\sigma_{ij} = \sigma_{ji}$ for $i, j = x, y, z$. The symmetry is required because angular momentum has to be balanced (Greve and Blatter 2009, p.33-34), that is, to prevent the cube from rotating (Hooke 2005, p.12; Cuffey and Paterson 2010, p.676).

Strain

When ice is under stress, it will start deforming; this is called strain. Normal strain is defined as the change in length of a line segment divided by its original length, that is $\sigma_{ii} = \Delta l/l$. For an infinitesimal distance $\bar{\boldsymbol{x}}$ along the x-direction, this becomes $\sigma_{xx} = \partial\bar{\boldsymbol{x}}/\partial x$. The normal strain in the y- and z-directions are defined similarly (Hooke 2005, p.262).

When ice deforms, ice crystals are being deformed at a (locally) constant rate. This steady state means that a stress- and velocity field established. Strain rates describe at what rate the mean velocities change within the materials. Therefore, strain rates can also be written in terms of velocity gradients, which can be derived for example from remote sensing studies over larger areas. It can be shown (Hooke 2005, p.262-264; Van Der Veen 2013, p.9-10; Cuffey and Paterson 2010, p.679-680) that strain rates ϵ_{ij} are related to velocities by

$$\dot{\epsilon}_{ij} = \frac{1}{2}\left(\frac{\partial u_i}{\partial x_j} + \frac{\partial u_j}{\partial x_i}\right) \tag{2.5}$$

where $u = u, v, w$ for the x-, y-, and z-directions, respectively. Eq. (2.5) holds for both normal strain and shear strain, and the strain rate tensor $\dot{\epsilon}$ contains nine components. For normal strain where $i = j = x$, the strain rate is $\dot{\epsilon}_{xx} = \frac{\partial u}{\partial x}$. Conversely, if velocities vary for example in the x- and y-direction along any horizontal plane z (which is usually the case for real glaciers), the shear strain rate becomes

$$\dot{\epsilon}_{xy} = \frac{1}{2}\left(\frac{\partial u}{\partial y} + \frac{\partial v}{\partial x}\right) \tag{2.6}$$

The same symmetry as for the stress tensor applies for the resulting strain-rate tensor $\boldsymbol{\epsilon}$, which thus also have six independent components (Van Der Veen 2013, p.10; Hooke 2005).

The rate of deformation (strain rate) in a particular direction depends both on the stress in that direction, as well as all other stresses acting on the material. The effective shear stress τ_e is defined so that

$$2\tau_e^2 = \tau_{xx}^2 + \tau_{yy}^2 + \tau_{zz}^2 + 2(\tau_{xy}^2 + \tau_{xz}^2 + \tau_{yz}^2) \tag{2.7}$$

The corresponding effective strain rate, $\dot{\sigma_e}$, is defined in a similar way. Derivations of Eq. (2.7) and corresponding effective shear stress can be found in Hooke (2005), p.257-258 and Van der Veen (2013), p.11-12. Generally, magnitudes of vectors are

independent of the orientation of the coordinate axes used. For a second-order tensor, there are three such quantities, called invariants. The first invariant of the Cauchy stress tensor is the sum of the components along the main diagonal $Tr(\boldsymbol{\sigma}) = \sigma_{xx} + \sigma_{yy} + \sigma_{zz}$. In contrast, the first invariant of the deviatoric stress tensor is zero. The effective stress defined in Eq. (2.7) is the second invariant of this tensor (Cuffey and Paterson 2010, p.676-677; Van Der Veen 2013, p.11-12).

The effect of applied stress on any material (for example ice) depends on its *rheology*, which is its behaviour (for example its deformation) in response to stress. Thus, we now turn our attention to the behaviour of glacier ice under stress.

2.1.2 Ice rheology

Ice forms from compression of randomly distributed snow grains. When ice flow, the orientation of ice crystals changes in accordance to the stress applied. This effect, called anisotropy, can be used to infer past flow directions, significant for example when interpreting ice cores records (e.g. Dahl-Jensen and Gundestrup 1987; Durand et al. 2007) or layering seen in radar imagery from the ice sheets). However in most modelling applications, this effect is ignored and ice is considered isotropic, meaning randomly distributed crystal orientations (Hutter 1983).

The vertical variation in density in a glacier is minor - only the snow and firn layers experiences compression by overlying mass. Density changes with depth or temperature for glacier ice are very small (Hooke 2005; Partridge 2013). Since the vertical extent of snow and ice layers are so small compared to the total depth of the ice column, ice can is assumed to be incompressible - mass and density are not changing, and only deviatoric stresses cause deformation. This is expressed as

$$\dot{\epsilon_{ii}} = 0 \iff \frac{\partial u}{\partial x} + \frac{\partial v}{\partial y} + \frac{\partial w}{\partial z} = 0, \tag{2.8}$$

where u, v, z are the velocity components in the $x-, y-$ and $z-$directions. To relate the applied stress to the resulting deformation (strain rate), a constitutive relation is required (Van Der Veen 2013, p.30). Practically all modelling exercises in glaciology rely on pioneering work done by JF. Nye and J. Glen in the 1950s (Glen 1952; Nye 1953; Glen 1955); their constitutive relation is an empirically based law based on laboratory experiments of the creep of ice:

$$\dot{\epsilon}_{ij} = A\tau_e^{n-1}\tau_{ij} \tag{2.9}$$

Eq. (2.9) is called Nye's generalization of Glen's law, or just Glen's flow law. It states that the strain rate in a specific direction depends both on the stress τ_{ij} in this particular direction, as well as the all remaining stresses (the effective stress τ_e) acting on the material (Van Der Veen 2013, p.30-4; Hooke 2005, p.16).

The parameters n and A in the flow law are empirically determined. The exponent is usually set to 3 in ice sheet modelling, supported by laboratory experiments (Hooke 1981; Budd and Jacka 1989) and theoretical work (Weertman 1973), although some experiments point towards that n may be less than 3 for lower stresses (<200 kPa), more

common in glaciers (Alley 1992; Montagnat and Duval 2004). However, for temperate (isothermal) glaciers, experiments measuring the tilt of boreholes over time indicate shear patterns suggesting a value of n = 3 to 4 (Raymond 1980).

Ice deforms in a viscoelastic way, meaning it has both elastic (reaction to deformation) and viscous (reaction to rate of deformation) properties. The elastic effects are often neglected, a reasonable assumption for time scales of days or longer. Glacier ice is then treated as a viscous fluid, with its viscosity dependent on the stress applied. This type of material is known as a non-Newtonian or power-law fluid.

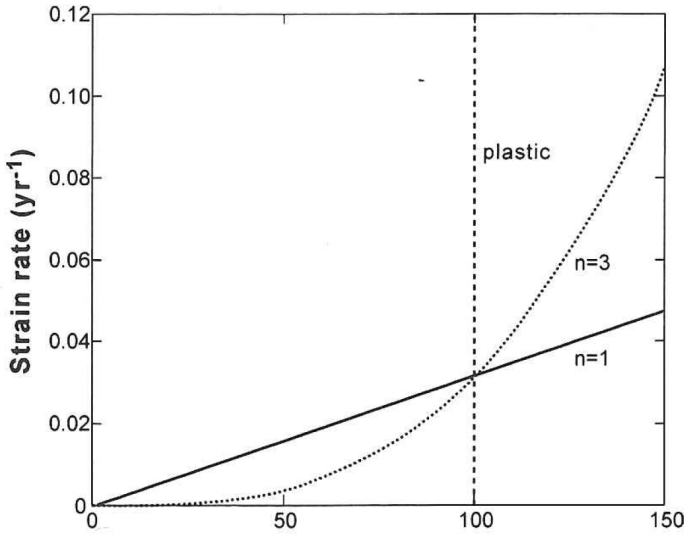

Figure 2.2: Different types of creep relations for ice. The non-Newtonian power-law relation with n = 3 is in between the relations for a linear viscous (n = 1) and perfectly plastic materials (no deformation before a yield stress, and instantaneous deformation when reaching the yield stress, here showed as 100 kPa). Figure from Cuffey and Paterson (2010), p.62.

The viscosity of ice is thus a ratio of stress to strain rate; a measure of how much ice is deforming in response to stress. For a purely viscous fluid, the strain rates depends on the viscosity η through

$$\boldsymbol{\sigma}' = 2\eta\dot{\boldsymbol{\epsilon}} \tag{2.10}$$

where $\boldsymbol{\sigma}'$ is the deviatoric stress tensor and η the effective viscosity. By combining Eq. (2.10) with Glen's flow law, we find that the viscosity of glacier ice is

$$\eta = \frac{1}{2A\tau^{n-1}} \tag{2.11}$$

The rate factor (sometimes called creep parameter) $A = A(T)$ in Glen's flow law depends on several factors, such as temperature, crystal fabric and impurities, of which the effect of temperature is most well-known (Cuffey and Paterson 2010). A depends on

temperature using a simple Arrhenius relationship so that

$$A(T) = \left(A_0 exp\left(\frac{-Q}{RT_h} \right) \right), \tag{2.12}$$

where A_0 is a flow factor, Q the activation energy for ice creep, R the universal gas constant, $T_h = T - \beta P$ the absolute temperature after correction for the pressure-dependency βP of the melting point of ice and β is the rate of change of the melting point with pressure. However, Eq. (2.12) is only valid for temperatures -10°C or lower. Cuffey and Paterson (2010), p.64-77, discusses a modified relation for $T_h > -10°\mathrm{C}$, accounting for the switch of activation energy Q at a transition temperature $T^* \approx -10°C$ (Fig. 2.3):

$$A = A_0 exp\left(-\frac{Q_c}{R} \left[\frac{1}{T_h} - \frac{1}{T_*} \right] \right), \tag{2.13}$$

where $n = 3$, $T_* = 263 + \beta P$ is the transition temperature modified by the pressure-dependency, $Q_c = Q^+$ for $T_h > T_*$. The activation energy Q^+ for warm ice is calibrated against field data and a value of A for temperate glaciers is recommended based on additional calibration against numerical models accounting for the entire stress regime (Cuffey and Paterson 2010, p.72-3).

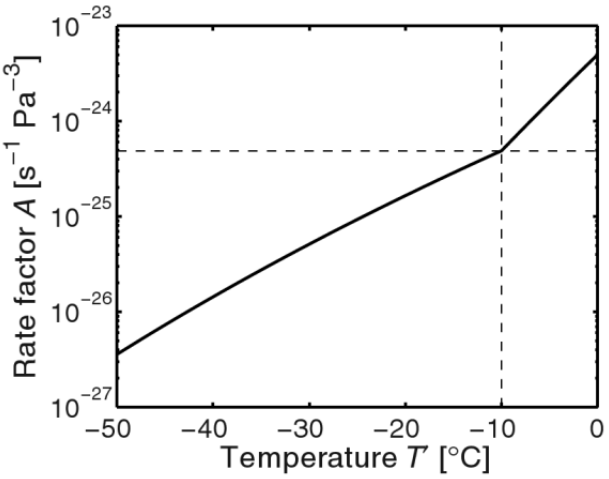

Figure 2.3: Temperature dependency of the rate factor A in Glen's flow law. Temperatures are given relative to their pressure-melting point. The piecewise definition of the pre-constant A_0 and the activation energy Q cause the kink at $-10°\mathrm{C}$. Figure from Greve and Blatter (2009), p.55.

2.1.3 Basal motion

The way we have described ice flow so far applies only to deformation of ice as a viscous fluid. Because of frictional heat or geothermal heat fluxes from below, glaciers can reach the melting point at their bed, water is produced, and the ice starts to slide. For entirely temperate glaciers, this is possible throughout the entire bed, and sliding can

be the dominant control of surface velocities (Cuffey and Paterson 2010). Basal sliding is probably the least understood process in glaciology, largely because of the difficulty involved in observing the glacier bed directly. In comparison, understanding of ice deformation is much better, even though inaccuracies remain due to ice impurities, water content, anisotropy and the dependence of flow law parameters to temperature and stress conditions. In addition to ice deformation and basal sliding, a third mechanism can affect glacier flow, namely deformation of sediments at the glacier bed (termed soft beds). Here, we focus on non-deformable beds only, since the ice cap Hardangerjøkulen in this study is assumed to have a hard bed (see Sect. 3.3).

We now describe three mechanisms of basal motion; *regelation*, *ice creep* and *cavitation*. Finally, we describe the role of subglacial drainage structures and efficiency. The role of water in basal sliding is highlighted since it provides the basis to discuss the sliding implementation used in this in this thesis (Sect. 4.1.2 and Sect. 6.3)).

Consider a small obstacle at the glacier bed. Cryostatic pressure on the stoss side of the obstacle is higher, the melting point is lowered and meltwater is produced. This meltwater flows toward the distal side of the obstacle, where cryostatic pressure is lower. The lower pressure raises the melting point, refreezing occurs and latent heat is released. This heat is conducted through the obstacle to the relatively colder upglacier side, providing a positive feedback (Van Der Veen 2013, p.182-83). The water produced allows ice to slide on a thin (microns thick) water film created (Fowler 2011, p.656). This process is called *regelation*, first proposed by Weertman (1957). Because heat conduction is most effective over short distances, regelation is most relevant at small spatial scales (< 10 cm).

Weertman also proposed that the high stress at the obstacle enables enhanced ice creep (plastic flow) so that ice can move around the obstacle (Hooke 2005, p.150). This process dominates on larger obstacles (> 1 m). We now turn our focus to processes relevant to the intermediate obstacles size (10 cm to 1 m).

Recently, scientific interest has moved away from regelation and towards viscous flow of ice over an uneven bed (e.g. Fowler 1987; Schoof 2005). It is widely accepted that basal water pressure is important to sliding (e.g. Weertman 1957; Lliboutry 1968; Budd and Jenssen 1987; Schoof 2005). This can be linked to the *effective pressure* N by

$$N = P_i - P_w = \rho_i g H - P_w, \tag{2.14}$$

where P_i is the cryostatic (ice overburden) pressure and P_w is the water pressure (e.g. Budd et al. 1979; Walder 1986). High water pressures can cause ice-bed separation at the lee side of bed obstacles - a process called *cavitation* (Lliboutry 1968). This happens at the so called *separation pressure* (Iken 1981), depending on bed roughness. Water is then temporarily stored in cavities, the small space opened up on the distal side of the obstacle. Parts of the bed drowned by the water in the cavity does not exert any drag on the ice. Ice therefore speeds up at this location, forcing the basal shear to increase at parts of the bed still in contact with ice. Basal shear stress is in this way redistributed from smaller obstacles covered by the cavity water to adjacent larger obstacles. Thus at low velocities and low degree of cavitation, basal drag is higher. However, as cavities grow more extensively, water pressure further rises. More areas are drowned and the

area supporting the ice is very small, enhancing sliding velocities.

There is a limit to how much sliding velocities can increase from cavitation, related to how much drag bed undulations can exert on the ice, which is determined by the obstacle slope. The first to propose such limiting slopes was Iken (1981), and this limit has consequently been called Iken's bound:

$$\frac{\tau_b}{N} = tan\alpha \tag{2.15}$$

where α is the upglacier slope of the obstacle. Schoof (2005) showed that such a limit on basal drag exist for an arbitrary bed, unless bed obstacles include vertical faces.

There is no simple relation between surface melt and glacier acceleration (Dunse 2011). More surface meltwater generally causes basal water pressures to rise and basal sliding to increase. However, if meltwater input triggers a transition from an hydraulically inefficient, high-pressurized (e.g. linked-cavities) drainage system to an efficient, low-pressurized (e.g. channelized) drainage system, glacier motion may actually be slowed down due to the drop in effective pressure at the base (Schoof 2010). Much attention during the last decade have been directed towards the role of surface water input to the subglacial drainage system and its effect on glacier flow. While still heavily debated, several studies (e.g. Bartholomaus et al. 2008; Sundal et al. 2011; Tedstone et al. 2013) suggest that water inputs to efficient, low-pressurized hydrological systems have small effects on annual velocities. In Sect. 6.3, the spatial and temporal controls of sliding in light of the results of this thesis are discussed.

2.1.4 Mass continuity

At every point on a glacier, mass has to be conserved - thickness can only be changed due accumulation, ablation or ice flow. Usually, density is considered constant over a glacier (Sect. 2.1.2), so that conservation of mass implies conservation of ice volume. Since time-evolving models all rely on mass continuity, this equation is derived here for completeness, following Bamber and Payne (2004), p.184-85, and van der Veen (2013), p.119-21.

Assuming ice flow in the x-direction only, we can write the ice flux q_{in} (per unit width) into a vertical section of ice as $q_{in} = HU(x)$, where H is ice thickness and $U(x)$ is ice velocity in the ice direction. The flux out of this section is then $q_{out} = HU(x + \Delta x)$ for an ice column with width x in the flow direction. Surface mass exchange can be expressed as a mass balance rate $\dot{M}$, where $\dot{M} > 0$ denotes accumulation and $\dot{M} < 0$ ablation. We can include basal melting $\dot{S}$ here, however this is normally negligible for applications not involving ice shelves or volcanic areas with anomalous geothermal heat. The surface input flux (per unit width) will thus be $q_{sfc} = \dot{M}\Delta x$. If horizontal fluxes are not in balance (that is if $q_{in} \neq q_{out}$), column thickness will have to change at a rate $\partial H/\partial t$. The resulting volume change of the column is

$$\frac{\partial H}{\partial t}\Delta x \tag{2.16}$$

Mass (volume) conservation can then be written

$$\frac{\partial H}{\partial t}\Delta x = q_{in} - q_{out} + q_{sfc} = HU(x) - HU(x + \Delta x) + \dot{M}\Delta x \tag{2.17}$$

We arrive at the continuity equation by dividing both sides by Δx and taking the limit $\Delta x \to 0$:

$$\frac{\partial H}{\partial t} = -\frac{\partial (HU)}{\partial x} + \dot{M} = -\left[H\frac{\partial U}{\partial x} + U\frac{\partial H}{\partial x}\right] + \dot{M} \tag{2.18}$$

Physically, the change in ice thickness $\partial H/\partial t$ represents the longitudinal strain rate, or the rate of downglacier stretching or compression of the ice column. For example, if velocity $U_{in} > U_{out}$ (that is, $\partial U/\partial x > 0$), stretching occurs in the flow direction and thinning in the vertical direction. On the right hand side in Eq. (2.18), the first term in the brackets represents changes in column thickness associated with velocity variations, whereas the second term in the brackets (velocity times thickness gradient) represent ice thickness change due to advection of (usually) thicker ice from upglacier (Benn and Evans 2010, p.145-46).

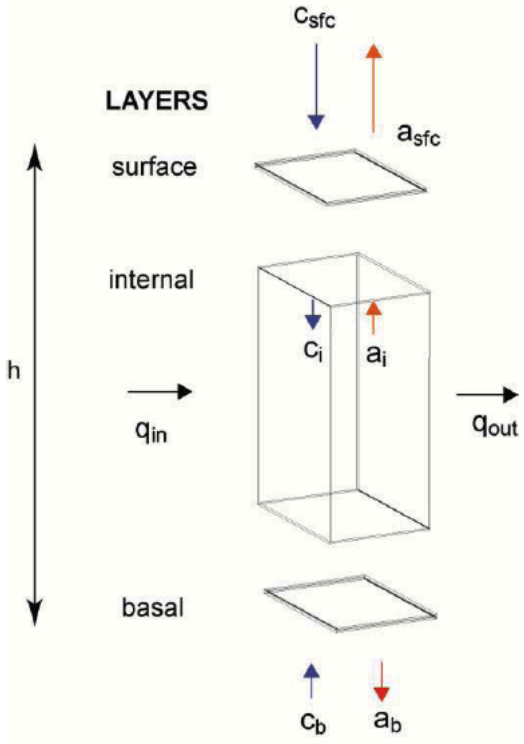

Figure 2.4: Inputs to and outputs from a schematic glacier column, where c stands for accumulation and a for ablation. Figure from Cogley et al. (2011).

Extending Eq. (2.18) to include the horizontal y-direction, we write the two-

dimensional (vertically integrated) continuity equation as

$$\frac{\partial H}{\partial t} = -\frac{\partial (HU)}{\partial x} - \frac{\partial (HV)}{\partial y} + \dot{M} = -\nabla \cdot (H\boldsymbol{U}) + \dot{M} \tag{2.19}$$

where $\boldsymbol{U} = \boldsymbol{U}(U, V, W)$ represents the x,y and z-directions. In this two-dimensional continuity equation, velocity is assumed constant with depth z.

Eq. (2.19) is hugely useful for time-dependent (*prognostic*) glacier modelling. The right-hand side is determined by ice flux divergence and surface mass balance. These quantities can be estimated from *diagnostic* equations and do not depend on time. They express the balance between quantities estimated from glacier geometry (stresses, strains and resulting velocities) and surface mass balance (accumulation versus ablation) at a specific point in time. Based on the calculation of the right-hand side, the rate of thickness change in time can be determined.

A more formal derivation of the continuity equation can be found in van der Veen (2013), p.121-22.

2.1.5 Ice flow approximations

Full Stokes stress balance

The full Stokes equations are the most complete description of ice flow. These equations are computationally demanding to solve, and are therefore often simplified under varying assumptions, for example using scaling arguments. The accuracy of underlying assumptions will vary with the characteristics of the flow in question. *Ice flow approximations* arise from such simplifications and can vary in their degree of complexity (Partridge 2013). Full Stokes equations and commonly used approximations in ice modelling are outlined here. A justification of the use of such approximations for Hardangerjøkulen ice cap is included in Sect. 4.1.1.

We saw in the previous section that mass always has to be conserved. Conservation of mass can be written more generally written as

$$\frac{\partial \rho}{\partial t} + \nabla \cdot \rho v = 0 \tag{2.20}$$

We concluded in Sect. 2.1.2 that ice can be considered incompressible. An incompressible material is one where for a moving volume element, the rate of density change following any motion is zero, that is

$$\frac{D\rho}{Dt} = 0 \tag{2.21}$$

With this assumption, Eq. (2.20) simplifies to

$$\nabla \cdot \boldsymbol{v} = \frac{\partial v}{\partial x} + \frac{\partial u}{\partial y} + \frac{\partial w}{\partial z} = 0 \tag{2.22}$$

Hence, the velocity divergence is zero at any point. Furthermore, conservation of momentum is expressed as

$$\rho \frac{d\boldsymbol{v}}{dt} = \nabla \sigma + \rho \boldsymbol{g} \tag{2.23}$$

Assuming that acceleration is negligible (e.g. Reist, Rappaz, et al. 2005) and that the only body force acting on ice is gravity (e.g. Van Der Veen 1989), the full Stokes stress balance for an ice mass can be written as

$$\nabla \cdot \boldsymbol{\sigma} + \rho_i \boldsymbol{g} = \mathbf{0} \tag{2.24}$$

where $\nabla \cdot \boldsymbol{\sigma}$ is the divergence vector of the stress tensor $\boldsymbol{\sigma}$, ρ_i is ice density, $\boldsymbol{g}$ is gravitational acceleration. We can assume that $g_x, g_y \approx 0 \Rightarrow g_z = \boldsymbol{g}$ (hydrostatic approximation).

Stress gradients across a volume of ice can be expanded from Eq. (2.24) as

$$\frac{\partial \sigma_{xx}}{\partial x} + \frac{\partial \sigma_{xy}}{\partial y} + \frac{\partial \sigma_{xz}}{\partial z} = -\rho g_x = 0 \tag{2.25}$$

$$\frac{\partial \sigma_{xy}}{\partial x} + \frac{\partial \sigma_{yy}}{\partial y} + \frac{\partial \sigma_{yz}}{\partial z} = -\rho g_y = 0 \tag{2.26}$$

$$\frac{\partial \sigma_{xz}}{\partial x} + \frac{\partial \sigma_{yz}}{\partial y} + \frac{\partial \sigma_{zz}}{\partial z} = -\rho g_z \tag{2.27}$$

Using Glen's flow law (Eq. 2.10) and the constitutive relation for incompressible viscous fluids (Eq. 2.11), the full stress balance in Eq. (2.24) can be defined in terms of velocities and pressure:

$$\frac{\partial}{\partial x}\left(2\eta \frac{\partial u}{\partial x}\right) + \frac{\partial}{\partial y}\left(\eta \frac{\partial u}{\partial y} + \eta \frac{\partial v}{\partial x}\right) + \frac{\partial}{\partial z}\left(\eta \frac{\partial u}{\partial z} + \eta \frac{\partial w}{\partial x}\right) - \frac{\partial p}{\partial x} = 0 \tag{2.28}$$

$$\frac{\partial}{\partial x}\left(\eta \frac{\partial u}{\partial y} + \eta \frac{\partial v}{\partial x}\right) + \frac{\partial}{\partial y}\left(2\eta \frac{\partial v}{\partial y}\right) + \frac{\partial}{\partial z}\left(\eta \frac{\partial v}{\partial z} + \eta \frac{\partial w}{\partial y}\right) - \frac{\partial p}{\partial y} = 0 \tag{2.29}$$

$$\frac{\partial}{\partial x}\left(\eta \frac{\partial u}{\partial z} + \eta \frac{\partial w}{\partial x}\right) + \frac{\partial}{\partial y}\left(\eta \frac{\partial v}{\partial z} + \eta \frac{\partial w}{\partial y}\right) + \frac{\partial}{\partial z}\left(2\eta \frac{\partial w}{\partial z}\right) - \frac{\partial p}{\partial z} - \rho g = 0 \tag{2.30}$$

Shallow Ice Approximation

The Shallow Ice Approximation (SIA) is the most widely used simplification of ice flow, based on a scaling analysis of the full Stokes stress balance (Hutter 1983; Morland 1984). This scaling argument is based on the assumption that typical glacier length L, is much larger than the typical ice thickness H. The aspect-ratio ϵ is then defined as

$$\epsilon = \frac{H}{L}, \tag{2.31}$$

where ϵ describes the "shallowness" of an ice mass. An aspect-ratio much smaller than unity is required for the SIA to be valid. Generally, the smaller the ϵ, the more accurate is the SIA (Le Meur et al. 2004; Winkelmann et al. 2011). For Hardangerjøkulen, the characteristic horizontal scale is 4 to 8 km, and the characteristic ice thickness 200 m, giving an ϵ of 0.05 to 0.025, which is acceptable (Le Meur and Vincent 2003; Giesen 2009).

SIA is valid where vertical shear stresses dominates over horizontal shear stresses, so that basal drag τ_b locally balances the driving stress τ_d. Lateral and longitudinal shear stresses are neglected, and deformational velocities is directly given by the ice thickness and surface slope:

$$u_d = \frac{2A|\tau_d|^{n-1}\tau_d H}{n+1} \tag{2.32}$$

where the driving stress τ_d is given as

$$\tau_d = -\rho_i g H \nabla s \tag{2.33}$$

We use a depth-averaged (2D) SIA model, so we integrate Eq. (2.32) over the ice column, becoming

$$u_d = \frac{2AH}{n+2}\tau_d^n \tag{2.34}$$

For a full derivation of Eq. (2.34), see Van Der Veen 2013, Section 4.2 or Greve and Blatter 2009, Section 5.4.

Even though the stress balance for SIA is local, interaction with up- and downstream flow is included, since the divergence of the mass flux in the mass continuity equation (Eq. 2.19) affects ice thickness.

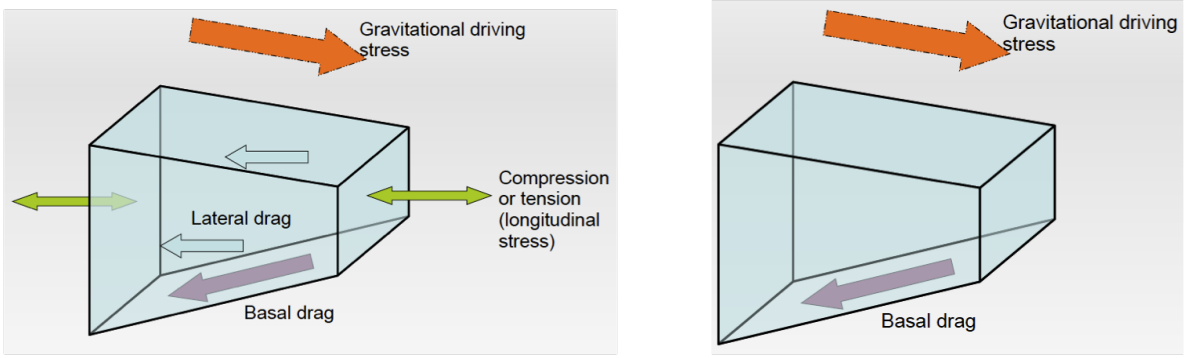

(a) (b)

Figure 2.5: (a) All stresses involved in glacier flow (full Stokes model); (b) The Shallow Ice Approximation: driving stress $\tau_d = \rho_i g H \nabla s$ is assumed to be completely balance locally by the basal drag τ_b. Figures modified after van der Veen (1999).

With the assumptions of the SIA, the full Stokes stress balance from Eq. (2.25)-(2.27) is reduced to a balance between the vertical shear stresses and the hydrostatic pressure

gradients:

$$\tau_{xz} = \frac{\partial p}{\partial x} \tag{2.35}$$

$$\tau_{yz} = \frac{\partial p}{\partial y} \tag{2.36}$$

$$0 = \frac{\partial p}{\partial z} + \rho g \tag{2.37}$$

These stress balance equations can be expressed in terms of ice viscosity and velocity gradients, analogously to the full Stokes stress balance in Eq. (2.28)-(2.29):

$$\frac{\partial}{\partial z}\left(\eta \frac{\partial u}{\partial z}\right) + \frac{\partial p}{\partial x} = 0, \tag{2.38}$$

$$\frac{\partial}{\partial z}\left(\eta \frac{\partial v}{\partial z}\right) + \frac{\partial p}{\partial y} = 0, \tag{2.39}$$

where ice viscosity η is given by Eq. (2.11).

If we integrate the stress balance in Eq. (2.35)-(2.37) over the ice column, we obtain the (2D) vertically integrated stress equations:

$$\tau_{xz} = -\rho g(h - z)\frac{\partial h}{\partial x} \tag{2.40}$$

$$\tau_{yz} = -\rho g(h - z)\frac{\partial h}{\partial y} \tag{2.41}$$

$$p = -\rho g(h - z) \tag{2.42}$$

where h is surface elevation and z (positive upward) is the height within the ice column (Dunse 2011; Van Der Veen 2013).

Dropping all terms except the two vertical shear stresses τ_{xz} and τ_{yz} in the full stress balance is key to why SIA is so computationally cheap - it only involves calculating the local stress balance analytically directly from geometry, without having to (numerically) solve a partial differential equation. Touching on model numerics, this stress balance results in sparse matrices (containing mostly zero entries), which require far less memory allocation than the full matrices resulting from the full Stokes balance.

SIA-models are strictly speaking only valid when ice is frozen to bedrock, since it only involves calculation of ice deformation for a given stress (velocity) field. To incorporate sliding for the non-frozen beds of temperate glaciers, SIA models usually add a sliding velocity depending directly on the driving stress (Eq. 2.33; Winkelmann et al. 2011). The sliding implementation used in this study is detailed in Sect. 4.1.2.

2.2 Mass balance

2.2.1 Surface mass balance

Surface mass exchanges dominate the mass budget of most glaciers, except those terminating in lakes, the ocean or overlying geothermally active areas. We can write the surface mass balance rate $\dot{b}_{sfc}$ at a point as

$$\dot{b}_{sfc} = \dot{c}_s + \dot{c}_a - \dot{a}_s + \dot{c}_r - \dot{s} + \dot{c}_w \tag{2.43}$$

where $\dot{c}_s$ is snowfall, $\dot{c}_a$ avalanche deposition, $\dot{a}_s$ melt, $\dot{c}_r$ refreezing of water, $\dot{s}$ sublimation and $\dot{c}_w$ wind deposition. For many glaciers, snowfall and melt dominates the surface mass balance, and Eq. (2.43) simplifies to $\dot{b}_{sfc} = \dot{c}_s - \dot{a}_s$. The units for the mass balance *rate* $\dot{b}_{sfc}$ are kg m^{-2} yr^{-1}. If we treat mass balance as mass per unit area, that is the *specific mass balance*, we usually express this as mm water equivalent (mm w.e.). This since 1 kg of water, having a density of $\rho_w = 1000$ kgm^{-3}, is 1 mm deep when distributed over 1 m^2. When comparing mass balances for different glaciers, we often use the unit m w.e. instead (Cuffey and Paterson 2010, p.94-6; Cogley 2005).

The glaciological mass balance year is for mid- to high latitudes defined from 1 October to 31 September. This is subdivided into winter balance from October to April, and summer balance from May to September. Glaciological (sometimes also termed 'direct') winter mass balance measurements are carried out by snow probing down to the summer surface of the previous year. This is called the stratigraphic method. In order to convert snow depth to a volume change in water equivalents, snow density samples are taken from snowpits at a few locations. Snow density is then interpolated over the glacier surface. At the end of the ablation season in late September or early October, the summer balance is measured on stakes drilled into the glacier surface. Net glacier-wide balance is then obtained by interpolation over the entire glacier surface (Cogley et al. 2011). Alternatively, summer and winter balance are measured on selected dates in autumn and spring. This is called the 'fixed-date' system.

Using point measurements for $\dot{b}_w$ (winter) with the glaciological method, the glacier-wide (area-averaged) specific winter balance B_w can be computed for the whole glacier area S by

$$\dot{B_w} = \frac{1}{S}\int_S \dot{b_w} ds \tag{2.44}$$

B_s (summer) and B_n (net) is computed in analogous ways.

Apart from the glaciological method, there are several other methods to determine the mass balance of a glacier. Commonly, these *geodetic methods* measure the elevation change $\partial H/\partial t$ and integrate this over the glacier area. This could be done by means of airborne platforms, by comparing topographic maps (DEMs) from different years or by repeated altitude profiles using a differential global positioning system (dGPS). These methods are described in full by Bamber and Payne (2004).

2.2.2 Mass balance variation with altitude

A glacier can be divided into two areas depending on their net (annual) specific mass balance b_n. The area where b_n is positive is called the *accumulation zone* and where b_n is negative is the *ablation zone*. The boundary between the two zones is called the *equilibrium-line* at which $b_n = 0$. The averaged altitude for the equilibrium-line is called the equilibrium-line altitude (ELA). At temperate glaciers, the position of the ELA roughly coincides with the snowline at the end of the summer, although the exact location of the ELA is determined by glacier geometry, topography effects and other local factors. Therefore, the the equilibrium-line should maybe be viewed as a *zone* rather than a strict line. Since the ELA is linked to the specific net mass balance, changes in the ELA can be interpreted as direct indications of changes in climatic conditions. A rise of the ELA corresponds to a negative mass balance, and if sustained for several years, the glacier may retreat at the terminus (Kaser et al. 2003; Cuffey and Paterson 2010; Cogley et al. 2011).

It is important to note that there is not a direct correspondence between terminus changes and the mass balance in a specific year. The lag or *response time* depends on glacier hypsometry (distribution of area with elevation), as well as the mass balance turnover of the glacier (Johannesson et al. 1989). This mass balance throughput can be quantified by the gradient of mass balance with elevation ($\partial b_n / \partial z$), also called the mass balance profile. In general, the larger the gradient (steeper mass balance profile), the faster the glacier has to flow to remain its geometry. Therefore it will be more sensitive to climate, implying a shorter time between an imposed climate anomaly and frontal response (Meier 1984). Notably, potting mass balance variations with elevation, mass balance is plotted as the *dependent* variable on the x-axis, while the independent variable, elevation, is plotted along the y-axis (Fig. 2.6). Thus, the mass balance profile of a typical maritime glacier with a large mass balance gradient (large difference in b_n between the ablation and the accumulation zone) will have a *smaller* slope in such a plot, than a continental glacier with a small mass balance gradient.

2.2.3 Mass balance and climate

The mean specific mass balance directly reflects the meteorological quantities over a year. For mid-latitude glaciers, the summer balance is largely determined by temperature, while (solid) precipitation dictates the winter balance. We can define the *mass balance sensitivity* as the change in mean glacier-wide mass balance to a 1°K increase for temperature (C_T) and 10 % for precipitation (C_P; Oerlemans 2001). The mass balance for maritime glaciers (for example those of the Norwegian west coast) are generally more sensitive to climate change. This is mainly due to three factors. First, the albedo feedback is stronger, since the winter snowpack is thicker and lasts longer, and thus reflect sunlight over a longer period. Second, a temperature change will have a large effect on the partitioning between snow and rain. Third, ablation seasons are longer, since maritime glacier extend to lower elevations (Oerlemans 1992; Oerlemans 2001).

The mass balance sensitivity approach should be seen as a first estimate, since it only considers the effect of two parameters (T and P) on mass balance. A more complete

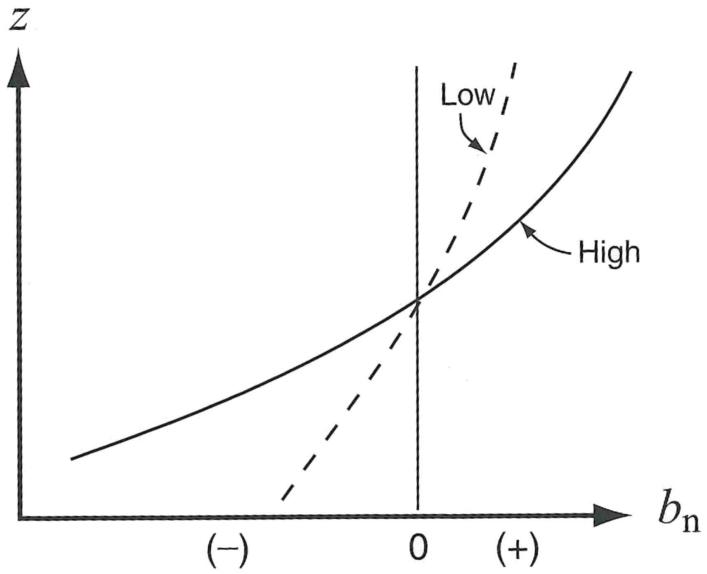

Figure 2.6: Schematic of high (large) and low (small) mass balance gradients. Typically, a maritime glacier will have a large mass balance gradient, while for a continental glacier it will be small.

approach is to take into account variables like cloud cover and humidity (Cuffey and Paterson 2010, p.107).

When air temperature rises, both downward sensible heat flux and the incoming longwave radiation balance increases. Since the temperature of the glacier surface cannot exceed 0 $°C$, the surface cannot compensate for this warming by emitting more longwave radiation, and melt occurs. This illustrates one aspect of why glaciers are so sensitive to climate (Oerlemans 1997). A review of the full energy balance and its relationship with climate can be found in, for example, Greuell and Genthon (2004).

Even though the specific mass balance is directly linked to the prevailing meteorological over a year, caution is needed about using the mass balance as a climate indicator. Part of the long-term variation in mass balance is also related to geometric changes. This can be illustrated by imposing a step-change in climate forcing (Fig. 2.7). While the actual climate has changed to a new state (the climate signal B'), it takes some time (in this example for Nigardsbreen, southwestern Norway, 200 years) for the glacier geometry to full adjust to this change, and consequently for the mass balance to reach zero again (Oerlemans 2001, p.103-104). Moreover, if a persistent climate change is experienced (for example the warming since the LIA or during the last few decades), the glacier may not be able to adjust fast enough, and will be in disequilibrium with the current climate. However, is may require many years of observations to distinguish this disequilibrium from interannual variations (Cuffey and Paterson 2010, p.112).

In addition, the time lag between mass balance and glacier response also depends on ice flow, since any added mass to the glacier surface is transported to lower elevations. Therefore, even though mass balance may stay constant, geometry adjustments may continue for many years as illustrated in Fig. (2.7). Conversely, mass balance may

change even during periods of constant climate, since glacier extent and shape may change.

A commonly used concept in terms of climatic responses of glaciers is the *steady state*. If the mass balance of a glacier is zero for many years, the glacier extent and shape will eventually remain constant. This period is usually longer for a larger glacier. While the concept of steady state is useful theoretically, real glaciers never reach an exact steady state (Cuffey and Paterson 2010, p.113).

The *mass balance-altitude* feedback plays a key role in such a scenario. In essence, if an ice mass is growing, it will extend to higher altitudes, where the colder climate will cause even less melting. Conversely, surface lowering into warmer altitudes will reinforce further melt (Oerlemans 1980). The importance of this feedback depends partly on ice dynamics. In dynamically inactive areas, such as flat areas of ice caps and ice sheets, local surface thinning may be much faster than local ablation rates (negative mass balance). Surface lowering also reduces the driving stress τ_d behind ice flow, since τ_d is proportional to ice thickness H and surface slope ∇s (Eq. 2.33), which both decreases if surface lowering is larger than terminus retreat (Haeberli et al. 2007).

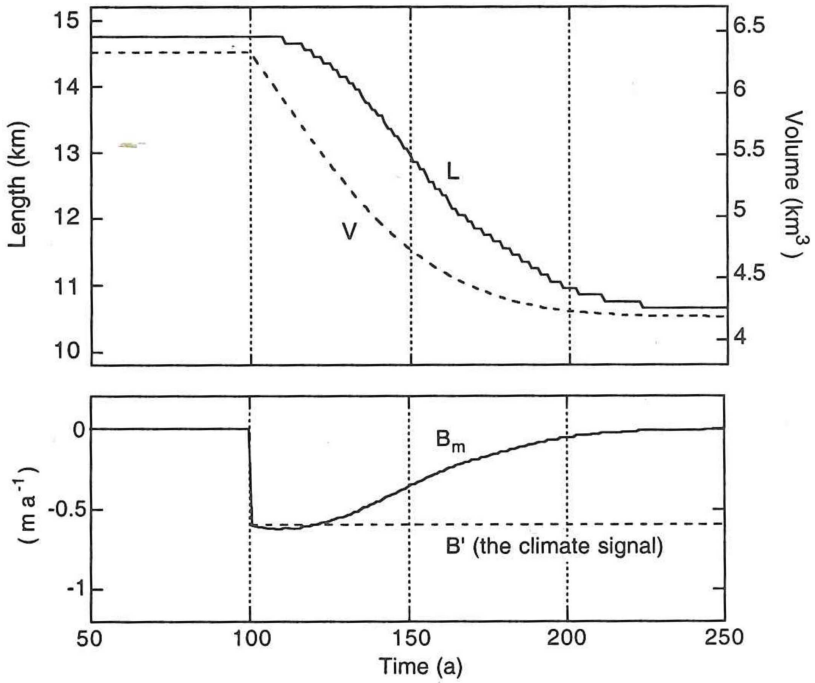

Figure 2.7: Calculated length, volume and mass balance response of Nigardsbreen to a step mass balance change of -0.5 m w.e. If we are "unlucky" enough to measure the mass balance between year 140 and 160, we may suggest that climate is getting colder or snowier, while in reality the glacier is just dynamically adapting its shape to a new climate state. Figure from Oerlemans (2001).

2.3 Introduction to ice modelling

2.3.1 What is an ice sheet model?

Since the 1970s, the use of computer models in glaciology has become increasingly common (Rutt et al. 2009). It is now one of the most important tools to reconstruct past ice sheets and glaciers, explore processes controlling their dynamics and predict their future behaviour and interaction with other subsystems of the Earth.

An ice sheet model can be thought of as computer code developed to simulate the behaviour of glaciers and ice sheets (Van Der Veen 2013). In essence, models consists of physical quantities and processes, represented by sets of equations. These are solved to determine how the system will act under certain given conditions (Benn and Evans 2010). Thoughtful use of numerical models can facilitate better understanding of the response to intrinsic and extrinsic processes for an ice mass. Models are based on physical laws and assumptions regarded to be important in describing glacier flow. Inevitably, models introduce errors, because they ignore or simplify the reality. Thus, the saying goes *"All models are wrong, but some are useful"*. The practical question is then how wrong do they have to be to not be useful (Box and Draper 1987). As an analogy, consider that a map is a model of the real world, but good maps are still hugely useful.

Models can be either diagnostic or prognostic. *Diagnostic* models are used to study a certain process or subsystem of an ice mass, whereas *prognostic* models describe change in a process or variable over time. Diagnostic models are usually calibrated against observations. Subsequent parameter studies can determine the sensitivity to poorly constrained processes (for example basal sliding), without actually understanding the process itself physically. Commonly, such models are run to a steady state with acceptable agreement to the actual ice mass geometry. Prognostic models on the other hand is applied to simulate behaviour of real ice masses and their response to climate over time. Parameters are adjusted so that model results matches with observations. As we will see, this is not the same as evaluating model performance or testing whether the actual physical processes are described well (Van Der Veen 2013).

2.3.2 Can we trust models?

One danger is to view a model as a "black box" or a substitute for reality (observations). This calls for model evaluations, which can be separated into *validation*, *calibration* and *confirmation*. It should be realized that models can never be *verified*, that is, the truth can never be demonstrated (Oreskes et al. 1994). In the context of glacier models, verification of the laws controlling ice flow would require following the movement of every single ice crystal in the glacier over its entire history. Obviously, this is not possible (Van Der Veen 2013). Thus, models are at best approximations of glacier systems and lumped behaviour of its constituent parts (Benn and Evans 2010).

Validation of models involves testing for errors associated with the way the governing equations are solved, e.g. numerical solution scheme and grid resolution. Of course, this is based on the assumption that the underlying equations are accurate representations of

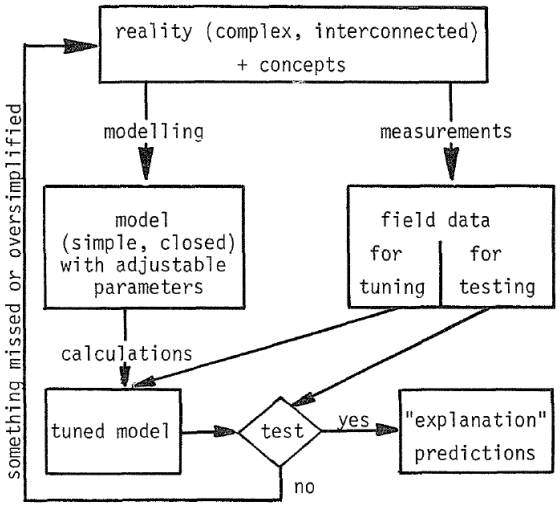

Figure 2.8: Possible workflow for a modelling study, showing the dependency of field observations both to calibrate (tune) the model, and to validate the model with additional field data (independent of the first set of observations). Figure from Waddington and Walder (1987).

actual glacier flow (Van Der Veen 1999). In this light, errors can arise from (a) solving the equations wrong; or (b) solving the wrong equations. Validation can be done through model intercomparisons, such as EISMINT (Huybrechts et al. 1996; Payne et al. 2000) and ISMIP-HOM (Pattyn et al. 2008) where a standardized simplified model set-up is used with different models, or by comparing to any available exact analytical solutions (Bueler et al. 2007).

If the model are thought to solve the right equations and does it well, focus moves to how well the model can reproduce actual observations. This is called *calibration*, and involves tuning of poorly understood parameters in order to match observations with model predictions at an acceptable uncertainty. If this succeeds, this means that parameters can be adjusted to make the model behave like the real world. This does not necessarily imply that the model accurately describe the processes involved, just that the combined effect of many processes can be represented by the model (Van Der Veen 2013). From a more general point of view, this is relevant to model development. If new understanding of a process is implemented into an ice model, it is not certain that the model representation will be closer to reality. Rather, it is more likely that model results will be farther from the actual behaviour, since model results rely on that small errors in various processes cancel each other out.

To actually *confirm* whether models describe the physical processes involved, model results should be compared with observations not used in the calibration process. The more observations that are matched with model predictions, the more faith one can have in that the model consists of realistic representations of natural processes. However, complete confirmation is impossible, as this would mean that the model has been fully verified. In here lies a key challenge when evaluating models and it also largely decides to what degree the model is useful or not. If confidence cannot be placed in the physical

understanding of ice processes the model are based on, it does not matter how well the numerics are done or how beautifully the results are plotted. It certainly does not move science further either.

Moreover, there are also inherent uncertainties in the observations the model is tested against. Therefore, it makes sense to test model predictions against all field measurements available. Further, it points out the mutual dependence on models and observations. If observations are not available to constrain models, it is difficult to place any confidence in model results. Conversely, if model studies were not at hand, it could well be that we are wasting our time trying to observe the wrong phenomena and missing out on what really matters. The model process is summarized in Fig. 2.8.

2.3.3 Importance of sensitivity analysis

Many parameters and boundary conditions used in models are poorly known, vary from glacier to glacier as well as within a single glacier. There may be several reasons to perform a sensitivity analysis, including to determine: (1) which parameters/processes are poorly understood and therefore need further research; (2) which parameters are insignificant and can be ignored or greatly simplified in the model; (3) which inputs/processes contribute most to output outcome and variability; (4) the consequence of final results by changing a given input parameter (Hamby 1994).

For example, we can perform a simple test to a parameter by varying it within some plausible limits. For example, suppose the temperature in a glacier is believed to be around -5 %, and unlikely to be below -7°C or above -1°C. We may then do a *sensitivity test* where we set the temperature to the most extreme, least extreme, and most likely values. This way we determine their effects (or robustness) on model outcome (Hooke 2005, p.302-303). There may also be the need to test some intermediate values, since the model response may not be linear to the parameter choices.

Since there are many parameters in a model, it quickly becomes a formidable task to test all possible combinations of values. Moreover, the sensitivity to a certain parameter or boundary condition will likely vary spatially, in fact it would be surprising if the sensitivity was equal everywhere. Recently, progress in methods like *adjoint modelling* (MacAyeal 1993; Heimbach and Bugnion 2009; Morlighem et al. 2013) enables calculation of sensitivities in space for a large number of parameters. The use of such methods fall outside the scope of this study, but remain an option for future work.

3 Data: Hardangerjøkulen ice cap

3.1 Geometry

3.1.1 Surface topography

Hardangerjøkulen (60°55'N, 7°25'E) is a plateau glacier or ice cap. It is the sixth largest ice mass in mainland Norway (Andreassen et al. 2012a) with an area of 73 km^2 in 2010 (Kjøllmoen et al. 2011; Andreassen et al. 2012b). The ice cap interior is rather flat (Fig. 3.2), with steeper outlet glaciers draining the plateau, the largest being Rembesdalskåka (W-SW, 17.4 km^2), Midtdalsbreen (NE; 6.8 km^2), Blåisen (NE; 6.6 km^2) and Vestre Leirbotnskåka (S-SE; 8 km^2), see Fig. 3.1. Surface elevation ranges from 1854 to 1066 m a.s.l. (Kjøllmoen et al. 2011) with 80 % of the area of the ice cap situated above the mean ELA at 1640 m a.s.l (Giesen 2009). For the largest outlet glacier Rembesdalskåka, the same percentage was 70 % based on net surface mass balance for 35 years during the period 1965-2007. Rembesdalskåka drains towards lake Rembesdalsvatnet, located 1 km from the glacier terminus (Kjøllmoen et al. 2011) (Fig. 3.1). With the development of hydropower in the area in the 1970s, both lake Rembesdalsvatnet and lake Nedre Demmevatnet was dammed and their water levels are thus controlled. The damming was partly done in response to repeated jøkulhlaups (glacier outburst floods) from lake Demmevatnet, the most recent events occurring in 1937 and 1938 (Liestøl 1956; Elvehøy et al. 1997).

Several surveys of the surface topography of the whole ice cap has been conducted; in 1920-25, 1961, 1995 and 2010. The first available data is a terrestrial map D33 (Norwegian: Gradteigskart D33) in 1:100 000. This map is drawn based on photogrammetry in 1927-28 (H. Elvehøy, pers. comm.). On 31^{st} August 1961, aerial photos was taken by Fjellanger Widerøe AS to produce a glacier map (1:20 000) with 10 m contour lines (Elvehøy et al. 1997 ; "Volume change Hardangerjkulen"). On 31^{st} August 1995 (Fjellanger Widerøe AS), new aerial photos were collected and a 1:50 000 map with 20 m contours were produced ("Volume change Hardangerjkulen"). The most recent airborne laser scanning was conducted on 29^{th} September 2010 and has an accuracy of 0.3 m (Andreassen et al. 2012b).

3.1.2 Ice thickness and bed topography

There has been numerous efforts to map the subglacial topography of Hardangerjøkulen. First attempts were done in 1963, when three seismic reflection and refraction profiles was collected in the upper drainage basin of Rembesdalskåka and the upper and lower part of Vestre Leirbotnskåka (Sellevold and Kloster 1964). Ice thickness from the seismic survey were not corrected for surface elevation change between 1963 and 1995 due to uncertainties in horizontal position and estimation of altitude in the two maps compared (Elvehøy et al. 1997). The surface change for this area of Hardangerjøkulen between 1961 and 1995 is ± 10 m w.e. ("Volume change Hardangerjkulen"). Measurements continued by NVE in 1965-66, when a hot water drill was used to estimate the ice thickness at

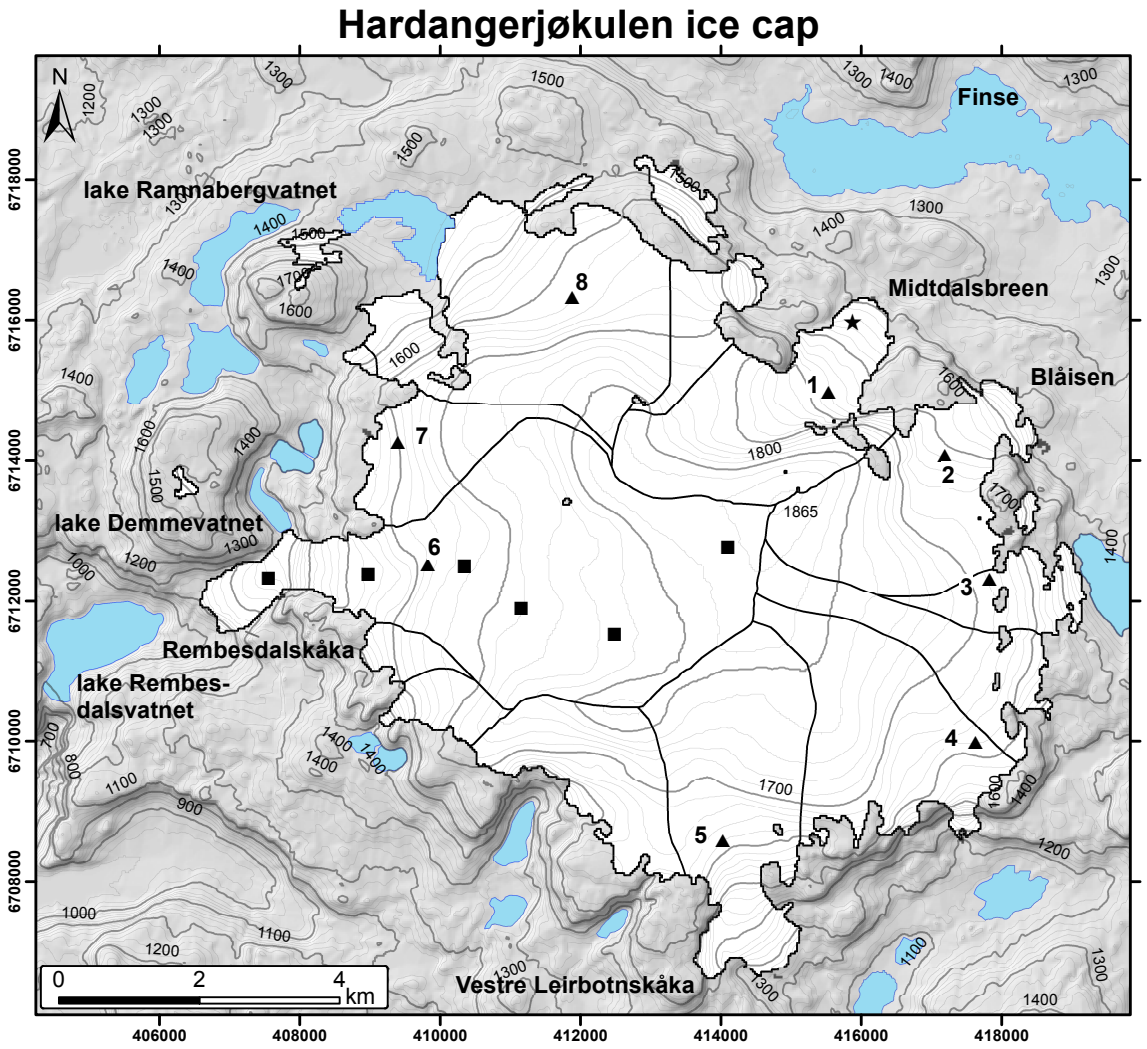

Figure 3.1: Map of Hardangerjøkulen, modified after Giesen (2009). Contour interval is 20 m and created from a digital elevation model by Statens Kartverk, 1995. The reference system is UTM zone 32N (EUREF89). Ice cap outline and drainage basins from 2003 are indicated (data from Cryoclim.net), as well as lakes surrounding the ice cap (drawn after Statens Kartverk N50 1:50 000). Shown are GPS positions for velocity measurements (numbered triangles), mass balance stakes from NVE (squares) and location of the automatic weather station (star).

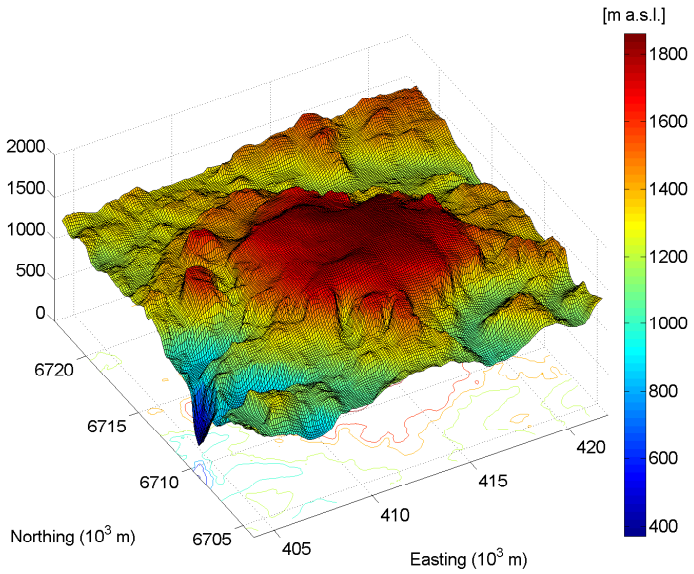

Figure 3.2: Surface topography of Hardangerjøkulen ice cap and surrounding areas in 1995. Data from Statens Kartverk.

several locations in the ablation zone of Rembesdalskåka. After comparisons with radar investigations in 1996, 20 out of 39 boreholes drilled in the 1960s were found unreliable and were thus rejected (Elvehøy et al. 1997).

The first radar (Radio Echo Sounding, RES) profiles were obtained in March 1988 by Y. Gjessing and H. Bjørnsson. An ice thickness map with 100 m contours were created, covering parts of the accumulation area of the ice cap. Subsequent comparison with radar measurements in the 1996 lead to large adjustments of the map from 1988 (Elvehøy et al. 1997; Giesen 2009). Further RES investigations were done in spring 1995 as a part of a Master thesis by Østen (1998). He did numerous tracks in the ablation zone of Midtdalsbreen, using a low-frequency pulse-radar system with a 6-10 MHz antenna. The RES setup were the same as detailed in Kennett and Sætrang (1987), with the only modification being that retrieved radar signals were stored on a computer instead of on camera film. In the past, the screen of the oscilloscope used were photographed and ice thickness estimated from the photos (Elvehøy et al. 1997). The upper parts of Midtdalsbreen were later covered by K. Melvold (NVE) in 2001, 2002 and 2004 (Melvold, unpubl. data; Giesen 2009; Willis et al. 2012). Ice thickness was also measured on Rembesdalskåka, close to lake Demmevatn, in September 1996 for use in an assessment of future jøkulhlaups. Results could not be obtained in heavily crevassed areas, and only where ice thickness exceeded 50 m. A maximum ice thickness of 200 m were measured at the lower reach of the ice fall. The bottom reflection signal was of variable quality; mean uncertainties in ice thickness is assumed to be ± 15 m (Elvehøy et al. 1997).

Considering the long measurement period in 1963-2008, it may seem problematic to combine all data described above to produce an ice thickness map. Nonetheless, outlet glacier length measurements (Fig. 3.7) and mass balance observations (Fig. 3.9) for this

(a)

(b)

Figure 3.3: (a) North-facing outlet glacier Midtdalsbreen. Imagery from Google Earth/Landsat. (b) Southwest-facing Rembesdalskåka outlet glacier, lake Rembesdalsvatnet and the interior of Hardangerjøkulen. Imagery from norgei3D.no. (a) and (b) are tilted satellite imagery from a viewpoint c. 2 km above the ground. Scale bars are approximate and most accurate where they are placed. Scale will be different in top and bottom parts of the images. Some distortion in areas of steep topography occurs.

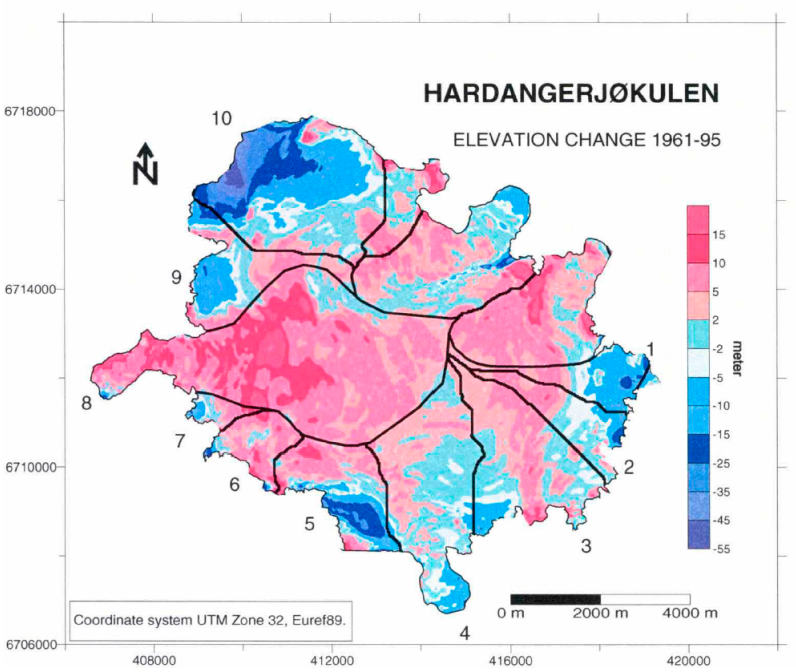

Figure 3.4: Difference between 1961 and 1995 surface elevations (DEMs). Note the asymmetric scale. Figure from Andreassen and Elvehøy (2001).

period suggest that Hardangerjøkulen was close to a balance state during this time span. Moreover, surface elevation changes from 1961 to 1995 was ± 10 m w.e. for most of the ice cap ("Volume change Hardangerjkulen"). This is similar to or lower than the uncertainties quoted for the ice thickness measurements.

To produce a final ice thickness map, a combination of automatic and manual interpolation and extrapolation was used (Elvehøy et al. 1997; Giesen 2009; Willis et al. 2012). Where measurements were dense (e.g. on Midtdalsbreen), ice thickness was interpolated using methods detailed in (Melvold and Schuler 2008). In areas with sparse measurements, ice thickness H was estimated directly from the surface slope α, assuming perfect plasticity (Paterson 1994):

$$H = \frac{\tau_0}{\rho_i g \nabla s}, \tag{3.1}$$

where τ_0 is the yield stress, ρ_i ice density, g gravitational acceleration and ∇s the surface slope. Based on detailed ice thickness measurements and knowledge of the surface slope on Midtdalsbreen, a yield stress of 150-180 kPa was used. Some manual interpolation was needed at ice divides and ice ridges (small surface slopes) and close to ice margins to obtain a smooth decrease in ice thickness (Giesen 2009).

The latest updated bed topography map was published by (Melvold et al. 2011), based on additional radar measurements as well the DEM derived from airborne laser scanning (Lidar) in 2010 (Melvold, pers. comm; Andreassen et al. 2012b). Patterns are similar to the bed topography produced with the bed topograhy map derived from the surface DEM from 1995, but some differences occur, mainly on the north-eastern outlet

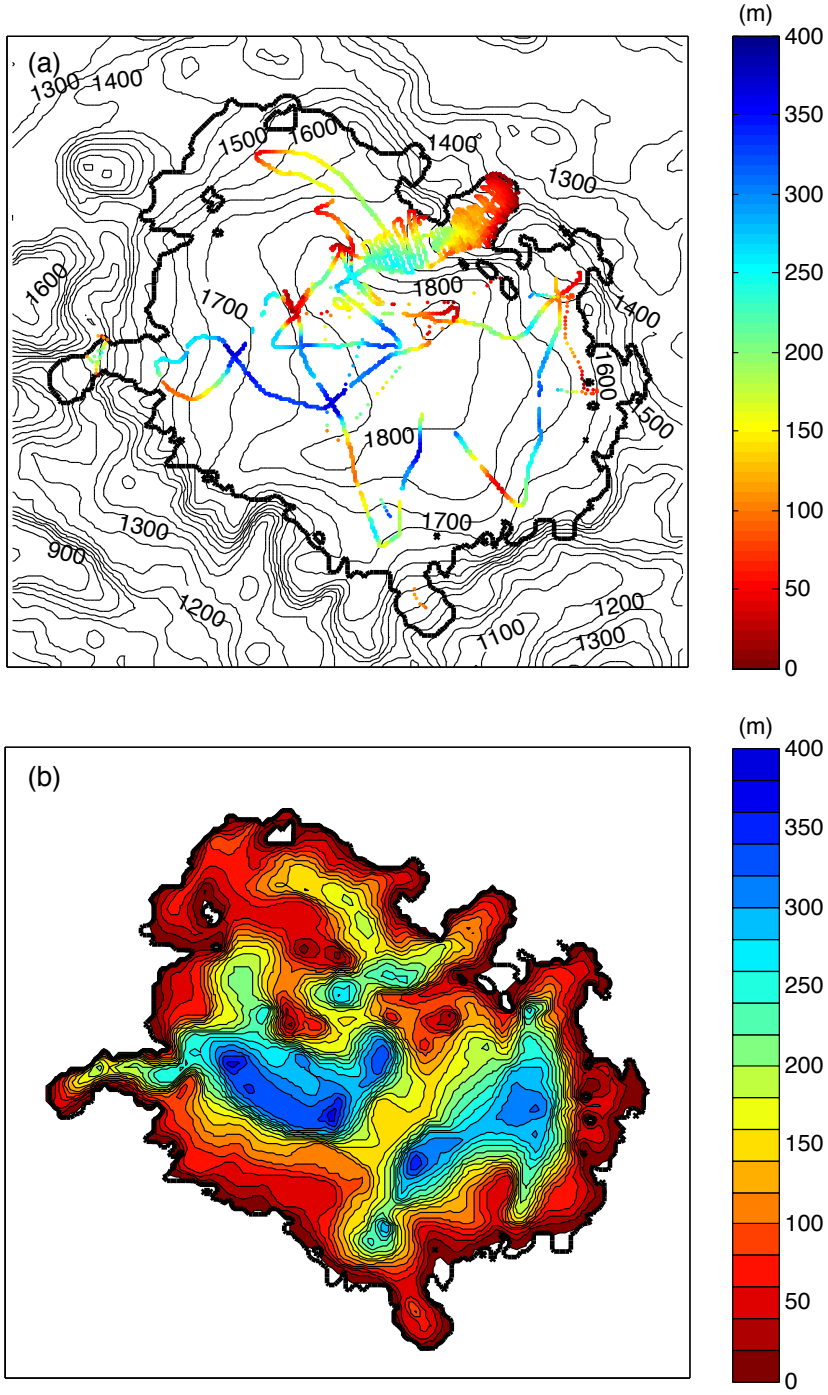

Figure 3.5: (a) Ice thickness data from studies 1963-2008 described in the text. (b) Ice thickness calculated from the surface DEM from 1995 and thickness measurements from studies 1963-2008, as described in the text. Note color scale is reversed from other ice thickness figures used in this thesis. Figures from Giesen (2009), data from K. Melvold, NVE.

glaciers Midtdalsbreen and Blåisen, where ice thickness from the later investigation appears somewhat larger than the ones used by (Giesen 2009). To ensure a more direct comparison to modelling efforts by Giesen (2009), we choose not to include the new measurements from (Melvold et al. 2011) at this stage. Further discussion about the accuracy of the bedrock topography and its potential implications for ice flow is included in Sect. 6.

3.1.3 Geometry changes since the Little Ice Age

The LIA maximum for Midtdalsbreen is dated to AD 1750 with lichenometry by Andersen and Sollid (1971). For Rembesdalskåka, the outermost terminal moraine has not been dated, but is assumed to originate from the LIA maximum. The end moraine was even more prominent before the proglacial lake Rembesdalsvatnet was dammed in the 1970s (H. Elvehøy, pers. comm. w. R. Giesen).

Length observations at Rembesdalskåka began in 1917 by J. Rekstad, Bergen Museum (Fig. 3.7a). Measurements have subsequently been done during several discontinuous periods, and is since 1995 done annually. For Midtdalsbreen, glacier length measurements was started by A. Nesje at University of Bergen in 1982 and an annual record since then exist (Fig. 3.7b; Giesen 2009 ; Kjøllmoen et al. 2011).

The terrestrial map based on photogrammetry in 1927-28 show that the glacier front reached the proglacial river delta in lake Rembesdalsvatnet, c. 885 m a.s.l. (Fig. 3.6), an area now regulated by the damming of the lake in the 1970s. The front of Rembesdalskåka was advancing during 1919-21, and deposited an end moraine 23 m in front of the glacier terminus measured in 1935, presumably in 1927-28 as indicated by Liestøl (1956) in Fig. 3.6. From 1935 to 1961, the glacier melted back almost a kilometre.

In the corresponding period 1934-1961, Midtalsbreen retreated around 500 m. Between 1961 and 1982, when the direct front measurements started, the terminus change of Midtdalsbreen was small, while Rembesdalskåka retreated slightly.

Both outlet glaciers advanced in response to the snowy winters in the early 1990s. The terminus change for from 1988 to 2000 for Rembesdalskåka was +147 m and for Midtdalsbreen +46 m. From their positions in 2000, the two have retreated 332 m and 164 m, respectively (Andreassen et al. 2005; Kjøllmoen et al. 2011; Cryoclim.net).

While relative terminus changes have a fairly high accuracy, deriving length records from such measurements is not straightforward, since it depends on the flowline used. Here we use the same flowline for Rembesdalskåka as NVE use for their measurements (H. Elvehøy, pers. comm.). For Midtdalsbreen, we use a slightly modified flowline from that of NVE. Moreover, length records corresponding to other surveys (Sect. 3.1.1) are used to complement the direct measurements. Since we use multiple sources of data to derive a single length record; a conservative uncertainty estimate of outlet glacier lengths in Fig. 3.7 is ±200 m. This is likely smaller for the most recent part of the record.

In addition to outlet glacier front measurements, a few surveys of the full ice cap extent has been done, some outlined above in Sect. 3.1.1. These are summarized in

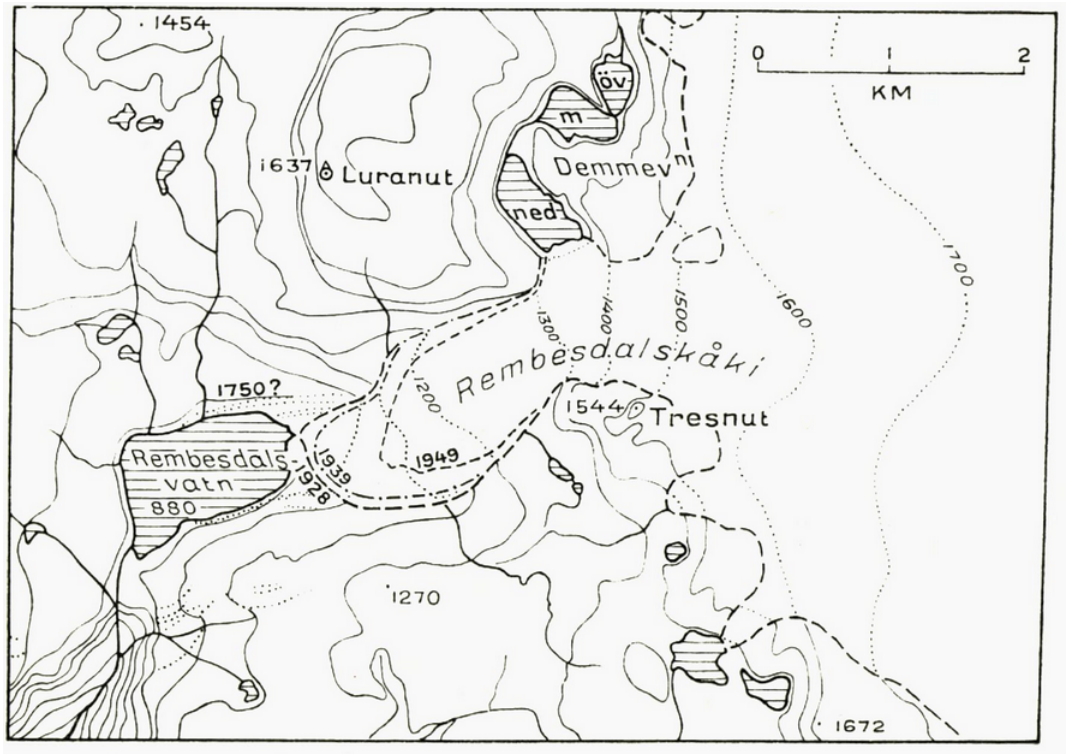

Figure 3.6: Map of Rembedalskåka front positions, as reported by Liestøl 1956.

Table 3.1.

3.2 Climate and mass balance

3.2.1 Present climate

Southern Norway is located on the stormtrack of the Northern Hemisphere westerly wind belt and is heavily influenced by the moist, warm air picked up from the Atlantic Ocean. When these winds reach the mountainous west coast, orographic lifting occurs and precipitation falls as rain or snow, depending on elevation. Conversely, eastern Norway are located in a rain shadow of the mountains of western Norway and the high mountain plateau Hardangervidda.

Table 3.1: Overview of data for ice cap extent.

Year	**Area (km^2)**	**Data type**	**Accuracy**	**Data source/reference**
1750	114	Moraine evidence	?	Liestøl (1962); Andersen and Sollid (1971); Nesje (pers. comm.)
1936	78	Terrestrial map	?	Liestøl (1962)
1961	77.6	Aerial photo	20 m	Cryoclim.net
1961	76.9	Aerial photo	20 m	Andreassen & Winswold (2012)
1961	75.0	Aerial photo	20 m	Andreassen & Elvehøy (2001)
1973	73.8	N50 Map	?	Cryoclim.net
1988	73.9	LANDSAT5 MSS	30 m	Cryoclim.net
1995	73.6	Aerial photo	25 m	Cryoclim.net
1995	72.4	Aerial photo	25 m	Andreassen & Elvehøy (2001)
2003	72.2	LANDSAT5 TM	30 m	Andreassen & Winswold (2012)
2010	73	Airborne lidar	0.15 m	Andreassen et al. (2012b)

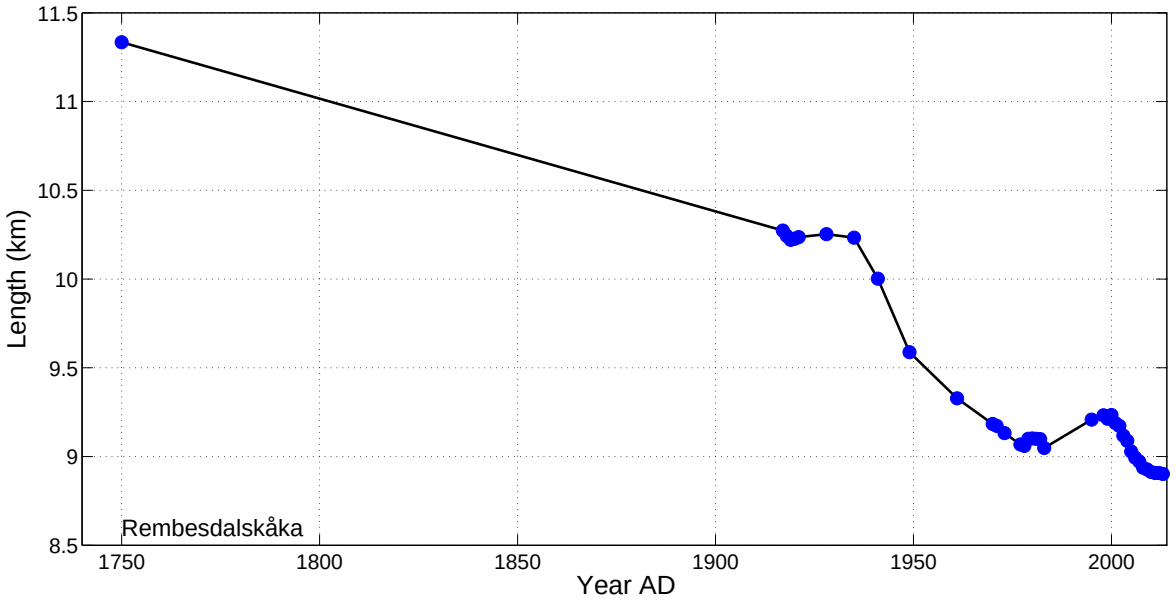

(a)

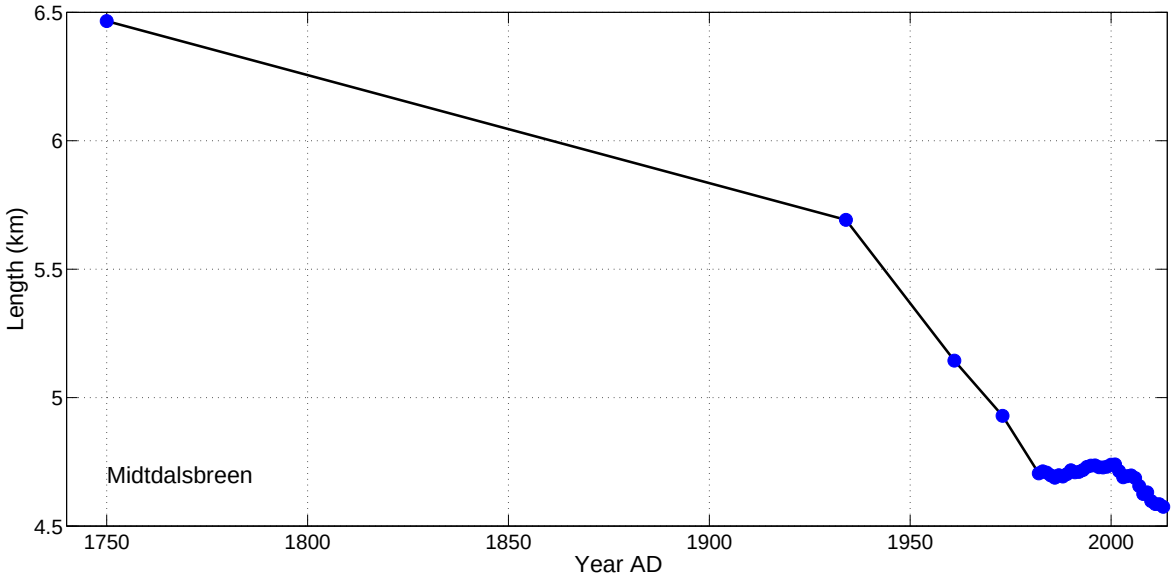

(b)

Figure 3.7: Length record for outlet glaciers (a) Rembesdalskåka and (b) Midtdalsbreen. Data from Cryoclim.net and Hallgeir Elvehøy, NVE.

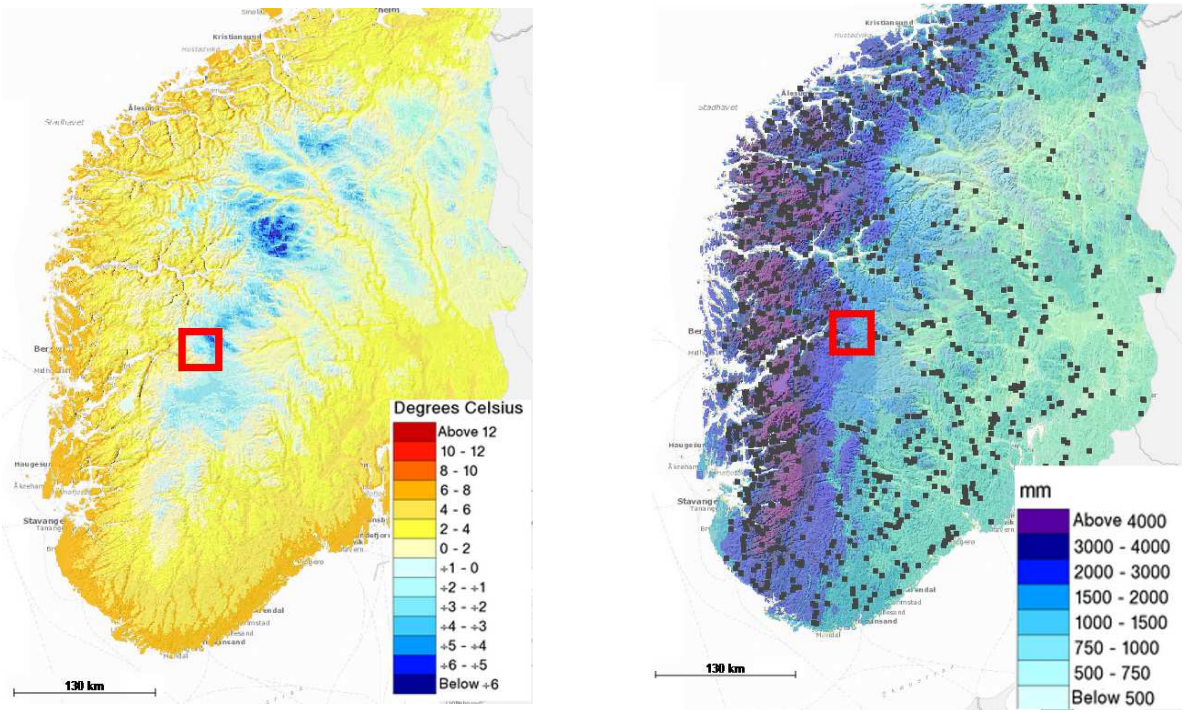

(a) (b)

Figure 3.8: (a) Mean annual temperature and (b) precipitation for southern Norway for the normal period 1971-2000. Black dots in (b) indicate location of hydropower stations. The Hardangerjøkulen ice cap is located at the main water divide, in between the maritime climate of the west coast and the dry continental climate of eastern Norway. Figures from seNorge.no, data from Norwegian Meteorological Institute and Norwegian Water and Energy Directorate (NVE).

This west-east precipitation gradient (Fig. 3.8b) is illustrated by the mean annual precipitation for 1961-1990 in Bergen, 65 km west of Hardangerjøkulen (red square), reaching 2250 mmyr^{-1}. In contrast, Oslo in eastern Norway have 763 mm precipitation per year. Liset, 17 km from the summit of Hardangerjøkulen and 12 km SSW of the SW facing Rembesdalskåka outlet glacier receives 1110 mmyr^{-1}. Finse, some 8 km north-east of the summit and 3 km from the front of the NE facing outlet glacier Midtdalsbreen, experiences 1030 mmyr^{-1}.

Temperatures for southern Norway are mainly determined by altitude and distance from the coast. For example, the warmest city of Norway is Bergen, with a mean annual temperature of 7.8°C, while the Jotunheimen area, home to several of Norway's continental glaciers, have the lowest temperatures in southern Norway. In the area closer to Hardangerjøkulen, the mean annual temperature for Finse is -2.1°C. Liset on the southern side lacks a temperature record covering the normal period 1961-1990 (data from eklima.no, Norwegian Meteorological Institute). Based on a five-year record (2001-2005) from an Automatic Weather Station (AWS) in the ablation zone of Midtdalsbreen, the mean annual air temperature here is -1.4°C (Giesen et al. 2008), with a typical

annual range of 15°C. This AWS is located around 400 m from the glacier front at an altitude of 1450 m a.s.l. (Fig. 3.1).

During the period 1875-2004, annual temperatures in southern Norway increased by 0.08 to 0.09 °C per decade (Hanssen-Bauer 2005). The largest trend was found for winter and spring, while the summer temperature trend was found not significant. During the 1930s, winter, summer and autumn temperatures were higher than normal (period 1961-1990). As a consequence, south Norwegian glaciers retreated rapidly and extensively (Andreassen et al. 2005). Subsequent cooling until the 1970s slowed the retreat down, while after 1980 a warming trend has been experienced.

For precipitation analysed for 1895-2004, southern Norway had a 2 % increase in autumn, while only some regions of southern Norway experienced a significant annual trend. For south-western Norway, precipitation amounts stayed relatively stable until the 1960s. After this, a statistically significant trend has been observed, mainly due to higher autumn and winter precipitation (Hanssen-Bauer 2005).

3.2.2 Little Ice Age climate

The term "Little Ice Age *glacierization*" is often used to describe glacier advances in Europe c. AD 1300-1950 (Matthews and Briffa 2005), although with considerable spatial and temporal variability. In general, Scandinavian glaciers started a pre-LIA advance during the 14th-16th centuries, followed by considerable growth during the late 17th and early 18th century, culminating during the mid-18th century (Grove 2001; Grove 2004; Nesje et al. 2008), although the LIA-maximum seem to be spatially and temporally asynchronous (Matthews and Briffa 2005).

In constrast, the "Little Ice Age *climate*" is usually defined for a period c. AD 1570-1900, when reconstructions and climate models indicate Northern Hemisphere temperatures 0.5-1.0°C lower than today (Shindell et al. 2001; Gouirand et al. 2007). There are considerable regional variations in LIA temperatures within the Northern Hemisphere, as shown from different proxy data records (IPCC, 2013). The colder climate and its variability during this period was likely caused by a combination of numerous large volcanic eruptions (Crowley 2000; Otterå et al. 2010) and low solar activity, namely the 'Maunder Minimum', AD 1645-1715, and 'Dalton Minimum' AD 1790-1830 (e.g. Lean et al. 1992).

3.2.3 Surface mass balance

The Norwegian Polar Institute started mass balance measurements on Rembesdalskåka (17.4 km^2) in 1963, investigations which the Norwegian Water Resources and Energy Directorate (NVE) took over in 1985 (e.g. Kjøllmoen et al. 2011). This continuous mass balance record (Fig. 3.9) is complemented by snow depth measurements along two profiles in the upper part of the glacier. The stake network and snow depth profiles from the early part of the record were very extensive. However, small year-to-year spatial variations in accumulation and ablation patterns lead to a reduction of the number of stakes to what is indicated in Fig. 3.1.

The annual mass turnover for Rembesdalskåka is around 2 m w.e. The mean net balance for the period 1963-2013 was close to zero (+0.04 m w.e.), divided into a winter balance of +2.09 m w.e. and a summer balance of -2.05 m w.e. (Fig. 3.9). Until 1988, Rembesdalskåka was in close to balance with climate.

For Midtdalsbreen, there are only mass balance measurements for 2000-2001 (Krantz 2002). Net mass balance were measured to +1.32 m w.e. for 2000 and -0.64 m w.e. in 2001. The same values for Rembesdalskåka were similar but slightly less positive, +1.43 m w.e. and -0.85 m w.e. respectively. This two-year time series is too short for a robust comparison between the northeast and southwest facing glaciers.

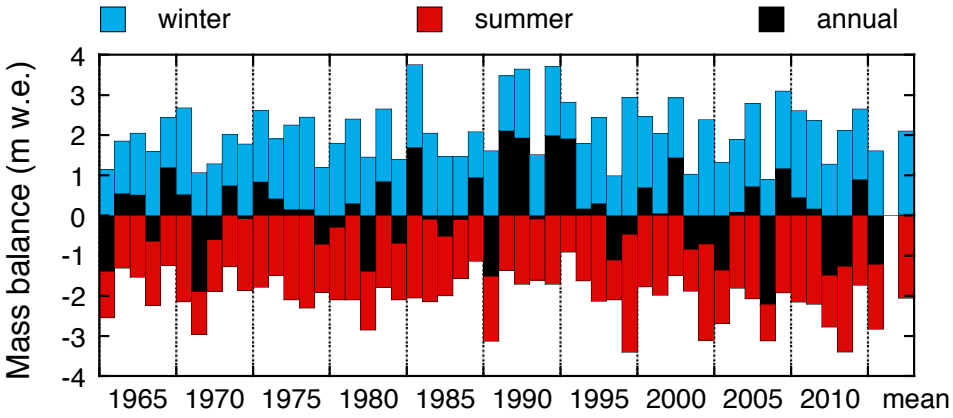

Figure 3.9: Winter, summer and net balance for Rembesdalskåka 1963-2013. The mean net balance over this period is also indicated. Data from NVE.

For the period 1963-2007, specific mass balance gradients exist from 35 of the 45 years (Giesen 2009). To facilitate a comparison as direct as possible with Giesen (2009), we use the same period and profiles and thus choose to not include the mass balance profiles from the years 2008-2013.

For the winter balance, the interannual variability around the mean winter profile is similar between years, while the summer balance has a larger range for lower elevations than at higher. The decrease in (winter) mass balance with elevation is probably explained by wind redistribution, but no studies have been done to quantify this effect on mass balance (Fig. 3.10a).

The net balance gradient have a similar shape for most years. The relationship between net mass balance and altitude is approximately linear in the ablation zone (Fig. 3.10b). The net mass balance is zero at 1640 m a.s.l., indicating the equilibrium-line altitude (ELA). Above the ELA, mass balance decreases with altitude. Looking at the winter profiles in Fig. 3.10a, there is a distinct bend in the mass balance profile for the highest altitudes, where mass balance decreases above 1775 m a.s.l.

In terms of volume (Fig. 3.10b), the largest contribution to mass balance come from the wide upper area of the Rembesdalskåka basin, where the mass balance profile has its maximum. The largest mass loss occurs around 1200 m a.s.l. in an area of the ablation zone wider than adjacent up- and downglacier areas (Giesen 2009).

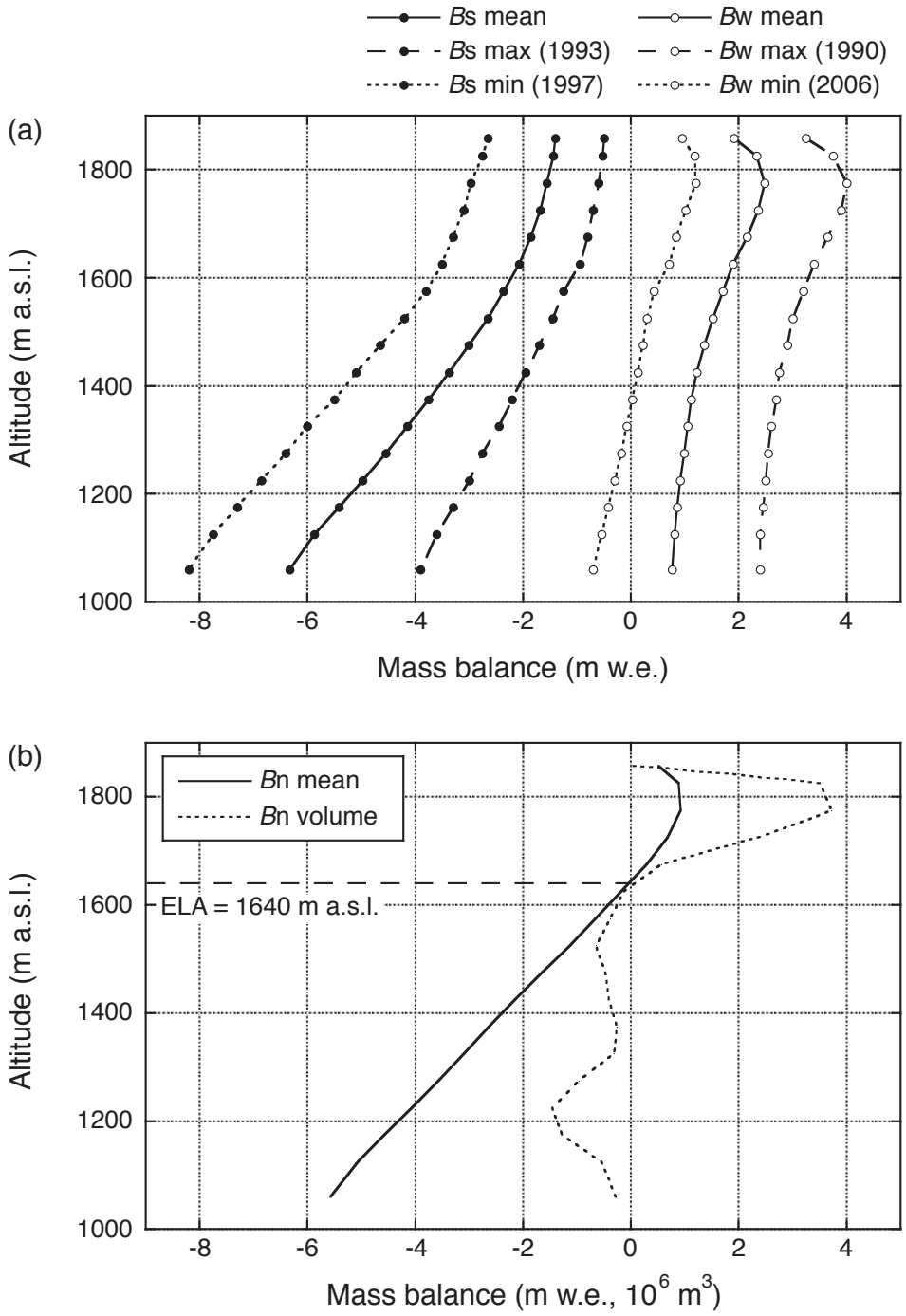

Figure 3.10: Mass balance profiles for Rembesdalskåka based on data from 35 profiles during 1965-2007. (a) Mean, maximum and minimum mass balance profiles for winter (B_w) and summer (B_s). (b) Mean net (B_n) specific and volume mass balance. Figures from Giesen (2009). Data from NVE.

3.3 Dynamics

3.3.1 Basal conditions

The geology below Hardangerjøkulen is part of a highly metamorphosed overthrust sheet, consisting of granitic gneiss and phyllite bedrock (Østrem and Ziegler 1969; Hagen 1978). Around the ice cap, the bedrock is of sedimentary type, possibly mylonite or sandstone (Askvik 2008). The sediment cover in surrounding areas is generally sparse (Andersen and Sollid 1971). Although bed conditions of Hardangerjøkulen are not well-known, given the sparse sediment cover around the ice cap, it seems likely that the bed can be characterised as a hard bed.

According to investigations described in Section 3.1, Hardangerjøkulen can be assumed a temperate glacier. However, Midtdalsbreen has based on temperature measurements been suggested to be cold-based in its lowermost parts (Hagen 1978; Konnestad 1996). Most recent studies by Reinardy et al. 2013 and a field visit in April, 2014 (Reinardy, unpubl. data), suggest that the cold-based area at the terminus of Midtdalsbreen is still present. Although affecting the formation of annual moraines as noted by Reinardy et al (2013), we assume that the effect of these cold ice regions on ice flow for Midtdalsbreen and Hardangerjøkulen as a whole is minor.

3.3.2 Surface velocities

Glacier velocities can vary over a range of timescales. Generally, summer velocities are higher than those in winter, and spring-time speed-ups of up to 900% of the average summer velocities has been observed at Midtdalsbreen, lasting a day or so in length (Willis 1995). This thesis focuses on glacier response on climatic timescales, meaning mean annual velocities is of concern rather than short-term motion events.

Ice velocities were measured in September 1996 on Rembesdalskåka, next to lake Demmevatnet, over a period of 26 hours. Measurements showed a ice flow of 30 cm day^{-1}, which corresponds to 110 m yr^{-1}. This short period can only give an order of magnitude estimation. Natural variations in ice flow will affect velocities over the course of a year (Elvehøy et al. 1997).

For the lower ablation zone of Midtdalsbreen, surface speeds were measured to 4-40 m yr^{-1} during summer 2000 (Vaksdal 2001). The mass balance for Midtdalsbreen in 2000 was +1.32 m w.e. There are no previous estimates of velocities for Midtdalsbreen.

Giesen (2009) measured velocities at eight GPS locations situated around the ELAs at the eight main outlet glaciers of the ice cap during the period of May 2005 - September 2007 (Table 3.2). GPS1 - 8 were placed on stakes drilled into the snow or ice. In addition, a GPS9 were put on top of the AWS on Midtdalsbreen. A stationary GPS10 located on a small hill adjacent to the terminus of Midtdalsbreen were used for comparison to determine the accuracy of the moving GPSs. A detailed description of the processing procedure can be found in Giesen (2009), p.46-47. Unfortunately, no GPS was functioning the whole period. Problems included loose wiring, buried and lost GPSs and one stake ending up in a crevasse. Notwithstanding these issues, the continuous data available show

highest velocities for the largest outlet glacier Rembesdalskåka (46 m yr^{-1}). Velocities at Midtdalsbreen (33 m yr^{-1} at the ELA and ∼20-22 m yr^{-1} at the AWS) are within the range of ablation zone summer velocities suggested by Vaksdal (2001) described above, albeit measured over a longer period.

Table 3.2: Mean surface velocities and direction for *in situ* GPS measurements at Hardangerjøkulen by Giesen (2009). Direction of movement is in degrees with respect to the north, where 0° represents northward flow and 90° eastward flow.

GPS #	**Start date**	**End date**	**Velocity** (myr^{-1})	**Direction** (°)	**Direction**
1	14 May 2005	18 Mar 2006	33.1	52.8	NE
2	15 May 2005	23 Oct 2005	18.9	33.4	NE
2	26 Mar 2006	28 Dec 2006	21.2	32.6	NE
3	26 Mar 2006	23 Nov 2006	7.1	12.3	NNE
4	26 Mar 2006	03 Oct 2006	6.2	108.4	ESE
6	13 May 2005	11 Nov 2005	46.3	269.7	W
6	26 Mar 2006	23 Sep 2006	46.4	272.9	W
7	14 May 2005	03 Dec 2005	6.6	250.8	WSW
8	14 May 2005	09 Nov 2005	8.5	223.8	SW
9	14 May 2005	14 Jul 2005	34.6	24.0	NNE
9	28 Aug 2005	19 Jun 2006	19.6	20.9	NNE
9	28 Mar 2007	14 Sep 2007	21.6	23.0	NNE

Since velocities only have been measured for single years or shorter, these observations mostly provide guidance rather than serving as data to calibrate or validate a model against. To the author's knowledge, there are no velocity data derived from remote sensing platforms (see Sect. 8).

4 Methods: Ice modelling

In this section, the methods used to model Hardangerjøkulen ice cap is outlined. The capabilities and mechanics of the ice flow model employed is first described, with a specific treatment of basal motion. Model setup and the calibration process with the present-day ice cap are then outlined. Finally, the climatic forcing used to model the ice cap since the Little Ice Age is described.

4.1 The Ice Sheet System model

The Ice Sheet System Model (ISSM) is a thermomechanical, finite element ice flow model developed at NASA Jet Propulsion Laboratory and University of California Irvine. ISSM is primarily developed for high-resolution, higher-order modelling of ice sheets using a parallel software architecture. There are many capabilities and modules in ISSM; only those relevant for this thesis are detailed here. For a complete description, including a more comprehensive section about model numerics and software architecture, see Larour et al (2012) and the ISSM website, http://issm.jpl.nasa.gov.

4.1.1 Ice flow approximation

Several approximations for ice flow can be used in ISSM. These include the Shallow Ice Approximation (SIA; Hutter 1983), Shallow Shelf Approximation (SSA; MacAyeal 1989), Higher-Order (HO; Blatter 1995; Pattyn 2003) and Full-Stokes (FS; Stokes 1845). These approximations are dealt with in more detail in Sect 2.1.5. A short discussion of the applicability of the SIA for Hardangerjøkulen is included here.

The SIA option in ISSM includes (i) a 2D depth-integrated version, meaning horizontal velocities correspond to averaged velocities over the ice column; (ii) a 3D option where velocities are allowed to vary with depth. For computational efficiency, and comparison with a previous modelling study (Giesen 2009), the 2D depth-averaged SIA is used throughout this thesis. The use of 3D SIA and higher-order modelling is a priority for future work.

The assumption of shallow ice become increasingly inaccurate when moving away from the flat interior of Hardangerjøkulen. Stress balances on outlet glaciers will not be completely local, as required by the SIA. Where bed and surface topography is less smooth, lateral drag against valley walls and longitudinal stresses will also be important. However, the SIA has proved accurate in representing glacier volume fluctuations on decadal and longer timescales (Leysinger-Vieli and Gudmundsson 2004), which is the prime concern of this study. They found no significant differences in advance and retreat rates for an alpine glacier when they compared a SIA-model with a model which included the full Stokes equations for the velocity and stress fields. They therefore argued that, at least in absence of large basal motion, studies focusing on ice volume variations and large scale geometry changes in response to climate forcing could use SIA-models without loss

of accuracy. Hardangerjøkulen has relatively gentle surface slopes and lacks areas of very fast flow. The SIA is therefore a viable option when studying this ice cap on climatic time scales. Similar studies on ice caps from Iceland (Gumundsson et al. 2009; Adalgeirsdóttir et al. 2011), Hardangerjøkulen (Giesen 2009; Giesen and Oerlemans 2010) and the French Alps (Le Meur et al. 2007) also indicate that ice-flow models employing the SIA on alpine glaciers and small ice caps on climatic timescales can be used with satisfactory results. Last but not least, because of its simplicity, SIA is very computationally efficient (Rutt et al. 2009). This enables modelling of ice cap evolution over long time scales (e.g. Abe-Ouchi et al. 2007; Flowers et al. 2008), without much computational time spent.

4.1.2 Ice deformation and sliding

Based on the Shallow Ice Approximation, we use Eq. (2.34) in Sect. 2.1.5 to calculate ice deformational velocities. Since Hardangerjøkulen is assumed entirely temperate (Sect. 3.3.1), the flow parameter is set to $A = 2.4 \times 10^{-24}$, as recommended for temperate glaciers by Cuffey and Paterson (2010), p.75 (Sect. 2.1.2).

Basal sliding introduces some challenges. The amount of basal slip requires a sliding relation (or "law"), usually relating the basal shear stress τ to the basal sliding velocity u_b (Fowler 2011, p.619). Models should ideally use a physically based sliding law, coupled to hydrologic conditions (Fleurian et al. 2014), commonly with the effective pressure N as a key variable. However, such models are rare due to both a lack of physical understanding of the subglacial environment, as well as the difficulty in modelling and coupling the hydrology with ice flow models through a sliding law in a feasible way. Because of these complexities, most ice flow models have used an *ad hoc* sliding relation, which has worked well for larger spatial scales at climatic timescales. The capabilities to simulate subglacial hydrology and couple this with the ice mechanic model in ISSM are under development and was not finished at the time of the experiments carried out in this thesis.

Several previous workers (e.g. Ritz et al. 1996; Payne et al. 2000; Rutt et al. 2009) employing the SIA use a sliding formulation where basal velocities are a function of the basal shear stress, which for the SIA is equivalent to setting basal velocities proportional to the driving stress:

$$u_b = -C\rho_i g H \nabla s, \tag{4.1}$$

where C is a (tuning) basal sliding parameter, which can be set spatially and temporally constant, or as a function of temperature, basal water depth, basal water pressure, bed roughness or other factors. The sliding velocity u_b is then simply added to the deformational velocity u_d, so that total surface velocity u becomes

$$u = u_d + u_b \tag{4.2}$$

In this study, the basal sliding parameter C is assumed inversely proportional to

elevation in a linear fashion:

$$C = C(z) = -az + b, \tag{4.3}$$

where a is the decrease in the sliding parameter with elevation and b is the intercept of this linear equation.

Many previous studies (e.g. Payne 1995; Ritz et al. 1996; Payne 1999; Payne et al. 2000; Giesen 2009; Le Brocq et al. 2009; Adalgeirsdóttir et al. 2011; Clason et al. 2014; Laumann and Nesje 2014) employing the Shallow Ice Approximation have used a spatially and temporally fixed sliding parameter in a Weertman-type sliding law. The above studies use slightly different variations of the Weertman sliding law, so a direct comparison of parameter values is not straightforward. Payne (1995) used a uniform sliding parameter of $5\times\ 10^{-3}$ myr^{-1} Pa^{-1}, whereas in the EISMINT comparison (Payne et al. 2000), a uniform $1\times\ 10^{-3}$ m yr^{-1} Pa^{-1} was used, albeit without giving a thorough reasoning behind chosen values.

LeBrocq et al. (2009) used a subglacial water-flow model for West Antarctica together with the Glimmer ice flow model (Rutt et al. 2009), using the same formulation for basal velocities, $u_b = C\rho g H \nabla s$ as in the current study. They found that the sliding parameter C varied over five orders of magnitude in response to available water, with C ranging from 1×10^{-5} to 1×10^{-1}. Of course, West Antarctica contains ice streams and velocities vary from 0 to 1000 myr^{-1}, in contrast to the maximum velocities for outlet glaciers of Hardangerjøkulen, measured to 5-50 myr^{-1}. In the present study, the sliding parameter C varies spatially from $\sim 3.5 \times 10^{-4}$ myr^{-1}Pa^{-1} at higher elevations to $\sim 5 \times 10^{-5}$ at 1000 m.a.s.l. (Fig. 4.1), where Rembesdalskåka is terminating.

Values used in this study are thus in the lower ranges of what LeBrocq et al. (2009) suggested, corresponding to areas away from ice streams in their experiments. Compared to what used by Payne (1995) and Payne et al. (2000) used to model ice sheets, the Hardangerjøkulen values are 1-2 orders of magnitude lower.

The goal of this parameterization is to capture the effect of meltwater production (implicitly, ablation) on the surface. Basal velocities are of course already explicitly a function of surface gradient and ice thickness as of Eq. (4.1).

4.1.3 Mass transport

For the vertically-integrated ice flow model used in this study, ISSM solves the two-dimensional continuity equation, derived in Sect. (2.1.4):

$$\frac{\partial H}{\partial t} = -\nabla \cdot (\overline{u} H) + \dot{M} - \dot{S} \tag{4.4}$$

where $\overline{u}$ is the vertically averaged ice velocity, $\dot{M}$ is the surface mass balance rate. The basal melt rate is assumed negligible (Sect. 2.1.4).

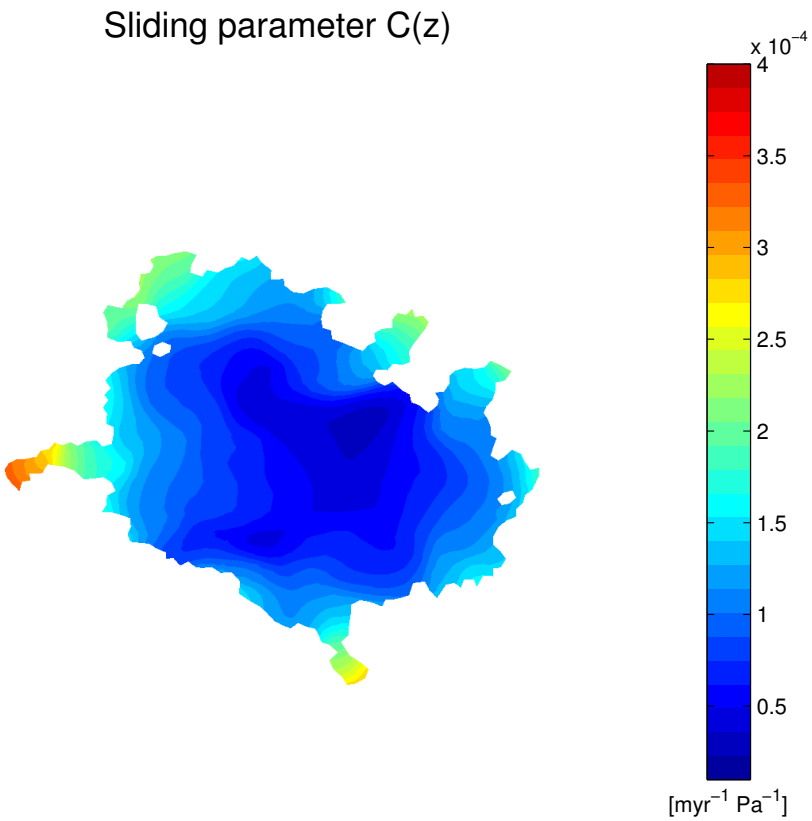

Figure 4.1: Spatial distribution of sliding parameter $C(z)$ used in this study. Basal velocities u_b are parameterized as $u_b = C(z)\rho g H \nabla s$, where $C(z)$ is inversely proportional to elevation in a linear fashion.

4.1.4 Mesh and time stepping

The area where model equations are solved is called the model *domain*, here a square including Hardangerjøkulen and surrounding areas. In order to solve these equations, the domain is broken down into smaller discrete segments. The most common numerical method for ice models is finite-differences, where the model domain is divided into a grid consisting of equally sized, rectangular grid cells. The values of neighbouring grid points and the distance to the grid point of interest are used to approximate gradients (derivatives) in parameter values (Hooke 2005). There are various techniques to numerically solve the associated differential equations. Details of such methods can be found in any textbook on numerical solutions of partial differential equations (e.g. Lapidus and Pinder 2011) and are not covered here.

In contrast, ISSM use the *finite-element* method to (numerically) approximate solutions for stresses, strain rates, mass transport or other physical quantities of interest. Instead of dividing the model domain into rectangles of the same size, values of functions are defined at the corners (called nodes or vertices) of triangular elements (Fischer et al. 2013). Inside elements, the value is interpolated based on values at neighbouring vertices. Analogous to the grid of finite-differences, the elements covering the domain is called a *mesh*. The finite-element method is covered in depth in many textbooks, e.g. Dhatt et al. 2012.

A main advantage of finite-elements is the ability to handle irregular geometries. While rectangular elements work well in areas of little change, the finite element mesh enables representation of complex geometries. ISSM includes adaptive mesh refinement capabilities (Larour et al. 2012), meaning that mesh resolution can be increased in regions of interest, and kept lower elsewhere where appropriate. Such meshes are called *anisotropic*, and make it possible to resolve smaller-scale processes while maintaining a relatively low computational cost. The mesh can be adjusted to a metric of the user's choice, for example ice thickness, ice/no ice, surface slope or observed velocities. Alternatively, the mesh can be adapted in a specific area, e.g. within a polygon defined by the user. At the time of writing, this mesh used in ISSM is fixed in time. This means that once the mesh is constructed, it will not adapt to ice cap evolution. Consequently, the mesh has to be defined so that it suits the present-day ice cap, as well as any anticipated changes in geometry when letting the ice cap grow or shrink in time.

ISSM uses a finite difference scheme in time, meaning model equations are solved at times with equal spacing. The model time step should be chosen short enough to ensure convergence when solving partial differential equations numerically, while maintaining a reasonable computational time. This is often expressed by the Courant-Friedrichs-Lewy (CFL) condition, which in an one-dimensional case is given by

$$\frac{u \cdot \Delta t}{\Delta x} \leq C \tag{4.5}$$

where u is the velocity, Δt the time step and Δx the length interval. C depends on the particular equation to be solved and not on Δt and Δx.

In practice, this means that an increased spatial resolution (a smaller Δx) requires a shorter time step Δt for the CFL condition to be fulfilled. A simultaneous consideration

of spatial and temporal model resolution is therefore needed. Here, a time step of 0.1 years was found low enough to avoid numerical instabilities. An anisotropic mesh was constructed based on a simple ice/no ice criterion corresponding to the present-day ice cap extent. A buffer zone around the ice cap is included to capture glacier advances at a higher resolution. For the ice cap, a 200 m resolution was used, while in the rest of the square model domain, the mesh is kept at 300 m. This results in a mesh of 5422 mesh vertices distributed over 10602 elements. The model used in this thesis is two-dimensional, but it is possible to make use of a 3D model in ISSM by simply extruding the mesh in the vertical, with any number of vertical layers. These can also be refined with depth, so that ice close to the bed are modelled at a higher resolution, where higher gradients of vertical shear exist.

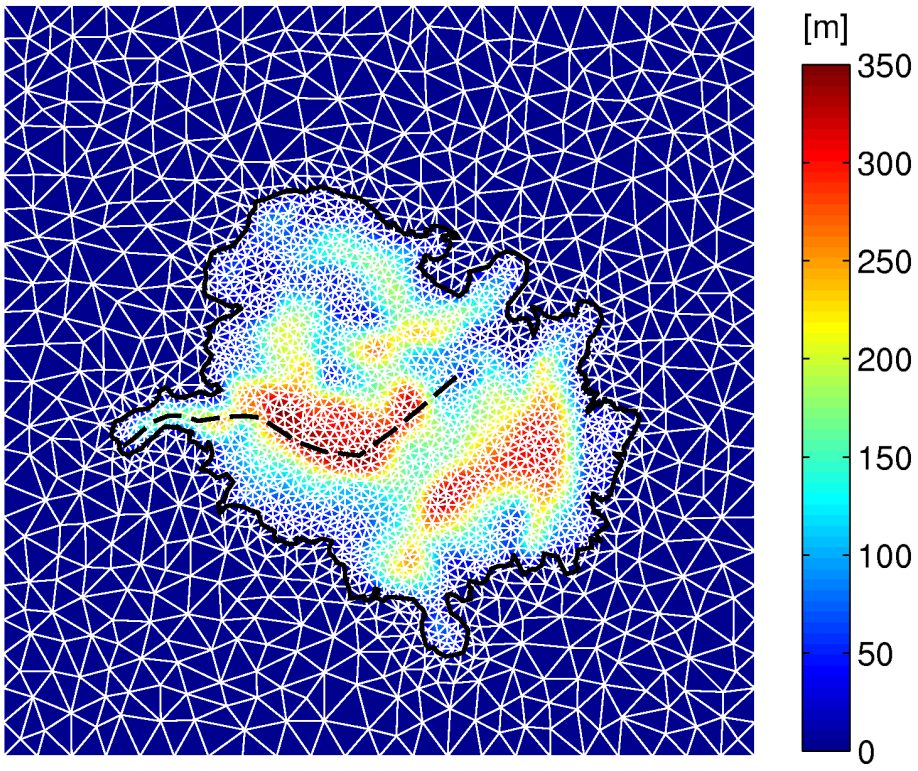

Figure 4.2: Ice thickness in 1995 with an example mesh overlay used in ISSM. Outline in 1995 and the flowline of the outlet glacier Rembesdalskåka are also shown. Mesh refinement is done according to an ice/no ice criterion, including a buffer zone around the ice cap to capture advances at higher resolution. To illustrate this concept, a 200 m/800 m mesh resolution is shown here, while a 200 m/300 m mesh was used in the actual model runs.

4.2 Model setup and calibration

In short, the methodology used in this study is as follows.
(1) Calibration runs to reproduce present-day ice cap forced with zero mass balance, with the aim of tuning the basal sliding parameter.
(2) Force the calibrated model from (1) with a positive mass balance anomaly to steady state, so that outlet glaciers fronts are in between present-day and their LIA-maximum positions.
(3) Use the steady-state geometry obtained in (2) as initial geometry for a historic run starting in AD 1600.
(4) Force the ice flow model with a mass balance history from AD 1600 until present. Until direct mass balance measurements begin in 1963, this mass balance history is optimized by matching modelled outlet glacier lengths to observed lengths.

We now describe steps (1)-(4) in more detail.

4.2.1 Sliding and ice rheology

To optimize the sliding parameter C, a trial-and-error method was used, with the main aim of reproducing the surface topography of Rembesdalskåka along its flowline. Midtdalsbreen could also have been used, but Rembesdalskåka was chosen since mass balance measurements and the resulting average mass balance gradient used in this study come from this glacier. First, different spatially constant values of C were tried. The model was forced with a zero mass-balance until a steady-state was reached. Since this sliding formulation was unsuccessful (Sect. 5.2.2) in reproducing present-day topography, a spatially variable sliding parameter C was employed, as described above in Sect. 4.1.2.

Optimal values for a and b in the sliding formulation $u_b = C(z)\rho g H \nabla s$, where $C(z) = -az + b$, were then found. The calibrated elevation dependency were constructed by first trying different values for the sliding parameter C close to the summit at 1850 m a.s.l., with a fixed gradient a. When a closer fit between modelled and observed surface was obtained, the intercept value b at 1850 m a.s.l. was fixed, and different gradients were tried from there, until an good fit between model and observed surface was obtained.

The ice stiffness parameter A for temperate ice in Glen's flow law was chosen as recommended by Cuffey and Paterson (2010), p.75. A comparison using the lower (softer) value recommended A by Paterson (1994) was also carried out (Sect. 5.2.3).

4.2.2 Mass balance

A mean reference mass balance gradient B_{ref} is derived from observed specific mass balance gradients, which exist for 35 of the 45 years spanning 1963-2008 (Sect. 3.2.3; Fig. 4.3). Mass balance $B(z,t)$ for any point in time are then imposed by shifting B_{ref} equally for all elevations by a mass balance anomaly $\Delta B(t)$:

$$B(z,t) = B_{ref}(z) + \Delta B(t) \tag{4.6}$$

B_{ref} should represent zero mass balance for the present-day surface topography. The measured mean net balance gradient for Rembesdalskåka was -0.175 m w.e., and B_{ref} is therefore the result of a shift of the mean observed gradient by this value (Oerlemans 1997; Giesen 2009).

A mass balance-altitude feedback is included in the model, by letting the mass balance $B(z,t)$ at a specific point to be recalculated for each time step according to the updated surface elevation.

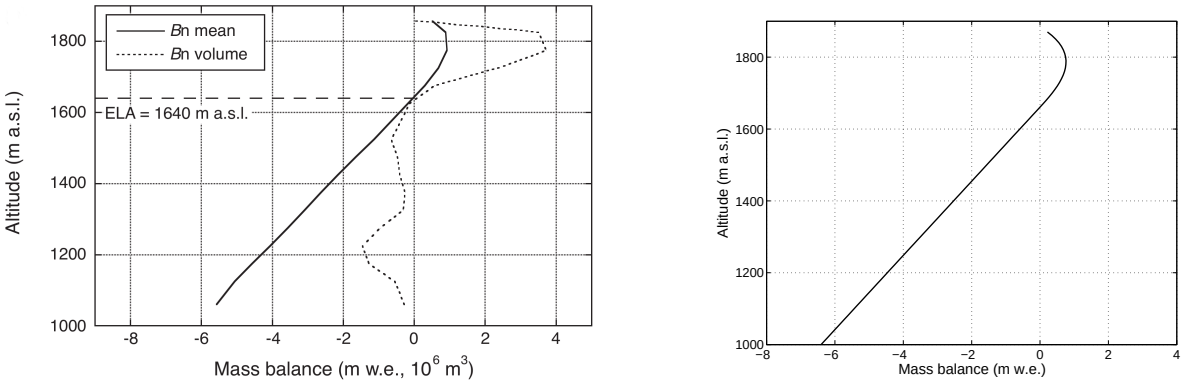

(a) (b)

Figure 4.3: (a) Observed mean net (B_n) specific and volume mass balance for 35 years between 1963-2008. Figure from Giesen (2009). Data from NVE. (b) Mean net mass balance profile used in the model runs, based on the net specific profile in (a). In the lower part, a linear gradient is imposed; for the highest elevations, a third-order polynomial is fitted to the observed values. Data from NVE.

4.2.3 Dynamic calibration

Since the mass balance record from Rembesdalskåka extends back to 1963, mass balance has to be reconstructed prior to this. For this purpose, an optimal mass balance history is found from before AD 1600 (before the LIA max) until 1963, using a dynamic calibration (Oerlemans 1997; Oerlemans 2001). This approach is based on matching the model against the moraine evidence and length records of the outlet glaciers Midtdalsbreen and Rembesdalskåka, while adjusting $\Delta B(t)$ accordingly. As a starting point, the mass balance histories obtained for Nigardsbreen (Oerlemans 1997) and Hardangerjøkulen (Giesen 2009) are used. These are then modified to match the outlet glacier length records. As a further constraint, modelled ice cap extents are compared with known past extents from old maps and aerial photographs from the 1900s. Additionally, observed surface topography (DEM) from 1995 are compared with the modelled surface. It is also possible to adjust the sliding parameter C during this process, since basal velocities may change with changes in surface melt, subglacial hydrology, basal roughness and perhaps other factors (Sect. 4.1.2). However for simplicity, the calibrated sliding parameter $C(z) = -az + b$ is kept to what is obtained from the reproduction of the present-day

surface topography.

Moraine evidence shows that outlet glaciers advanced to their maximum extent around AD 1750. As long as this LIA-maximum extent is matched, the initial topography is not important for the post-LIA front positions. Model runs therefore start from a steady-state ice cap at AD 1600, in between the present-day ice cap margin and the LIA-maximum moraines, corresponding to a mass balance anomaly by $\Delta B = +0.4$ m w.e. We then impose a LIA mass balance anomaly for a few decades in the late 17th and the early 18th centuries so that modelled and moraine derived lengths of Rembesdalskåka and Midtdalsbreen in AD 1750 agree reasonably well. The maximum for Midtdalsbreen was matched first since this is where the LIA-moraine has been dated to AD 1750.

5 Results

This chapter presents the main results from this thesis. In line with the main aim of this thesis, results regarding ice volume and outlet glacier variations are shown first. In the second half of this chapter, sensitivities to mass balance, sliding formulation and ice rheology are outlined. We show that the ice cap response to mass balance changes is non-linear, that a spatially variable sliding parameter is necessary and that the sensitivity to the choice of ice stiffness in the model is low.

5.1 Hardangerjøkulen since the Little Ice Age

We have investigated the climatic and glaciological responses of Hardangerjøkulen using a two-dimensional ice flow model, forced by a mass balance history found by comparing modelled and observed outlet glacier variations since the LIA. The optimized mass balance forcing (Fig. 5.1a) is applied to a steady-state ice cap from AD 1600, starting with a mass balance anomaly relative to the reference mass balance profile (Sect. 4.2.2) of +0.4 m w.e. An anomaly of +1.7 m w.e. is imposed from AD 1690-1720 to reproduce the LIA extents of the outlet glaciers Midtdalsbreen and Rembesdalskåka around AD 1750.

The historic runs all use a spatially variable sliding parameter, fixed in time according to present-day elevation, unless stated otherwise. A mass balance-altitude feedback (Sect. 2.2.2) is included in all experiments, and the mass balance gradient maximum is kept fixed at according to the reference profile derived for 1963-2005 (Sect. 4.2.2).

The resulting mean velocities of the ice cap (Fig. 5.1b) are rather stable between $\sim$12-18 myr^{-1}, with a slight increase during the LIA maximum. Since the ice motion is very small on the high plateau, the mean velocity is not very meaningful. Looking at the maximum velocity instead, occurring in the ice fall of Rembesdalskåka, we see a velocity decrease from the LIA maximum at $\sim$120 myr^{-1} to a present-day flow of $\sim$85 myr^{-1}, a drop of about 30 %. While this is a considerable change, we should be cautious when interpreting velocities derived from SIA models, since they have been shown inaccurate in representing small-scale dynamics (Sect. 6.1.2). The LIA maximum ice volume is modelled to 21 km^3 (Fig. 5.1c), a result hard to validate since we do not know the surface topography at this time, in addition to uncertainties in the ice cap extent. Until the present-day, Hardangerjøkulen is simulated to have lost roughly half of its volume in 1750. For the known ice volumes in 1961 and 1995, the model overestimates volume by $\sim$10 %, mainly due to too thick ice over the eastern ice cap.

The mass balance forcing used in Fig. 5.1a is found according to observed variations of the outlet glaciers Midtdalsbreen (NE) and Rembesdalskåka (SW). For the LIA maximum, we find it not possible to match both outlet glaciers simultaneously. Midtdalsbreen was chosen since the LIA maximum glacier extent has been dated to AD 1750 here, while no dates exist for Rembesdalskåka. When the model is matched to the Midtdalsbreen, the LIA maximum length agree well with moraine evidence, whereas Rembesdalskåka is too short (Fig. 5.2). Conversely, if the mass balance anomaly is

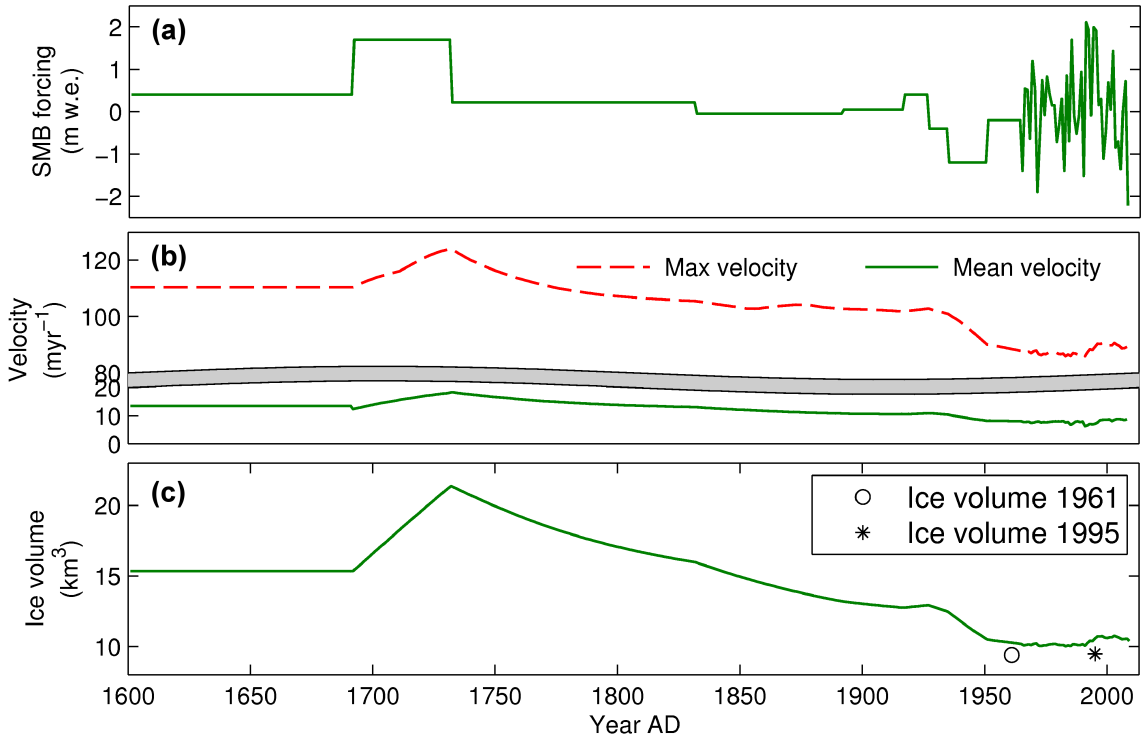

Figure 5.1: Modelled evolution of Hardangerjøkulen since the LIA. (a) Mass balance forcing; (b) Max and mean velocities (c) ice volume response. Note the break in the y-axis in (b).

changed to match Rembesdalskåka, Midtdalsbreen advances too far (not shown here).

The underestimation of Rembesdalskåka from the LIA maximum carries along to the early 1900s, where the glacier length is underestimated by ∼700 m (Fig. 5.4a). For this period, also Midtdalsbreen is too short (Fig. 5.4b), but the difference is only slightly larger than the spatial resolution of the model (200 m). After 1960, the differences between modelled and observed lengths are small and within the size of one mesh element in the model. Modelled surface profiles along the flowlines of Rembesdalskåka and Midtdalsbreen for selected years along with observed front positions are summarized in Fig. 5.3.

When we examine the fronts of Rembesdalskåka and Midtdalsbreen from a planview perspective (Fig. 5.4), we see that while the LIA length of Midtdalsbreen is well represented, the narrow ice-free corridor between Midtdalsbreen and Blåisen suggested from geomorpholocical evidence (Andersen and Sollid 1971; Sollid and Bjørkenes 1978) is missing. This improves for the 1900s, when a prominent nunatak separates the two outlet glaciers both in the model and reality. In general, the observed margins of the ablation zones of all the three outlet glaciers shown in Fig. 5.4 are very well reproduced after 1960. Discrepancies are generally similar to the model resolution.

If we assess the entire ice cap through time, we find that the margins at the LIA maximum in AD 1750 is generally well represented in the model (Fig. 5.5a), especially given the spatial and temporal uncertainty in the actual ice cap extent. Although the

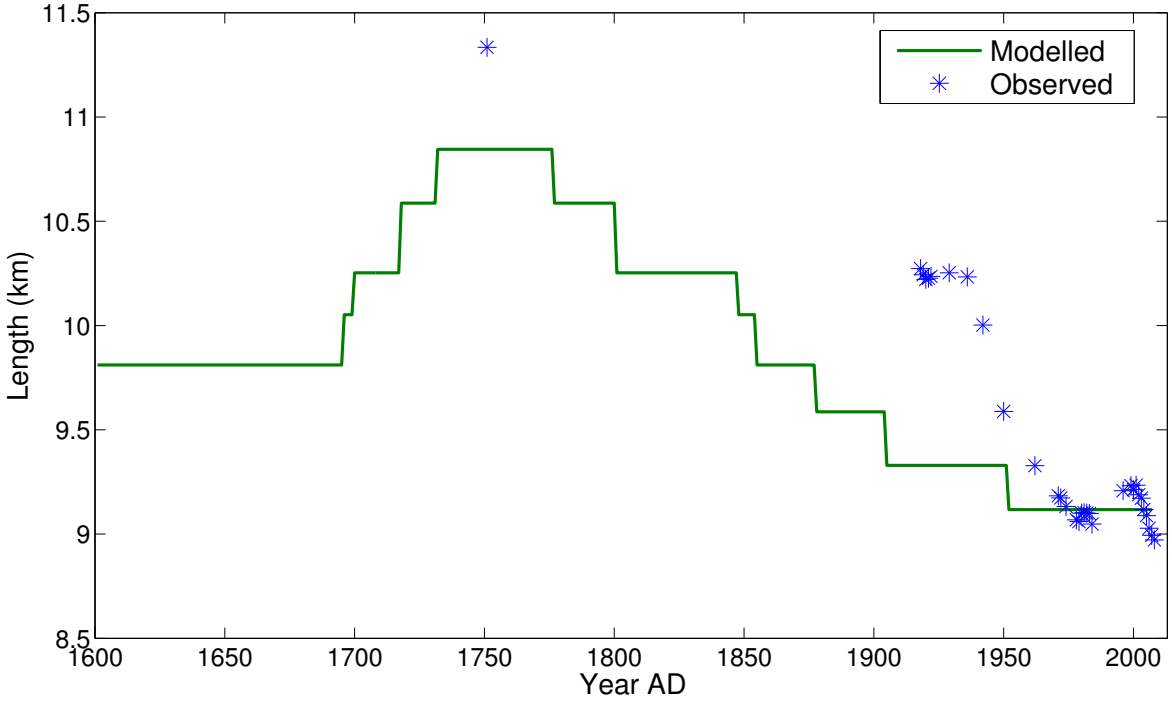

(a)

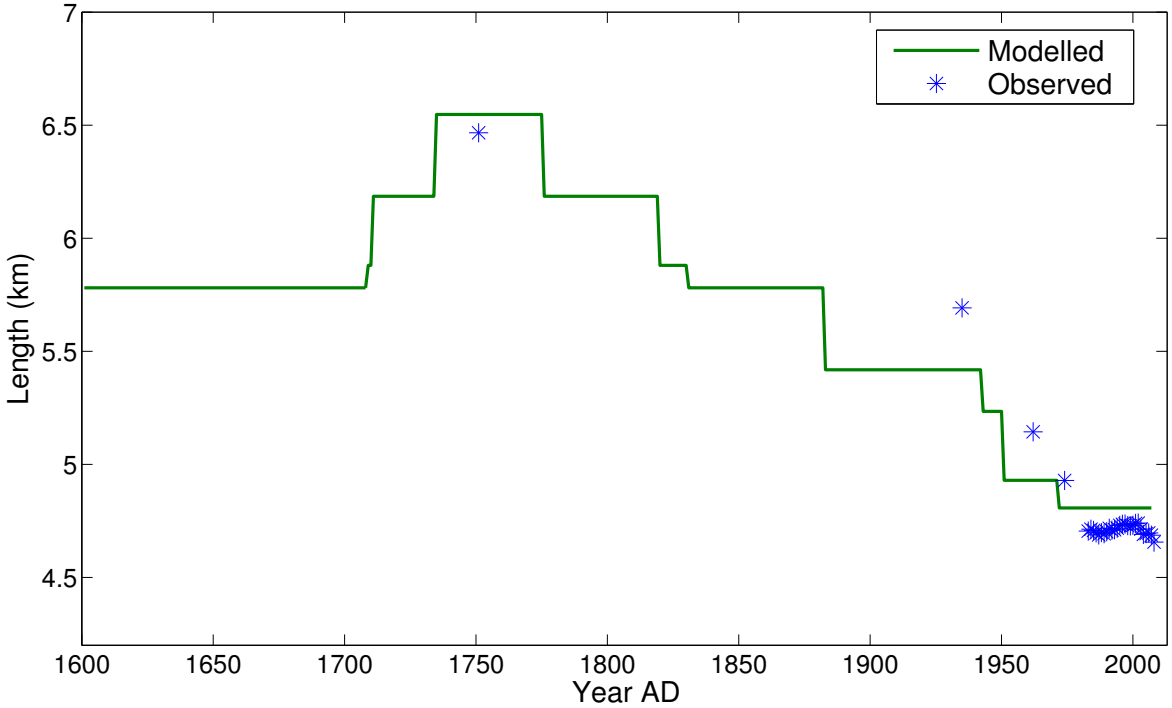

(b)

Figure 5.2: Modelled and observed length of the outlet glaciers (a) Rembesdalskåka and (b) Midtdalsbreen.

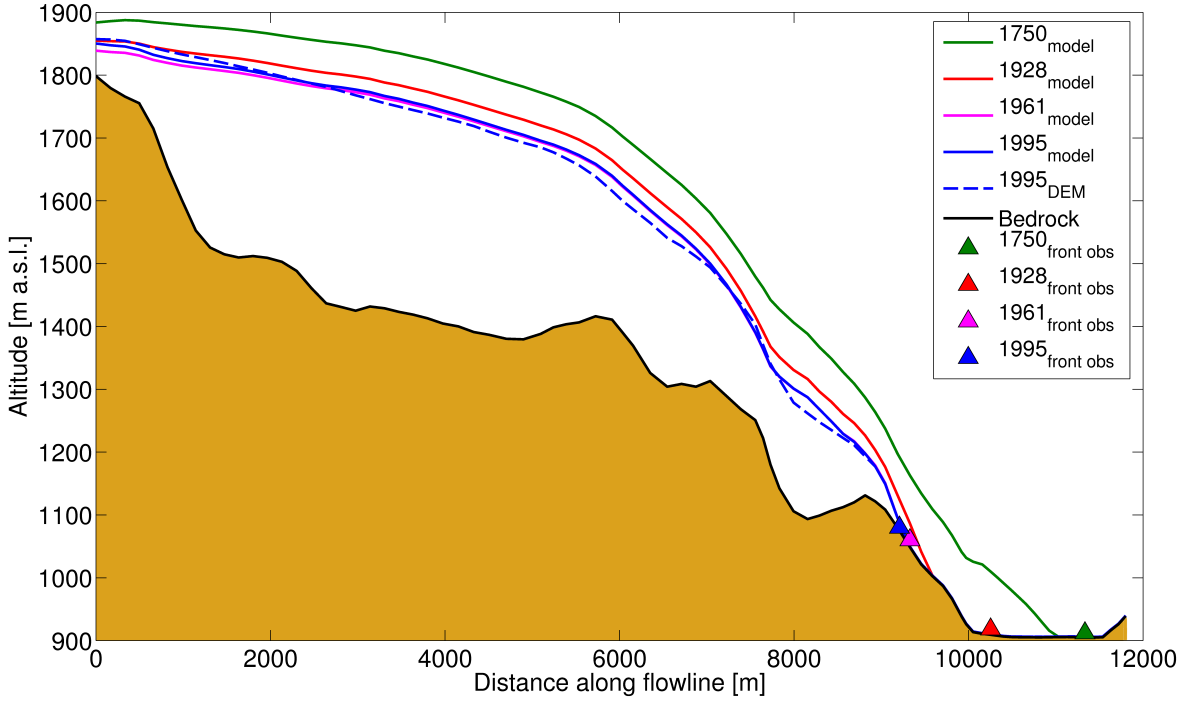

(a)

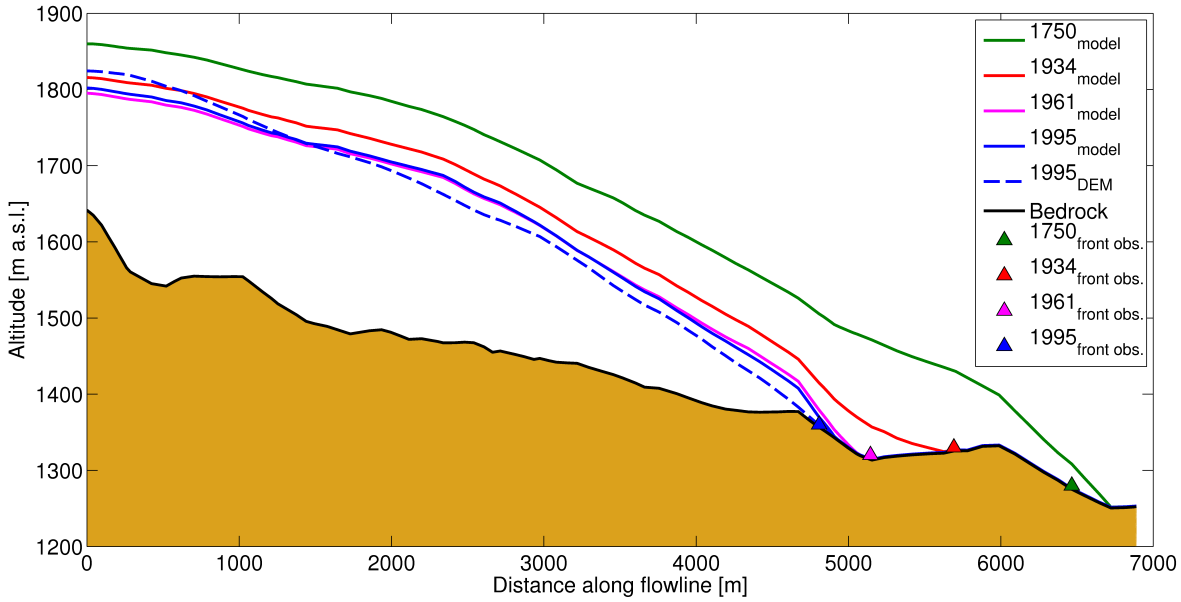

(b)

Figure 5.3: Modelled surface profiles along the flowlines of (a) Rembesdalskåka (b) Midtdalsbreen for selected years. Observed front positions from corresponding years are also shown. Note that the vertical scale are exaggerated compared to the horizontal, and that the horizontal scale for in (a) is smaller than in (b).

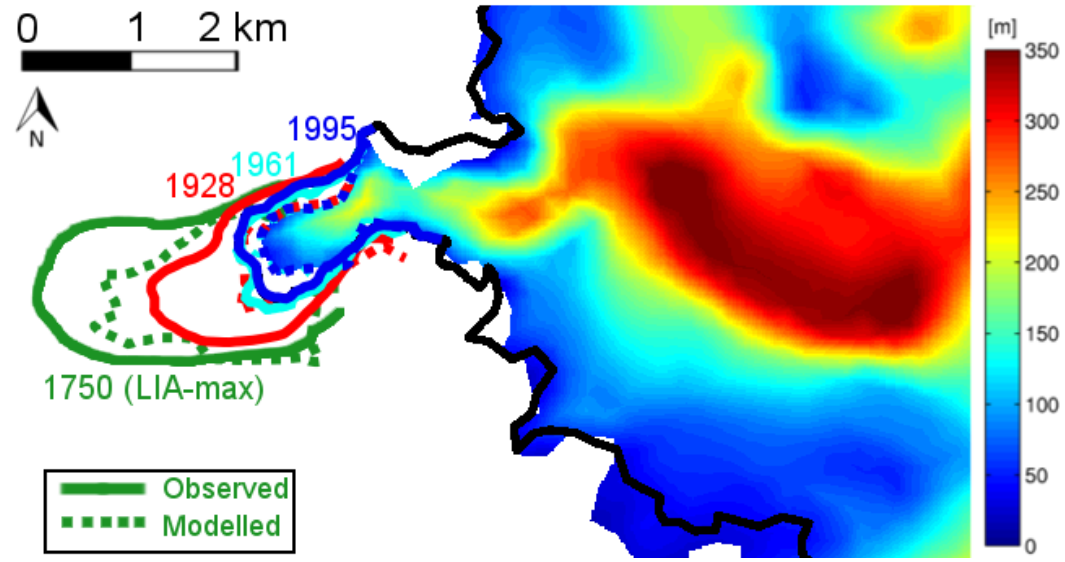

(a)

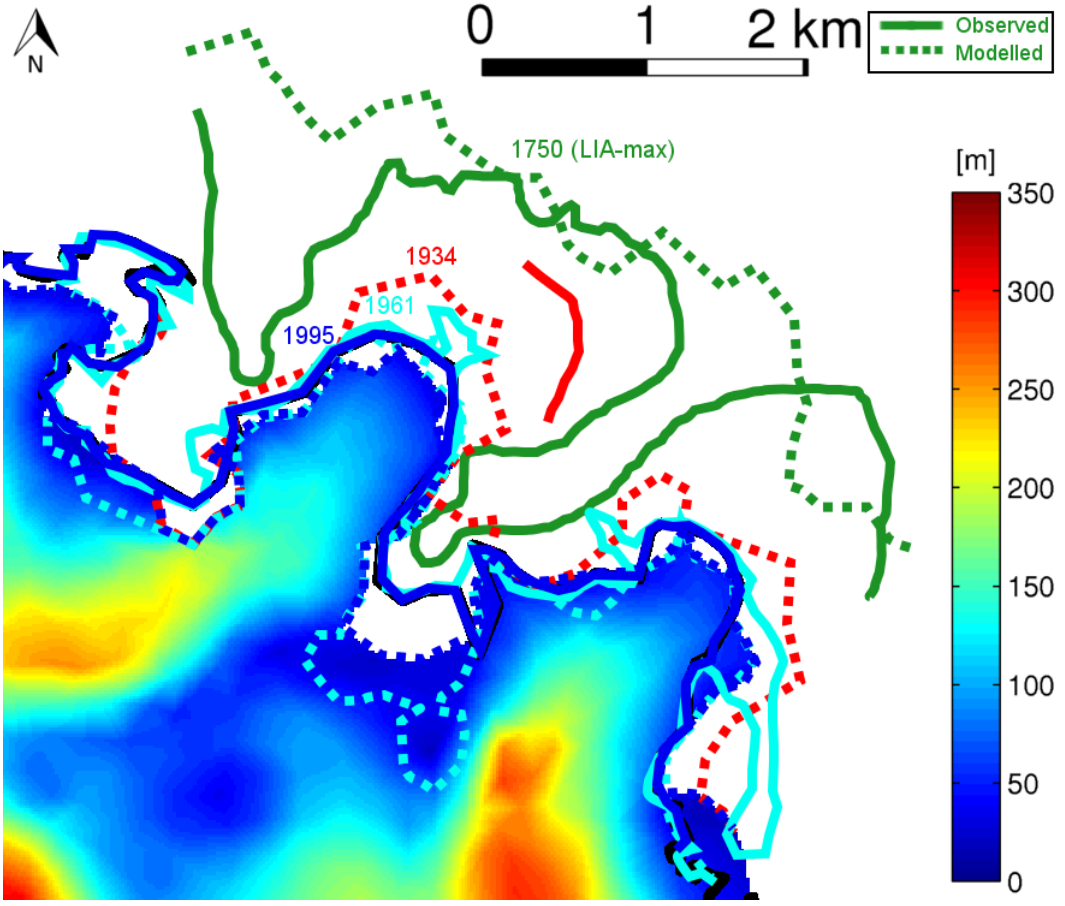

(b)

Figure 5.4: Observed and modelled fronts of (a) Rembesdalskåka and (b) Midtdalsbreen, Blåisen outlet glaciers. Modelled ice thickness in 1995 (colourbar) and observed ice cap extent are also shown (black).

outlet glaciers around 1930 are too short (Fig. 5.5b), the ice cap margin for the second half of the twentieth century is reproduced with a very high degree of detail (Fig. 5.5cd). One exception is the too small northwestern ice cap, however ice thickness in the missing area is small (< 50 m), so this mismatch contributes very little in terms of total ice volume.

By comparing the modelled surface topography by a DEM from 1995, we can assess model performance not only in terms of ice extent but also of ice cap shape (Fig. 5.6). In general, the flat plateau is best represented, while steeper marginal areas are overestimated. The modelled surface correspond to a high degree (± 20 m) to the observed topography for the interior part of the ice cap. In contrast, the steeper outlet glacier topographies are slightly overestimated ($\sim$50 m), while the model overestimates ice thickness along the eastern margin considerably ($\sim$50-80 m). The model also have problems with the steep areas just north of the ablation zone of Rembesdalskåka. Perhaps surprising is that the model surface in the ice fall of Rembesdalskåka is well represented.

Andreassen and Elvehøy (2001) computed surface elevation changes between two DEMs from 1961 and 1995 (Fig. 5.7a). Notably, they found ice thickening of 5-15 m over the majority of Rembesdalskåka and parts of Blåisen. The largest surface thinning occurred in the northwestern drainage basin ($\sim$10-55 m), as well as along the southern margin, west of the outlet glacier Vestre Leirbotnskåka. Comparing their results to the modelled elevation changes (Fig. 5.7b), the significant mass loss in the northwest is a common feature. The spatial variability of ice thickening over the plateau is however not reproduced by the model, even though the magnitudes of elevation change are approximately correct. Moreover, the slight observed surface lowering in the lower ablation zone of Midtdalsbreen is also captured in the model.

Using the mass balance forcing in Fig. 5.1a, modelled velocities over the entire ice cap through time (Fig. 5.8) reveal that outlet glaciers have faster ice flow than the plateau. Lower Rembesdalskåka is the most active area ($\sim$100 myr^{-1} at LIA maximum), while the other outlet glaciers have LIA speeds around 30-60 myr^{-1}.

The velocity field in 1750 and 1995 show further details, since vectors indicate both magnitude and direction of flow (Fig. 5.9). We see that the interior is moving very slowly (< 10 myr^{-1} for the LIA) and that the northwestern large drainage basin (10 km^2) is a relatively undynamic area. We can also identify different drainage basins based on the flow directions, with Rembesdalskåka (SW), Vestre Leirbotnskåka (SE), Midtdalsreen (NE) and Blåisen (NE) visible. Flow was apparently more confined at several places in 1750 than in 1995. In addition, two outlet glaciers seems to have formed along the southern margin during the LIA, features not observed today.

A comparison between the modelled ice flow at the LIA maximum in AD 1750 and present-day (Fig. 5.10) show that the margins have been slowing down by 10-60 myr^{-1}, whereas the ice cap plateau actually has speeded up, although very modestly (< 5 myr^{-1}). The biggest changes is modelled to have occurred at the terminus of Rembesdalskåka and Vestre- and Austre Leirbotnskåka.

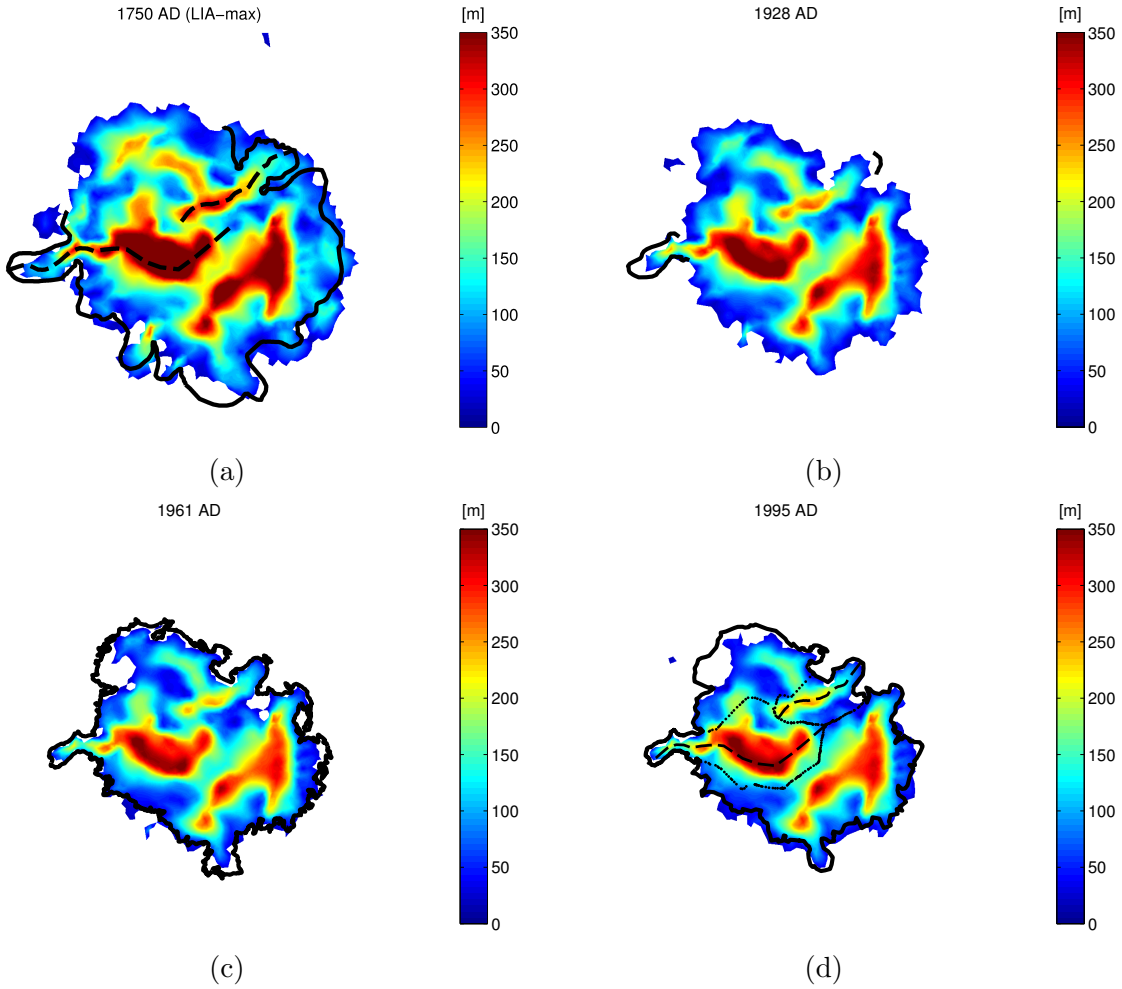

Figure 5.5: Modelled ice thickness of Hardangerjøkulen for (a) 1750; (b) 1928; (c) 1961; (d) 1995. Observed ice cap extents (Andersen and Sollid 1971; Sollid and Bjørkenes 1978; A.Nesje, pers. comm; H. Elvehøy, pers. comm; Cryoclim/NVE) for corresponding years are shown where available. In (a), the actual extent in the north-west is very uncertain and therefore not shown. The most accurate areas are from terminal moraines representing the fronts of Midtdalsbreen and Rembesdalskåka. Dashed flowlines are from 1995, so should be seen as indications rather than the actual flowlines in 1750. In (b), the front of Rembesdalskåka in 1928 and of Midtdalsbreen in 1934 are shown. Drainage basins of Rembesdalskåka and Midtdalsbreen as of 1995 are shown in (d), as well as main dashed flowlines for these outlet glaciers.

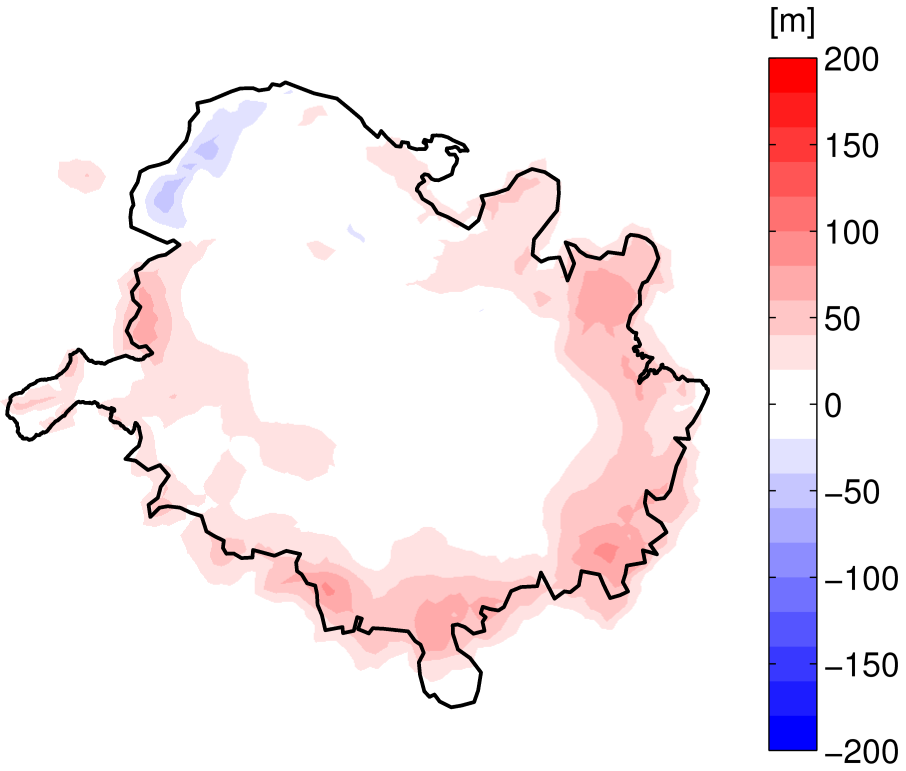

Figure 5.6: Difference between modelled and observed surface in 1995. Positive (negative) values indicate that the model overestimates (underestimates) surface elevation.

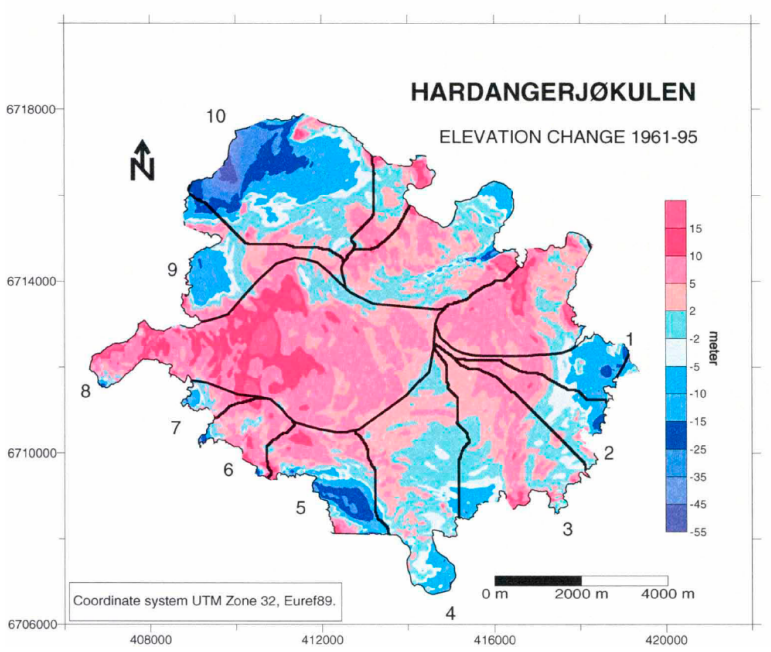

(a)

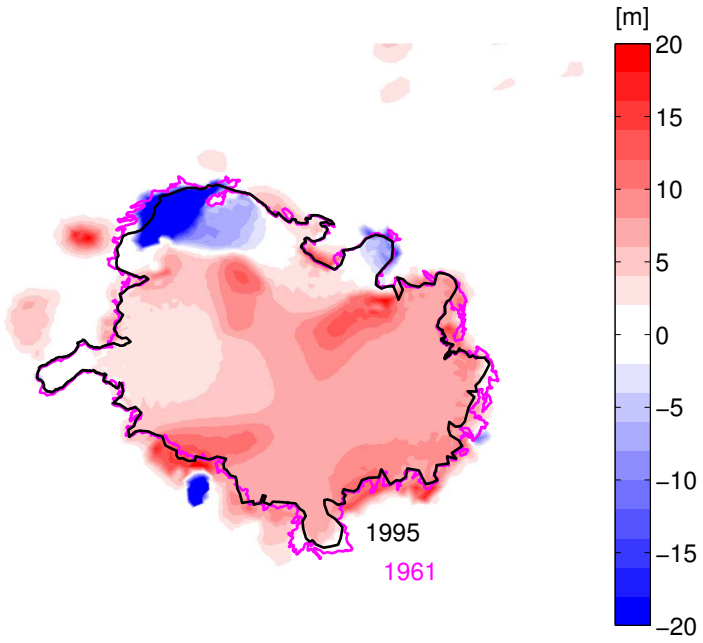

(b)

Figure 5.7: Surface elevation differences between modelled surface topography in 1961 and 1995. (a) Observed surface change from 1961 to 1995 ("Volume change Hardangerjkulen"). Note that their colour scale is asymmetric around zero and that color coding with unequal colorbar steps is used. Positive (negative) values indicate an elevation increase (decrease) from 1961 to 1995. (b) Modelled surface change from 1961 to 1995.

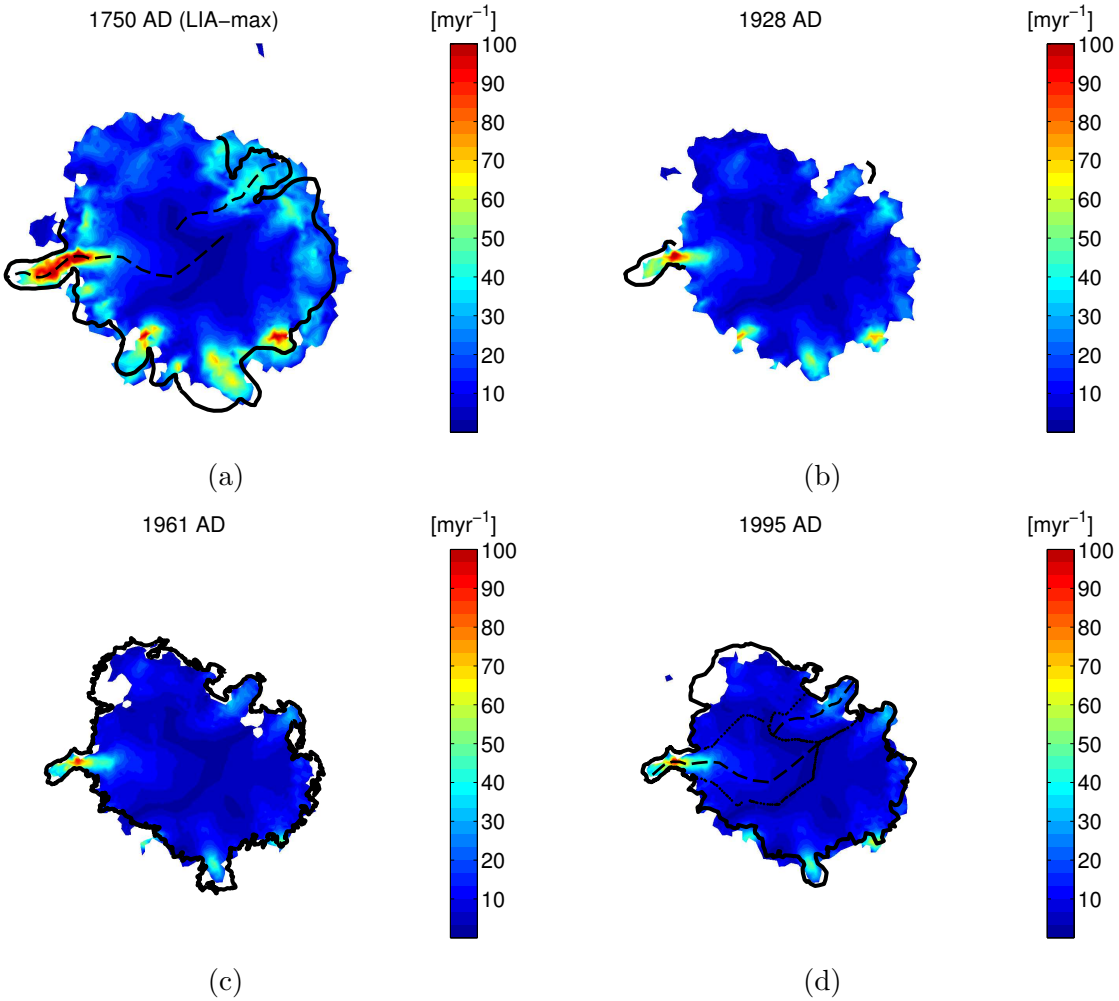

Figure 5.8: Modelled velocities in (a) 1750; (b) 1928; (c) 1961; (d) 1995. Observed ice cap extents for corresponding years are shown where available (details of these are described in Fig. 5.5)

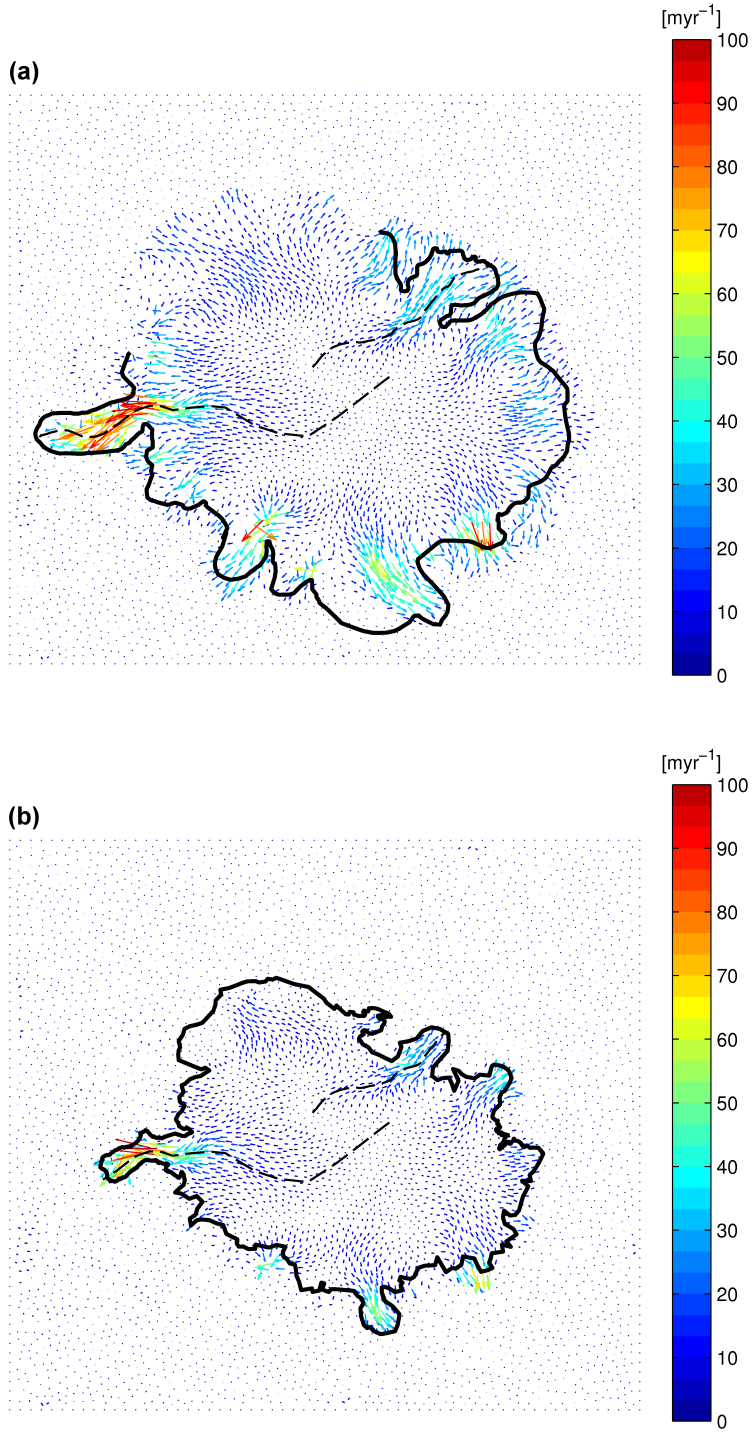

Figure 5.9: Modelled velocity field of Hardangerjøkulen in (a) 1750 and (b) 1995, with respective observed glacier extents. Colour and length of velocity vectors are indicative of depth-integrated velocity magnitude and direction, respectively. Dashed lines represent flowlines of Rembesdalskåka and Midtdalsbreen.

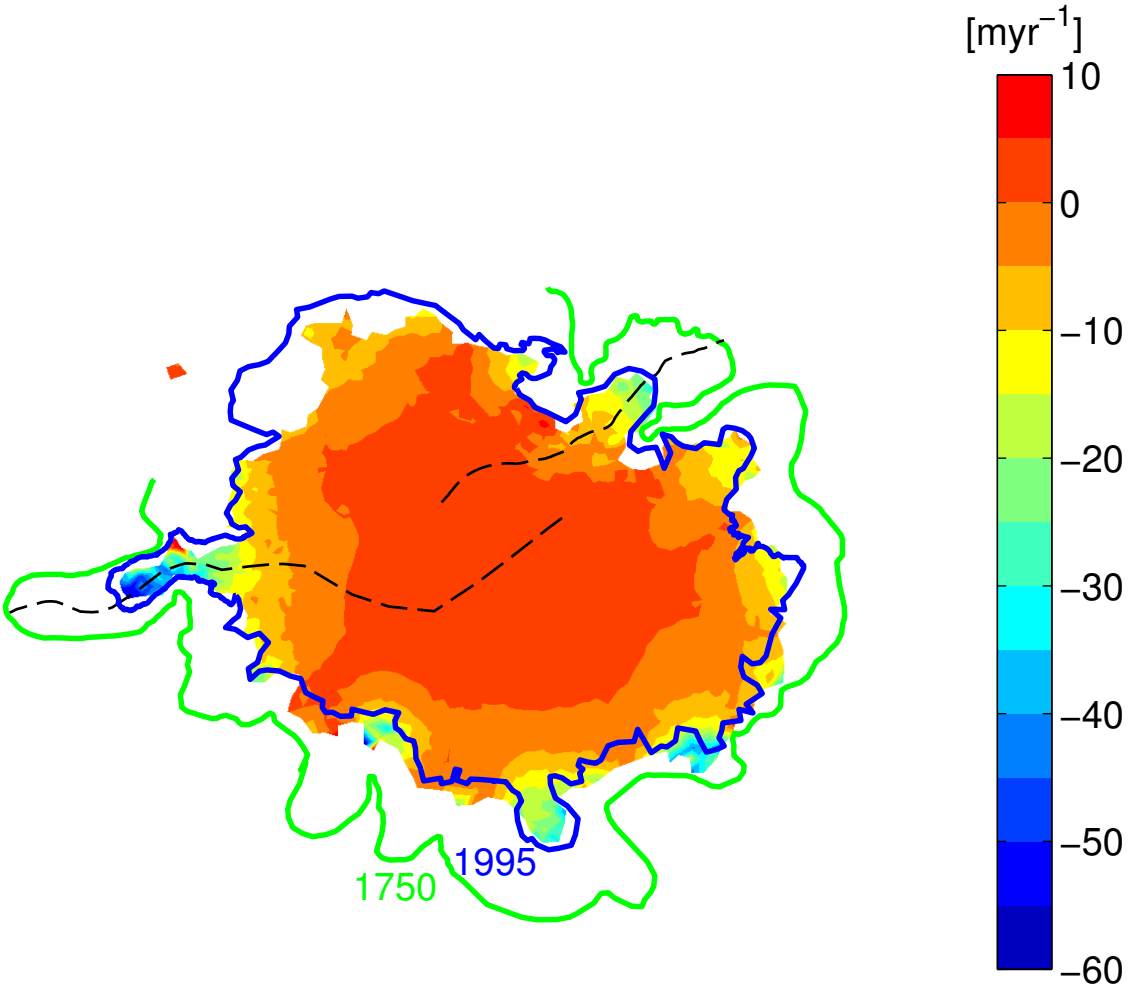

Figure 5.10: Modelled velocity change from 1750 AD (LIA-maximum) to 1995 AD with respective observed glacier extents. Negative (positive) values correspond to a velocity decrease (increase) between 1750 and 1995 AD. Velocity changes are shown for the modelled ice cap extent in 1995 only. Dashed lines represent flowlines of Rembesdalskåka and Midtdalsbreen.

5.2 Sensitivity experiments

5.2.1 A non-linear response to mass balance

To investigate Hardangerjøkulen's sensitivity to changes in mass balance, steady-state experiments were performed with present-day ice cap topography as starting point. The ice flow model was first forced with zero mass balance until an equilibrium state was found. From this state, we impose constant mass balance anomalies between -0.5 and +0.5 m w.e. and run the model to a new equilibrium, to assess ice volume and length responses. These runs were done with a fixed maximum in the mass balance profile. This means that the mass balance profile is shifted equally for all elevations for a given mass balance anomaly, and that the elevation of the maximum in the mass balance reference profile (Sect. 3.2.3) is kept fixed in time. In Sect. 6.2.2 and we discuss the effects of a mass balance profile maximum shifted vertically in time, according to surface elevation changes.

Results ('ISSM, SMB-altitude feedback') show a non-linear relationship between ice volume response and mass balance perturbations (Fig. 5.11). Hardangerjøkulen is found more sensitive to negative than positive mass balance changes. There is a distinct jump in steady-state ice volume for a mass balance anomaly of 0 to -0.1 m w.e. With such a mass balance change, around half of the ice volume is lost. For more negative mass balances (< -0.15 m.w.e), the ice volume loss is 90-95 %, with only some small ice patches left on the highest altitudes (not shown here).

Giesen (2009) also did experiments excluding the mass balance-altitude feedback, meaning the mass balance field is fixed according to present surface topography ('Giesen (2009), no SMB-altitude feedback'; Fig. 5.11). With this setup, a close to linear relationship between mass balance changes and ice volume response was found, and the ice cap was much less sensitive to mass balance changes (Giesen, 2009, p.158). In fact, half of the ice volume was still present at an anomaly of -0.5 m w.e. In other words, no drastic jump in ice cap response occurs when the mass balance-altitude feedback was excluded.

The differing sensitivities to positive and negative mass balances is nicely illustrated by outlet glacier length changes, shown in Fig. 5.12 for selected mass balance anomalies. We see that Midtdalsbreen and Rembesdalskåka only advances with about 10-25 % of their present-day lengths for mass balances of +0.3 to +0.5 m w.e., while for corresponding negative mass balance perturbations, they loose 85-100 % of their initial lengths. The length of Rembesdalskåka stabilizes around 1 km for anomalies of -0.3 and -0.5 m w.e. In these situations, there are just small ice patches left high on the plateau, see Fig. 5.3 for reference. The time scales of these retreats are 500-1500 years. However, we have to remember that the mass balance changes in these experiments are much smaller than for example projected under future warming over the next 100 years, so timescales of ice cap changes can likely be much shorter. These considerations are discussed in Sect. 6.4.

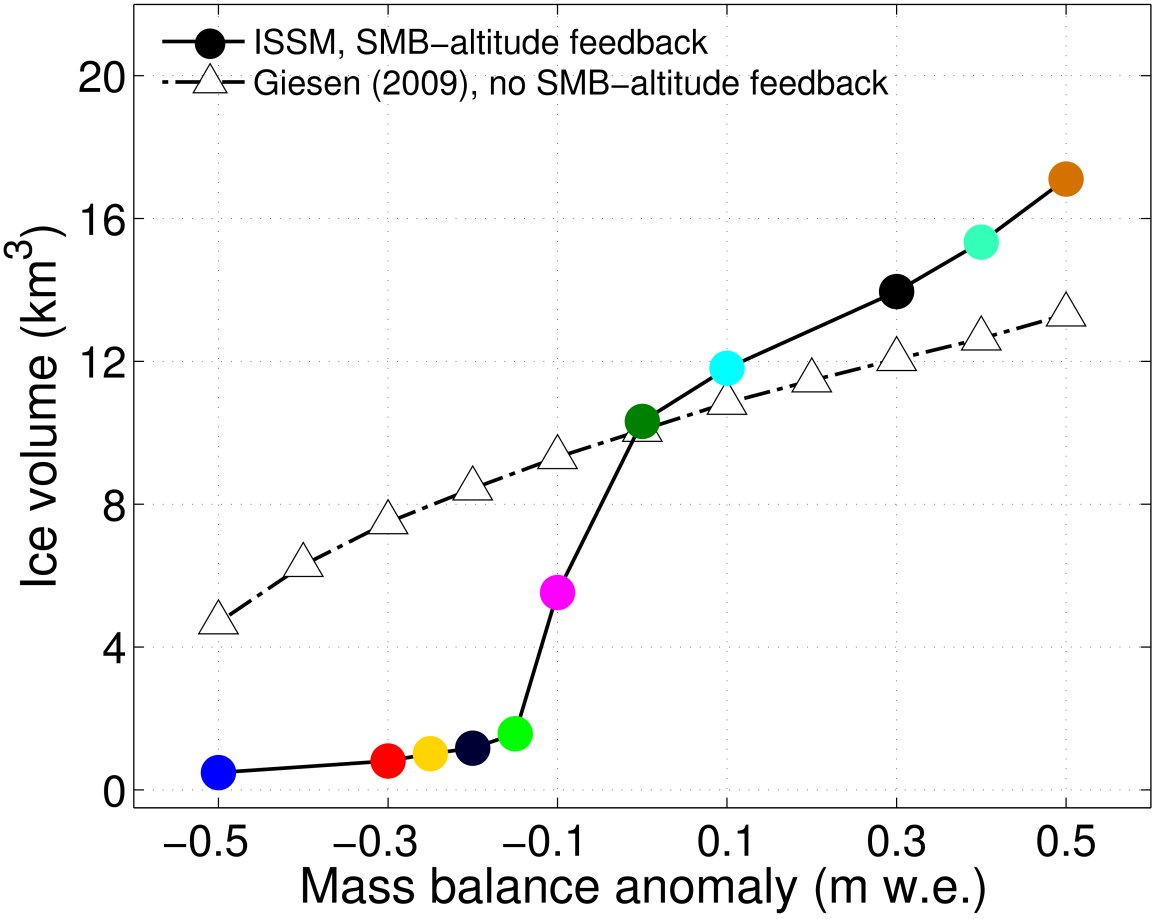

(a)

Figure 5.11: Steady-state ice volumes using a temporally fixed mass balance profile maximum from ISSM, shown together with a run without mass balance-feedback (mass balance profile fixed to the 1995 surface topography) from Giesen (2009). Mass balance anomaly colours correspond to colours in Fig. 5.12, showing outlet glacier length time series for different mass balance anomalies.

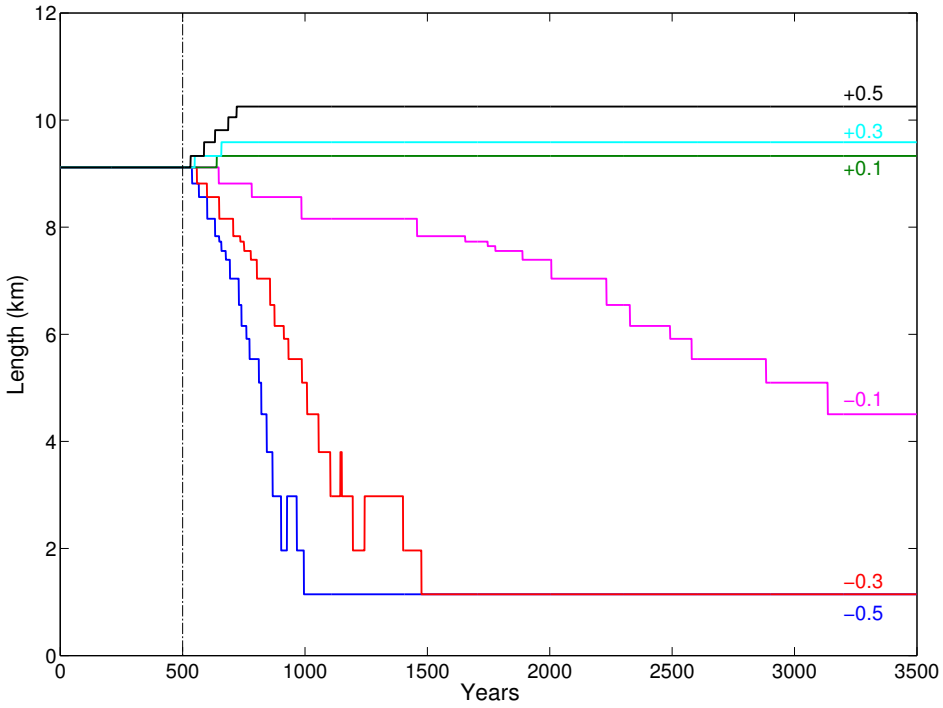

(a)

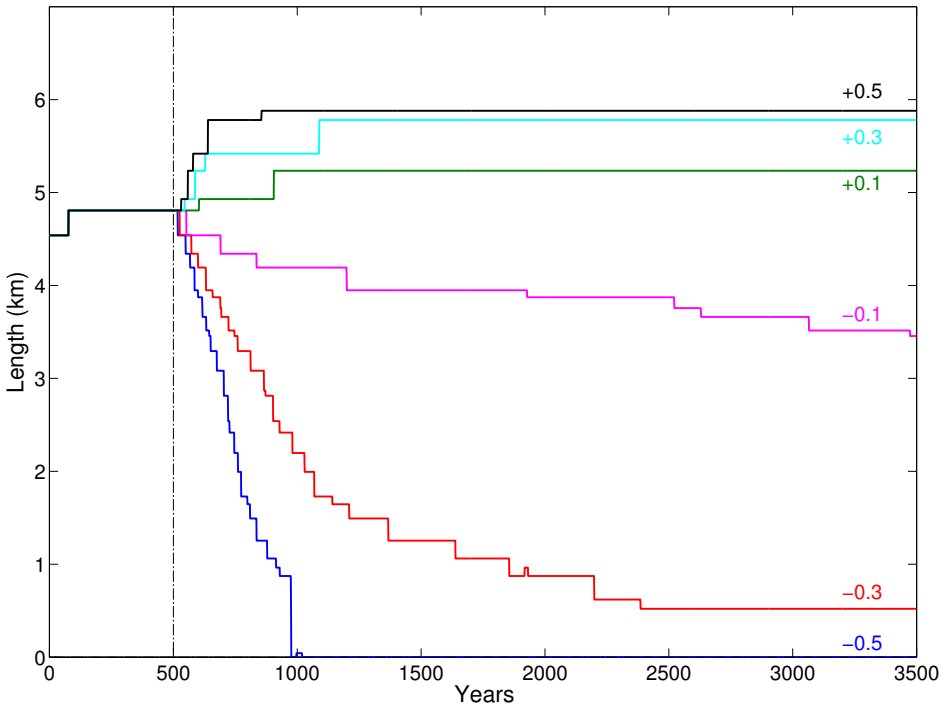

(b)

Figure 5.12: Length time series of (a) Rembesdalskåka and (b) Midtdalsbreen for selected mass balance anomalies. Colours correspond to mass balance anomalies Fig. 5.11

.

5.2.2 Spatially variable sliding necessary

As a part of the calibration process, different formulations of basal sliding were tested. Initially, a parameterization dependent on driving stress and a spatially constant sliding tuning parameter C was used. Basal velocities u_b is then computed by $u_b = -C\rho_i g H \nabla s$. With the goal of reproducing the present-day ice cap topography and extent, the model was forced with zero mass balance until a steady-state was reached. In particular, Rembesdalskåka was paid most attention to since the mass balance gradient used to force the model is derived from direct observations here. It is also the largest (17.4 km^3) and probably the most dynamic glacier.. This process differs from when the model is run from LIA until today (Sect. 5.1), since the ice cap then evolves based on the historic mass balance history found in the calibration against outlet glacier lengths.

Experiments forced with zero mass balance and a spatially constant sliding parameter C was not able to reproduce present-day topography. This setup resulted in a too flat accumulation zone and a too steep ablation zone. Varying the magnitude of the sliding parameter did only change surface elevations and not ice cap shape. When applying a elevation-dependent sliding parameter $C(z)$ instead, the agreement between modelled and observed topography is much better (dashed line in Fig. 5.13). Selected runs with a spatially constant sliding parameter C are shown in Fig. 5.13, using different fractions of the sliding parameter at the ELA, $C(z)_{ELA}$ (ELA $\sim$1640 m a.s.l.), found in the calibrated elevation-dependent sliding formulation. Besides the illustration in Fig. 5.13, the sliding parameter at the ELA $C(z)_{ELA}$ has no specific meaning.

Looking at surface topography for the entire ice cap (Fig. 5.14), the model underestimates the surface height in the northwestern areas (as in the historic run) by 20-100 m, while the eastern and southeastern margin is too thick (around 50 m and up to 100 m overestimation at places). In contrast, the interior ice cap thickness is generally reproduced within $\pm$20 m. Surfaces at Rembesdalskåka and Midtdalsbreen, the two outlet glaciers of prime interest, is reasonably represented. Regarding ice cap extent, the agreement is good, except for the southeastern part, where there is too much ice.

Again, we stress the difference between the historic run and the run starting from the present-day topography. A comparison with the 1995 DEM based on the historic run (Fig. 5.6) therefore differs from a comparison based on zero mass balance starting from present-day (Fig. 5.14), although they share some features (for example, the too thin northwestern ice cap and the too thick eastern areas).

A temporally fixed sliding parameter is generally used in this study (Sect. 4.1.2). While the sliding *parameter* $C(z)$ is fixed in time, basal velocities are not, since they also are proportional to the driving stress τ_d, which is determined by the time-evolving ice thickness and surface slope through $\tau_d = \rho g H \nabla s$. For the interested reader, we perform a test in Sect. 9 of how a temporally evolving field of the basal sliding parameter affects ice volumes, velocities and outlet glacier lengths since the LIA.

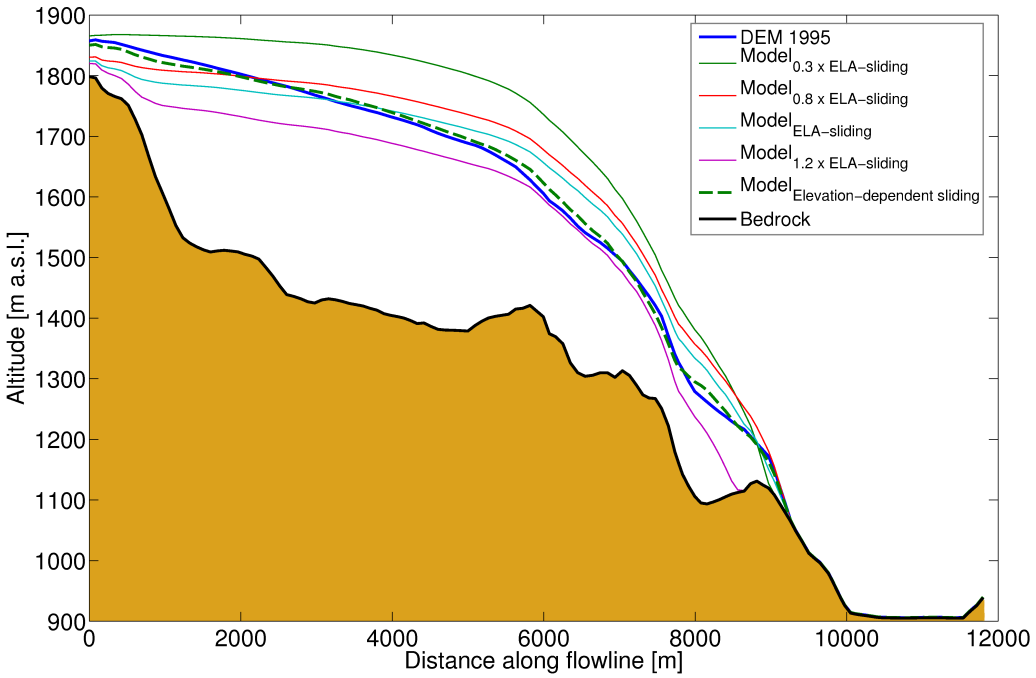

Figure 5.13: Modelled steady-state surface topography for Rembesdalskåka, forced with zero mass balance, using different sliding formulations. For runs with a spatially constant sliding parameter C, various fractions of the sliding parameter value at the equilibrium-line altitude in the elevation-dependent formulation $C(z)$ are shown.

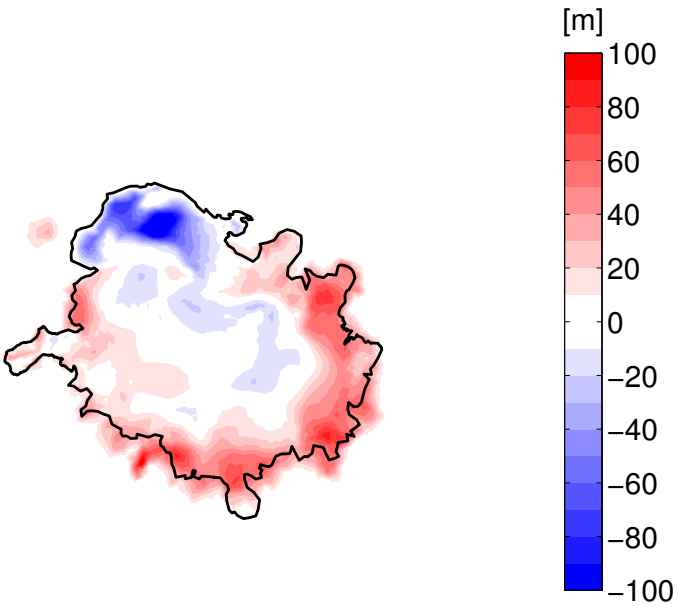

Figure 5.14: Surface elevation differences between modelled steady-state topography, forced with zero mass balance, and the surface DEM in 1995.

5.2.3 Low sensitivity to ice rheology

As a part of the calibration process, we investigated the effect of ice stiffness through the creep parameter A in Glen's flow law. For temperate ice, the recommended value for the parameter A differs by almost a factor of three between Paterson (1994) and Cuffey and Paterson (2010). In Paterson (1994), p.97, the recommended value $A_{Paterson}$ (6.8 x 10^{-24} $s^{-1}Pa^{-3}$) is based mainly on laboratory studies and studies of tilting boreholes in mountain glaciers (Raymond 1980; Paterson 1994). The recommended value by Cuffey and Paterson (2010), p.73, (2.4 x 10^{-24} $s^{-1}Pa^{-3}$) comes from averaged results from five numerical models of temperate glaciers in Iceland, the Alps, Scandinavia and Alaska (for references to these studies, see footnote of Table 3.3, p.73 in Cuffey and Paterson (2010)). These 'full-stress' models accounted for all stresses and were calibrated against observed surface velocities or changes in topography. For glacier dynamics, the most relevant results are those from calibration of full-stress models to large-scale flow, and the values from these experiments are therefore considered more reliable than earlier studies (Cuffey and Paterson 2010).

To get an idea of the effects of the updated creep parameter from Cuffey and Paterson (2010), here called A_{Cuffey}, steady-state runs for zero surface mass balance (SMB) as well as an mass balance anomaly of +0.4 m w.e. were done (Fig. 5.15). SMB = +0.4 m w.e. was chosen since the resulting steady-state ice cap using this mass balance anomaly is the starting point for the historic run starting in AD 1600. Difference in steady-state volumes for zero and non-zero mass balance are 0.73 % and 0.83 %, respectively. Differences in surface topography (Fig. 5.15ab) and surface velocities (Fig. 5.15cd) are generally within $\pm$ 5 myr^{-1}. Some exceptions with larger differences of 10-20 m exist using the non-zero mass balance, notably in the northwestern part of the ice cap. Here, ice accumulates for the stiffer 'Cuffey' rheology, while this does not happen when using the softer ice of Paterson (1994). Where the two resulting steady-state ice cap overlap, the Cuffey elevations are generally 2-4 m higher than from Paterson's rheology.

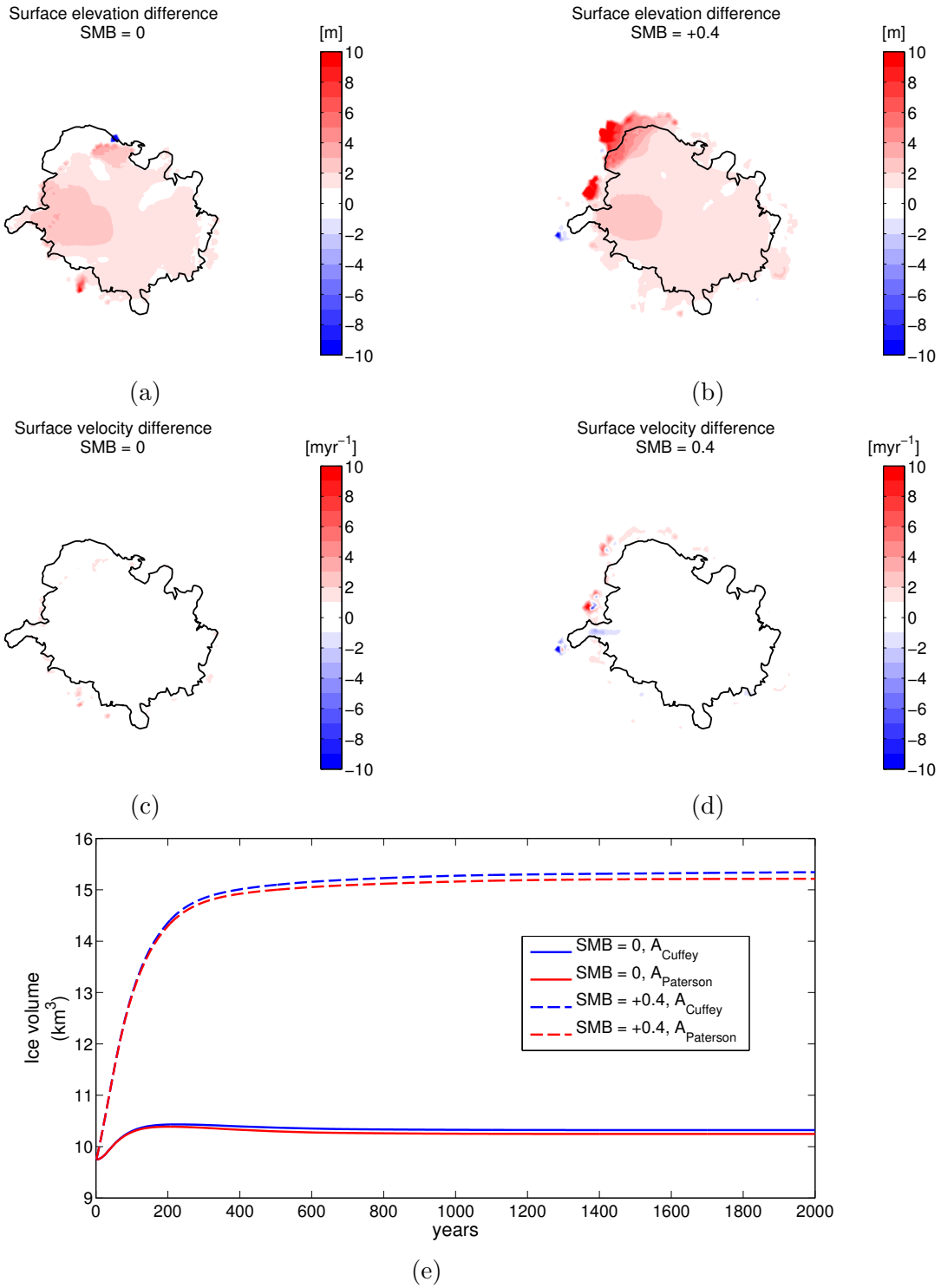

Figure 5.15: Effects of varying the ice stiffness parameter A in Glen's flow law, as recommended by Paterson (1994) and Cuffey and Paterson (2010); called $A_{Paterson}$ and A_{Cuffey}, respectively. A_{Cuffey} is around three times higher (stiffer) than $A_{Paterson}$. Shown are steady-state surface elevation differences for (a) SMB = 0; (b) SMB = +0.4 m w.e, and steady-state velocity differences for (c) SMB = 0; (d) SMB = 0.4 m w.e. (e) Ice volume time series. Positive values in (a)-(d) indicate higher (lower) magnitudes for the Cuffey (Paterson) rheology.

6 Discussion

The chosen methodology and results in this thesis will be discussed in this chapter. Findings are compared with previous studies and relevant wider implications are highlighted. Recommendations for further work are summarized in Chapter 8.

Given the purpose of reproducing observed outlet glacier lengths and areal extent of Hardangerjøkulen ice cap since the Little Ice Age, the model setup used in this thesis performs well. The LIA extent is reasonably well represented for most of the ice cap, although some areas do not correspond to geomorphological evidence (Fig. 5.5a). Still, considering spatial and temporal uncertainties in moraine evidence, uncertainty in the applicability of the present-day mass balance gradient during the LIA climate, as well as the inability to resolve small scale features with a mesh resolution of 200 m, the fit is good. The general outlet glacier retreat pattern is also reproduced, although the model underestimates outlet lengths during the early 1900s (Fig. 5.4). The match between modelled and observed ice cap extent is very good after 1960 (Fig. 5.5cd) and the modelled surface topography in 1995 corresponds well to observations (Fig. 5.6). This coincides with the period when direct mass balance measurements are used as forcing (Fig. 5.1a), indicating that accurate mass balance forcing is important.

Because the climatic response of Hardangerjøkulen since the LIA has been simulated reasonably well, we can conclude that the main aim of this thesis has been reached. Nevertheless, deeper insight into reasons behind the periods of agreement and disagreement between the model and observations requires an examination of the full model setup, including assumptions, parameterizations and input data used.

An important glacier characteristic is ice volume, since it accounts for both areal extent and ice thickness. In terms of hydrological applications such as hydropower, the total ice volume represents stored water which can be utilized for energy production. We do not know the ice volume of Hardangerjøkulen during the LIA, so there is no way to validate the modelled ice volume of 21 km^3 (Fig. 5.1c). In 1961 and 1995, the model overestimates observed ice volumes by $\sim$10 %, mostly due to too thick ice over the eastern ice cap. Ice thickness in this area was also overestimated in a model study by Giesen and Oerlemans (2010), suggesting a common explanation, although they overestimated ice thickness in the northern and northeastern ice cap more than this study. Potential causes of the eastern ice cap overestimation and other discrepancies are discussed in the text below, including SIA inaccuracy in steep terrain, the absence of horizontal mass balance gradient and errors in bedrock topography data.

The model shows a mutual front of the northern outlet glaciers Midtdalsbreen and Blåisen at the LIA-maximum. In contrast, geomorphological evidence (Fig. 5.4) suggests that there was an ice-free corridor between these two outlets (Andersen and Sollid 1971; Sollid and Bjørkenes 1978). Part of the explanation for this discrepancy could be the mesh resolution. Since the resolution of 200 m is similar to the proposed width of the ice-free corridor, it would be hard to resolve such features in the model. Another reason may be the exclusion of longitudinal stresses by the SIA. There is a very steep nunatak separating the two northern outlet glaciers Midtdalsbreen and Blåisen, with slopes larger than 0.5 (45°) at some places. The present western lower ablation zone of Blåisen is

also steep (surface slopes ∼0.15-0.30 or 13.5-27°; Fig. 6.1a). SIA likely has problems in these areas, since it has been suggested accurate only for bedrock slopes up to 0.2 (18°) (Le Meur et al. 2004). Further studies comparing SIA with HO- and FS-models in these areas will resolve these issues.

The modelled glacier length of Rembesdalskåka is too short (5.3a). This underestimation carries along to the 1900s, since the modelled glacier is retreating from the wrong position. Further, the bedrock slope is large (0.2-0.4, 18-36°) in the area of retreat from lake Rembesdalsvatnet during the 1900s. SIA may have problems with this area, given that SIA has reduced accuracy for steeper bed and surface slopes, as suggested by Leysinger-Vieli and Gudmundsson (2004) and Le Meur et al. (2004).

For the early 1900s, outlet glacier lengths are underestimated by the model (Fig. 5.2). A better match will likely be obtained by forcing with a slightly more positive (for example +0.2 m w.e. higher) mass balance for the preceding 150 years or so. The mass balance is not known for the 19th century, and the dynamic calibration approach used in this thesis (Sect. 4.2.3) would allow such an adjustment. Applying a simple mass balance model based on meteorological station data available for parts of this period could also be used to compute mass balance during this period. We choose not to go into further matching of the length records at this stage, but instead focus on model parameters and sensitivities. However, we will prioritize this point in coming work, since it will likely confirm whether the model can capture short time scale changes associated with for example the 1930-1960 retreat.

In terms of length responses to climate, the outlet glaciers respond to the mass balance anomaly imposed for the LIA, as well as that of the early 1900s. However, the advance during the snowy winters of the 1990s is not reproduced, except when using a temporally evolving basal sliding formulation (Fig. 9.3). However, this sliding formulation produces outlet glacier lengths that are further from the rest part of the record. To investigate length responses in more detail at relevant timescales, model resolution may have to be increased. At the current 200 m resolution, changes shorter than this will not be resolved. Moreover, it is expected that outlet glaciers will experience a short delay in their response due to the model resolution, since it will take some time for a mass balance anomaly to cause outlet glacier advance (retreat) to the next (previous) mesh element. Therefore, it is not so surprising that subdecadal climate variability, such as the NAO-induced positive mass balance of the 1990s, not results in an advance in the model within a few years.

The response to a climate perturbation can be assessed by changing the mass balance in the model when the ice cap is in balance with climate. The response time then can be estimated by the so called *e-folding time* (Oerlemans 2001), defined as $t_{rL} = L_2 - (L_2 - L_1)/e$, where L_1 is the length in equilibrium (steady-state) with the initial climate C_1, and L_2 steady-state length for a new climate C_2. Volume response time can be defined in an analogous way. As shown in Fig. 6.2, the response to a constant mass balance anomaly is non-linear and the ice cap almost entirely disappears for an anomaly of -0.15 m w.e. In addition, outlet glacier lengths and ice volumes are much more sensitive to negative than to positive mass balance changes. Since the response times depend on the mass balance perturbation, a single, characteristic response time

for Hardangerjøkulen, or for its outlet glaciers, is not applicable. These findings are consistent with Giesen (2009), who also found a non-linear relationship between mass balance and ice volume and length responses.

6.1 Applicability of the Shallow Ice Approximation

Using the Shallow Ice Approximation (SIA) is an important choice, since this governs how ice flow is represented in the model. In short, we have used the SIA to describe ice flow, with realistic mass balance and a spatially variable and temporally fixed sliding formulation. For this setup, SIA captures climatic timescale variations in ice cap extent and outlet glacier terminus positions. Even though the broader patterns are good, there are some mismatches, including: the underestimation of outlet lengths during the early 1900s; the inability to model the geomorpholocially suggested LIA-corridor between the northern outlet glaciers Midtdalsbreen and Blåisen; the overestimation of ice thickness for the eastern ice cap. We now discuss these discrepancies in detail, starting in light of the SIA. However, we do not expect potential inaccuracy of the SIA to alone explain these mismatches.

This thesis and previous glacier and ice cap modelling exercises (e.g. Le Meur et al. 2007; Gumundsson et al. 2009; Giesen 2009; Adalgeirsdóttir et al. 2011), as well as theoretical comparisons between SIA and Full Stokes (FS) models (Leysinger-Vieli and Gudmundsson 2004) suggest that it is viable to apply the SIA if interests are climatic rather than ice dynamical. Leysinger-Vieli and Gudmundsson (2004) compared a SIA-model with a FS-model for an alpine-like idealized glacier geometry, while neglecting basal sliding. No significant differences in advance and retreat rates were found between the two models. They therefore argued that in absence of large basal motion, length fluctuations of alpine glaciers on timescales longer than a few years can be modelled equally accurate with a SIA model.

Several investigators have done ice flow approximation intercomparisons for idealized glacier geometries. Theoretical work by Hindmarsh (2004) and Gudmundsson (2008) showed that the SIA can reproduce large scale flow, in the absence of significant basal sliding. Moreover, Le Meur et al. (2004) compared a 2D SIA finite-difference model and a FS finite-element model for synthetic glacier geometries. They found that bedrock slopes rather than the aspect-ratio ("shallowness") determined the accuracy. Bedrock slopes up to 0.2 (18°) were found to give good results for the SIA, while steeper beds caused the SIA solutions to diverge from the FS solutions.

Additionally, they performed 3D simulations and found that the exclusion of longitudinal stresses was the main reason undermining the validity of the SIA for larger bedrock slopes. It has previously been shown (Kamb and Echelmeyer 1986) that bedrock bumps affect longitudinal stresses over distances several times the ice thickness, effects not captured by the local stress balance of the SIA. In this light, the validity of the SIA depends rather on bedrock undulations than the characteristic aspect-ratio $\epsilon = [H]/[L]$ (Le Meur et al. 2004). At Hardangerjøkulen, there are many areas (Fig. 6.1b) where bedrock slopes are above 0.2 and longitudinal stresses may be important. For example,

northern part of lower Rembesdalskåka has slopes of 0.4-0.6 (36-54°), Midtdalsbreen and Blåisen has similar slopes in some areas and slopes along the southern and eastern ice cap reach 0.4-0.7 (36-63°) at places. These areas would all cause problems for the SIA. The inability of the SIA to handle the steep margins of the eastern ice cap could perhaps partly explain the overestimated ice thickness in this area, but this mismatch may also be related to erroneous bed topography data or an overestimation of the mass balance (Sect. 6.2.1 below). The southern ice cap is better represented but also has steep bedrock slopes, suggesting that SIA invalidity in steep bedrock areas is not the only reason behind the too thick eastern ice cap.

Given the arguments of Le Meur et al. (2004), it is tempting to suggest that the SIA is inaccurate for bedrock slopes above 0.2 at Hardangerjøkulen. However, all the simulations performed by Le Meur et al. (2004) considered very simple basal conditions, with flat bedrock geometries (no bed obstacles) and sliding ignored. Other theoretical studies (Hindmarsh 2004; Gudmundsson 2008) have highlighted that the SIA is accurate only for high basal traction, and that longitudinal stresses are increasingly important when basal sliding becomes important.

It is difficult to know how much sliding there could be before SIA validity deteriorates, but it likely depends on the climatic and glaciological setting. Moreover, the bed topography data used in this study are uncertain in places (Sect. 3.1.2). Care should therefore be taken before drawing too many conclusions on SIA accuracy based on the bedrock slopes in different areas of the ice cap, since the actual input data may be wrong. A comparison against a higher-order or Full Stokes model will shed light on these issues.

Lastly, mass balance is the other component (the first being ice dynamics) determining glacier responses to climate change. If our aim is to understand and predict the behaviour of a *real* glacier, then we have to give attention to mass balance. If the mass balance is inaccurate, then we get erroneous results no matter what ice mechanic model we use.

6.1.1 Relative importance of ice dynamics and mass balance

One of the very few studies comparing different ice flow approximations for a *real* glacier with realistic mass balance is Adhikari and Marshall (2013). They compare SIA, Higher Order (HO) and Full Stokes (FS) models under different climate scenarios for Haig Glacier (2.56 km^3) in the Canadian Rocky Mountains. They found that basal drag is the dominant resistive stress (70 %), while longitudinal stress gradients and lateral drag contributed 23 % and 7%, respectively. They attribute the longitudinal stress resistance to the compressive flow associated with the overdeepened bedrock shape, features also present at Hardangerjøkulen, for example in the ablation zone of Rembesdalskåka. They point out that lateral drag is limited by the wide glacier geometry, and caution that this may not be true for narrower valley glaciers. Regarding transient evolution of glacier volume and extent, the SIA perform well under their glacier retreat scenarios. Notably, ice velocities are very low ($\sim$6 myr^{-1}) at Haig Glacier and the overdeepened bed hinders significant horizontal ice flow, facilitating good SIA performance. These velocities are several times smaller than what has been measured for the outlet glaciers

of Hardangerjøkulen. In this setting, the mass balance rather than ice mechanics is decisive of the behaviour of Haig Glacier.

In contrast, when the glacier is advancing, ice velocities increase to a few tens of metres per year over a steeper bed topography. In this situation their SIA results simulates larger ice volumes than the HO and Full Stokes models (Adhikari and Marshall 2013). These velocities resemble the velocities at Hardangerjøkulen more. If we extend the findings for Haig Glacier to Hardangerjøkulen, the ice cap plateau and gently sloping bedrock sections of the outlet glaciers would be well represented by the SIA, while steeper terrain will not. However, such an analogy is not straightforward. Hardangerjøkulen has a larger mass turnover and outlet glacier velocities are generally higher, suggesting significance of basal sliding. Adhikari and Marshall (2013) neglect basal sliding based on lack of observed seasonal velocity variations, and therefore argue that ice deformation is the dominant flow mechanism. In contrast, seasonal speed-ups have been observed at Midtdalsbreen (Vaksdal 2001; Willis et al. 2012), even though the net effect on ice flow of such events is debatable (Sect. 6.3). As described above, several studies (Hindmarsh 2004; Leysinger-Vieli and Gudmundsson 2004; Gudmundsson 2008) have noted that low basal slip likely is needed for the SIA to be accurate. In this light, it is perhaps less surprising that SIA performs well at the "undynamic" Haig Glacier for glacier retreat. Indeed, Adhikari and Marshall (2013) suggest that higher-order mechanics are likely important for more dynamic situations. Hence, other similar studies are needed in different dynamic, climatic and topographic settings to understand the (in)significance of higher-order ice mechanics under climate forcing. Since we have not (yet) compared the SIA results with a HO- or FS-model for Hardangerjøkulen, we cannot conclude how accurate SIA is for Hardangerjøkulen in particular and ice caps in general. Such a comparison remains a priority for future work.

Lastly, because of the relatively poor knowledge about processes at glacier beds, uncertainties regarding spatial and temporal patterns of basal sliding may be larger than the difference between a simple and a physically complete ice flow model. If our goal is to understand and predict glacier behaviour under climate change, we advise that any ice flow model intercomparisons considering *real* glaciers should consider both ice mechanics and basal sliding (and of course, mass balance) in a physically meaningful way.

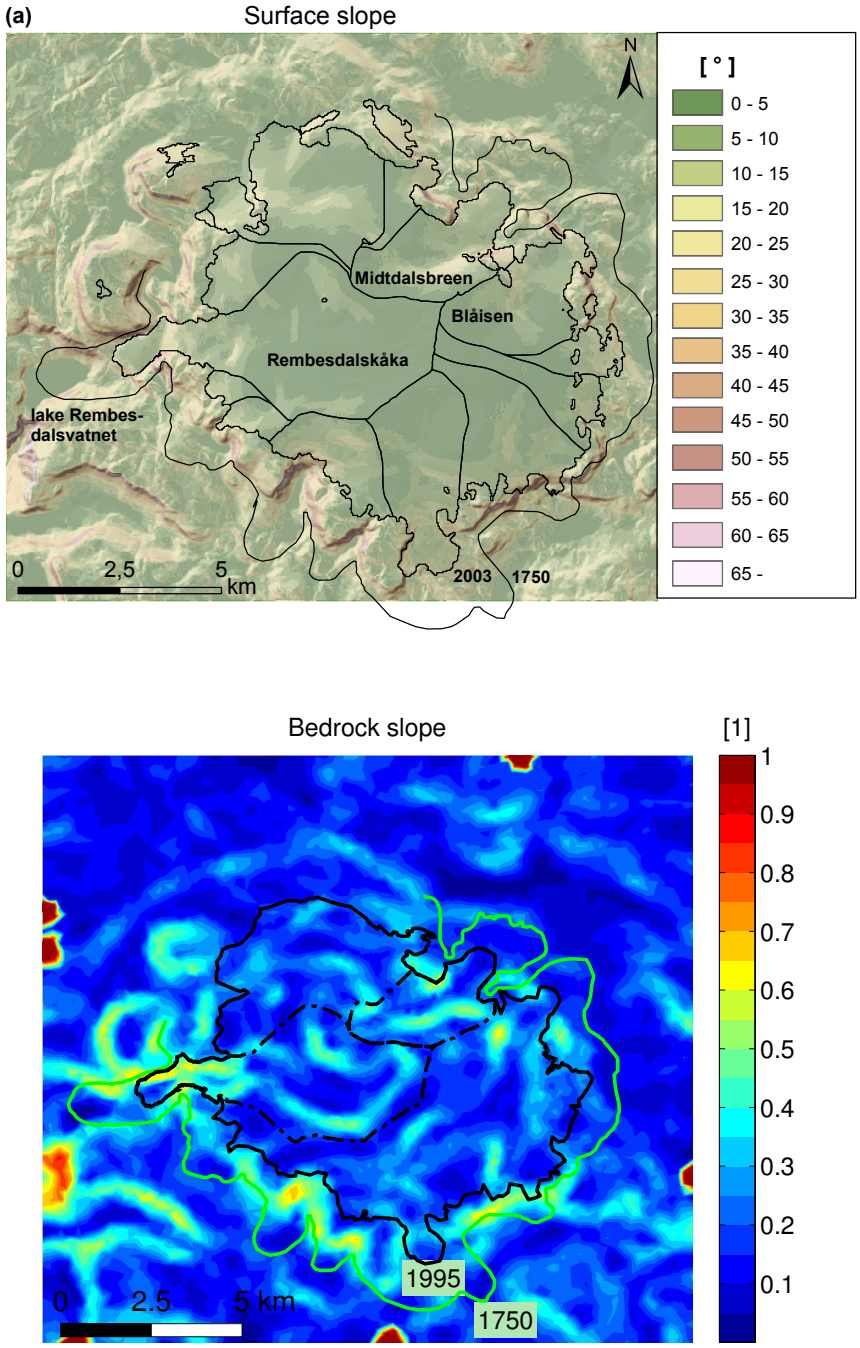

Figure 6.1: (a) Surface slopes of Hardangerjøkulen calculated from a 25 m surface DEM for 1995. Drainage basins indicated are from 2003 (differences are minor to 1995). Data from Statens Kartverk and Cryoclim.net. (b) Bedrock slopes at the 200 m mesh resolution used in the model. Ice cap extents from 1750 and 1995 are indicated in both figures, for which the 1750 extent go beyond the data boundaries of the 1995 DEM.

6.1.2 Modelling velocities with a SIA model?

Surface velocity measurements exist for several outlet glaciers, but only for single years. To the author's knowledge, no complete survey of ice velocities for the entire ice cap is available. Therefore, it is difficult to validate modelled velocities, let alone the simulated ice slowdown since the LIA. Notwithstanding this, modelled velocities at the ELA of Rembesdalskåka for 1995 ($\sim$40 myr^{-1}; Fig. 5.8a) are similar to what was measured for 2005-2006 (46 myr^{-1}; Table 3.2). Velocities for the other outlet glaciers also seem to be within $\pm$ 10 myr^{-1} of what is measured for single years (Vaksdal 2001; Giesen 2009). For Rembesdalskåka, the 26-hour qualitative velocity estimate in September 1996 (Elvehøy et al. 1997) of 110 myr^{-1} was measured in the area adjacent to lake Demmevatnet, close to the ice fall at Rembesdalskåka. The modelled velocities seem to correspond to within $\pm$ 20 myr^{-1} to these measurements. However, the short observation period as well as seasonal and interannual variations very strongly undermines the validation basis of these measurements.

We also saw that velocities at the ice cap plateau increased slightly ($<$ 5 myr^{-1}; Fig. 5.10). Since SIA velocities are proportional to ice thickness and surface slope, one of these must have changed. The ice thickness is smaller now than at the LIA maximum (Fig. 5.5), so increasing surface slopes caused by preferential thinning and retreat along the margins are likely responsible for this velocity change. However as discussed below, the insuitability of SIA to model surface velocities should make us cautious of these modelled changes.

Previous studies (e.g. Le Meur et al. 2004) have suggested that SIA tend to overestimate velocities in areas of steeper bed and surface slopes, because longitudinal stresses and lateral drag are neglected. Unfortunately, there are no velocity measurements where we expect the SIA to be least valid, e.g. in the steep ice fall in the ablation zone of Rembesdalskåka and at several places of steep bedrock slopes as seen in Fig. 6.1b. Adding higher-order ice flow physics may improve the representation of these steep regions. However, the lack of observed velocities for the ice cap in general and in this area in particular poses a challenge when it comes to validating model performance and constrain our ice dynamical understanding. This problem applies regardless of using a higher order model or not.

Several authors (e.g. Kamb and Echelmeyer 1986; Leysinger-Vieli and Gudmundsson 2004) have shown that SIA is unable to reproduce small-scale dynamics such as surface velocities. Additionally, since SIA requires high basal friction and neglects longitudinal stresses, SIA is unsuitable to model surface velocities (Le Meur and Vincent 2003; Leysinger-Vieli and Gudmundsson 2004). Weertman-type sliding laws as the one in this study, where sliding is determined by surface slope and ice thickness, has also been deemed inadequate to model sliding velocities (Vincent et al. 2000). The comparisons done with observed surface velocities may therefore not be meaningful. However, depth-integrated velocities across the glacier width can be correct. Since the ice flux (ice passing through a glacier column) gradient is determined by the surface mass balance, the flux must be roughly correct to ensure mass conservation (H. Gudmundsson, 1999, pers. comm. w. Vincent et al. 2000).

The aim of this thesis is to reproduce the observed ice cap and outlet glacier fluctuations over climatic time scales, rather than reproducing velocities at particular snapshots in time. If we measure velocities over a longer time period (at least a few years) and for various settings around the ice cap, we will deepen our dynamical insight and better understand the climatic response of Hardangerjøkulen. Rembesdalskåka would be a suitable starting point, since this seems to be the most dynamic part of the ice cap. Also the southeastern outlet Vestre Leirbotnskåka remain largely unstudied, despite its larger size (8 km^3) than both Midtdalsbreen (6.8 km^3) and Blåisen (6.6 km^3).

Obtaining velocities for the entire ice cap by means of remote sensing would of course be even better. A more complete velocity field could also give us the possibility to perform inversions for basal properties, a data assimilation method developed extensively within ISSM (Morlighem et al. 2010; Larour et al. 2014). Such data, especially in combination with a new hydrological model being implemented in ISSM (Fleurian et al. 2014), will advance our knowledge about ice dynamics and climatic response of Hardangerjøkulen in particular and smaller ice masses in general.

6.2 Mass balance

6.2.1 A west-east climatic gradient at Hardangerjøkulen?

The climate in southern Norway is dominated by a strong west-east precipitation gradient (Fig. 3.8b). Rembesdalskåka is facing the prevailing westerly wind direction and is expected to receive more snow than leeward Midtdalsbreen, affecting primarily winter mass balance. Rembesdalskåka may therefore be more sensitive to precipitation changes than Midtdalsbreen.

Differing mass balance regimes is indicated by Andreassen and Elvehøy (2001), who calculated the surface elevation change from 1961 to 1995 (Fig. 5.7) for the entire ice cap. They found that Rembesdalskåka had a mass surplus of 7 m w.e., while the cumulative mass balance for Midtdalsbreen was +2 m w.e.

Unfortunately, the two single years (2001-02; Krantz 2002) with mass balance measurements on Midtdalsbreen are not enough to assess systematic differences in mass balance regimes of Rembesdalskåka and Midtdalsbreen, let alone their sensitivity to temperature and precipitation. Considering that measurements already are carried out at nearby Rembesdalskåka, along with the logistically ideal location of Midtdalsbreen, extending the mass balance program at NVE to include Midtdalsbreen could be considered. Such data will enable us to better quantify meteorological influences on mass balance for either side of the ice cap. Further, combined with additional velocity measurements, it would give more insight into the relative importance of mass balance and ice dynamics. However, maintaining a continuous mass balance program of high quality is costly and labour intensive, and there may exist other unmeasured glaciers equally suitable for monitoring.

The inability to accurately model Rembesdalskåka and Midtdalsbreen simultaneously may be related to the mass balance formulation in the model. As implemented in this thesis, mass balance is only a function of elevation. Given the hypothesized west-east

gradient in winter accumulation, a potential improvement is to let mass balance vary both vertically and horizontally. A horizontal precipitation gradient was also assumed by Giesen (2009) and Giesen and Oerlemans (2010), but this effect was added artificially based on meteorological station data on respective sides of the ice cap rather than from *in situ* measurements. Quantification of the spatial variability of accumulation, for example along west to east transects over the ice cap, would be very valuable to understand the climatic response of Hardangerjøkulen.

The mass balance sensitivity to temperature (C_T) and precipitation (C_P) at Rembesdalskåka has been estimated by Rasmussen and Conway 2005 by a regression of mass balance and upper-air meteorological conditions. They found that sensitivity to temperature C_T was -0.64 m w.e. K^{-1} and to precipitation C_P +0.22 m w.e. $(10\%)^{-1}$. By applying a temperature-index model to nearby meteorological station data, De Woul and Hock 2005 found similar values (C_T = -0.66 m w.e. K^{-1} and C_P = +0.28 m w.e.$(10\%)^{-1}$), while a spatially distributed energy balance and mass balance model used by Giesen (2009) gave higher sensitivity for temperature and slightly higher for precipitation (C_T = -0.94 m w.e. K^{-1} and C_P = +0.30 m w.e.$(10\%)^{-1}$).

We can view these sensitivities in light of the LIA climate. There has been some debate about whether the LIA glacial advances in southern Norway were solely driven by lower temperatures or in concert with higher winter precipitation. Nesje and Dahl (2003) and Nesje et al. (2008) argue that lower temperatures alone cannot explain the LIA glacier advances. Rather, they suggested that higher snowfall associated with mild and humid winters were responsible. For the more continental Jotunheimen region northeast of Hardangerjøkulen, Rasmussen et al. 2010 found a LIA precipitation anomaly of 20-28 %, assuming a LIA temperature anomaly of -0.5 °C (e.g. Briffa et al. 1992; Nordli et al. 2003; Oerlemans 2005).

Suppose that the temperature at Hardangerjøkulen was 0.5° lower at the LIA maximum than today, and that precipitation was 25 % higher. Further, assume that the climatic sensitivities remained constant through time. Using the sensitivities C_T = -0.94 m w.e. K^{-1} and C_P = +0.30 m w.e.$(10\%)^{-1}$) from the spatially distributed energy balance model of Giesen (2009), this yields a mass balance anomaly of 1.23 m w.e. for the LIA maximum. This is not entirely dissimilar to the mass balance anomaly of +1.7 m w.e. imposed during 1690-1730 in the model. Of course, the imposed mass balance in the model is chosen to match the LIA maximum for the outlet glaciers, and its magnitude depends on the initial ice cap state. Since we did not know the ice cap geometry before 1750, we used an initial steady-state ice cap geometry corresponding to +0.4 m w.e. relative to present-day. However, we could also have chosen an initial state corresponding to +0.8 and a lower mass balance anomaly. Given these considerations, more knowledge of Hardangerjøkulen's geometry prior to 1750 would be very valuable, for example by means of geomorphological or sedimentary evidence. Such further work will render more robust insights regarding the forcing mechanisms and ice cap responses during the LIA.

Based on the proposed precipitation-driven LIA glacier maximum and higher mass turnover for Rembesdalskåka, we might be able to explain the mismatch between the modelled LIA outlet glacier lengths. If the LIA maximum for Rembesdalskåka is matched in the model, Midtdalsbreen advances too far. If the LIA maximum was caused

mainly by increased precipitation, the mass balance anomaly imposed in the model is representative for Rembesdalskåka rather than Midtdalsbreen. Thus, for the assumed west-east gradient in accumulation, Midtdalsbreen would have had a less positive mass balance anomaly and as a result not thickened and advanced as far. This would aid in the right direction of representing the two outlet glaciers simultaneously. A west-east precipitation gradient could also partly explain the thickness overestimation of the eastern ice cap for AD 1995, although there may be other equally important factors, for example errors in the bed topography data used and inaccuracy of the SIA in steep terrain.

Different climatic responses for the northern and southern sectors of the ice cap were also suggested by Nesje et al. (1994), who investigated a sediment core from lake Isdalsvatn downstream of the southwestern margin. By comparing with sediments from a lake receiving meltwater from the northeastern part of the ice cap (Dahl and Nesje 1994), they found that the glacial chronologies differed. For example, the southern side of Hardangerjøkulen had a short-lived advance around 7000 before present (BP), while the northern side of the ice cap was was completely absent between c. 7590 to 6285 BP. Consistent with what is hypothesized above, they proposed that differing glacier responses could partly be explained by the prevailing westerly winds and associated precipitation patterns. Further glacier reconstructions based on multiproxy approaches on lacustrine sediments (e.g. Vasskog et al. 2012; Bakke et al. 2013) could give more insight into differing continentality of the outlet glaciers of Hardangerjøkulen. For example, there are several lakes on the western and eastern sides of the ice cap receiving glacier meltwater. Such reconstructions should be of high temporal resolution and well-dated to be of glaciological and climatological value.

Given that the outlet glaciers respond(ed) differently to climate, this may also have implications for the timing of the LIA maximum at the two outlet glaciers. The terminal moraine at Midtdalsbreen is dated to AD 1750; Rembesdalskaka is assumed to have produced a terminal moraine at the same time. In the model, this means that the moraine positions is compared with the modelled positions in AD 1750 for both outlets, while in fact the true maximum for Rembesdalskåka may have had a different timing. The model resolution is probably too coarse to investigate the details of such asynchronous advances, let alone the uncertainty in the climatic forcing. Further, since the two outlet glaciers vary in size and dynamics, they will likely have different response times.

6.2.2 Improving the mass balance implementation

In addition to imposing a horizontal accumulation gradient over the ice cap (Sect. 6.2.1), the mass balance formulation could be improved in several ways. For example, the observed mass balance maximum at ∼1775 m a.s.l can been adapted in time according to changes in maximum ice cap elevation. This would be valid if we assume that the decrease in mass balance at the high plateau is related to the ice cap shape rather than elevation. Giesen (2009) showed that temporally shifting the mass balance maximum according to summit elevation plays a minor role when mass balance is slightly positive, but gives a more sensitive ice cap for negative mass balances. They also found that

including the mass balance-altitude feedback was the most important improvement of the mass balance implementation. Although these results come from a different ice flow model (modified version of Van Den Berg et al. 2008) than used in this study, they are derived with the same ice flow approximation (SIA) and the same mass balance profile as used in this thesis. Thus the major role of the mass balance-altitude feedback found by Giesen (2009) gives some comfort in using a mass balance gradient without a time-adaptive mass balance maximum. Implementing this in the model will be prioritized in future work.

We do not know the origin of the maximum in the mass balance profile at around ∼1775 m a.s.l. (Fig. 3.10), but a likely explanation is snow redistribution. If we seek to explicitly include effects of snow erosion and redeposition, we may use a parameterization based on surface curvature, which is a good indicator of regions of wind-induced snow redistribution (Blöschl et al. 1991). Huss et al. 2008 used a distributed temperature-index melt model (Hock 1999) coupled with an accumulation model to calculate seasonal mass balances for four glaciers in the Alps since 1865. They accounted for snowdrift by calculating the curvature from a surface DEM within a range of 200 m around each grid point. Giesen (2009) tested such an approach for Hardangerjøkulen, but since the plateau of the ice cap is too flat, no snow redistribution occurred based on the surface curvature (R. Giesen, pers. comm.).

In Fig. 6.2, we include results from Giesen (2009), who applied a SIA-model to Hardangerjøkulen with a similar setup. First, we compare their equivalent experiment using a mass balance profile maximum fixed in time according to initial surface topography ('Giesen (2009), fixed SMB max'). The non-linear mass balance sensitivity found in this thesis was also evident in Giesen (2009). Differences in steady-state volumes are similar, but ISSM is slightly more sensitive for small negative changes in mass balance: the jump in ice volume occurs between -0.1 and -0.2 m w.e. for Giesen (2009), while it arises between 0 and -0.1 m w.e. in ISSM. Second, the 'fixed SMB max' experiments are compared to runs with a mass balance profile maximum shifted vertically in time, according to changes in ice cap summit elevations ('Giesen (2009), adaptive SMB max'). Using this setup, the transition from 10 km^3 to no ice is somewhat less abrupt. The 'fixed' and 'adapted' mass balance profile maxima from Giesen (2009) renders similar results for negative mass balance changes, the difference being a somewhat more sensitive ice cap for the fixed maximum than for the adaptive.

For a -0.1 m w.e. mass balance anomaly, the steady state volumes for temporally fixed and adapted maximums from Giesen (2009) are almost equal. The absence of a temporally adapted mass balance gradient maximum in ISSM hence does not offer an explanation for the differing climate sensitivity to this slightly negative mass balance anomaly. Both models get a jump in the steady-state ice volume response around 0 to -0.2 m w.e.; for ISSM this jump occurs for a somewhat less negative mass balance. The differences may relate to a combination of several small differences between the models (e.g. spatially constant or variable sliding parameters, differing ice rheology, mesh resolution or discretization of the input fields used). While it is difficult to determine the exact importance of each of these, the models show the same pattern between ice volume responses and mass balance: a non-linear relationship not symmetric around the

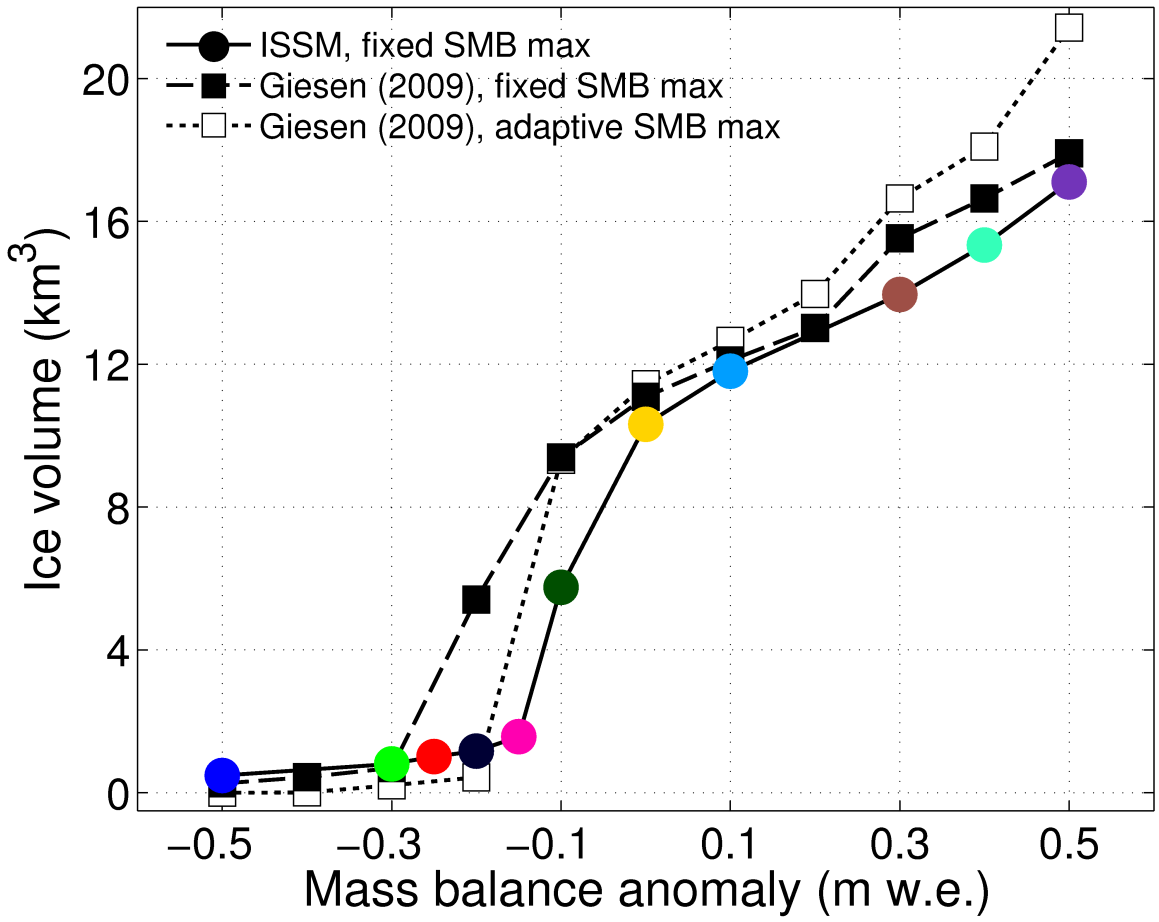

(a)

Figure 6.2: Steady-state ice volumes using a temporally fixed mass balance profile maximum from ISSM, shown together with corresponding fixed and time-adaptive experiments from Giesen (2009).

reference state, with Hardangerjøkulen being more sensitive to negative than positive mass balance perturbations. Regardless of the mass balance vertical maximum being fixed, or adapted in time according to surface topography changes, all three experiments in Fig. 6.2 show that Hardangerjøkulen almost vanishes or vanishes completely for negative mass balances below -0.3 m w.e.

Even though the mass balance formulation in this study works reasonably well, there are some uncertainties associated with applying the present-day mass balance profile in different climates. While it may be reasonable for smaller ice cap changes, it is probably not realistic when Hardjangerjøkulen grow or shrink considerably. Surface topography changes will affect accumulation distributions, especially if the ice cap splits up into individual outlet glaciers. In a warmer climate, the melt season will also be longer. This implies that the surface albedo will be lower for a longer time period every year, because earlier melt will expose bare ice earlier in the summer (Oerlemans and Hoogendoorn 1989). This is a positive feedback since lower albedo means that more melt occurs at a given temperature (equivalently, less energy is needed to melt a unit mass of ice than snow). Finally, solar insolation patterns may also change with a strongly altered surface topography, for example by shading effects of valley walls. Still, Giesen (2009) accounted for longer melt seasons and solar insolation changes when applying a spatially distributed energy balance model until 2100. They did not find very large changes in the mass balance gradient, indicating that on this timescale, the transferability of today's mass balance profile works well.

6.3 Basal motion

6.3.1 Physical basis of elevation-dependent sliding

In this thesis, we tried to account for the effect of surface meltwater on basal velocities by using a sliding parameter $C(z)$ linearly dependent on elevation. This formulation is able to reasonably reproduce the present-day topography when the model is run to steady-state with zero mass balance. It became clear that this is not possible with a spatially constant sliding parameter C. The elevation-dependent parameterization works well also when forcing with real mass balance, as evident by the good match between modelled and observed present-day topography for the historic run, although more accurate mass balance in the preceding period may partly explain this agreement. The argument for this formulation is that lower elevations have higher ablation rates and therefore produce more meltwater. This meltwater reaches the bed and increases basal water availability, which may enhance sliding.

An alternative is to use a sliding dependent on surface melt (Greve and Otsu 2007). Ablation varies approximately linearly with elevation at Hardangerjøkulen, except for the highest elevations, so we might expect the effects to be similar. However, ice cap topography change on different timescales than ablation rates. Situations may therefore arise when ablation has changed, while surface elevation has not (Sect. 2.2.3). It may therefore be more consistent to scale basal velocities to *in situ* ablation rates. This problem is intricately linked with other processes controlling basal sliding, such as

physical bed properties and subglacial drainage. These issues are discussed in Sect. 6.3.2 below.

Apart from the linearity of the mass balance gradient, the usefulness of this sliding formulation depends on (i) to what extent surface meltwater is routed directly to the bed; (ii) ability of basal water to modulate basal velocities and (iii) relative importance of other factors affecting basal velocities, such as bed roughness and subglacial drainage efficiency. The formulation used in this thesis assumes that surface meltwater is transferred vertically to the bed via crevasses, moulins and englacial passageways, without considerable horizontal water transfer (Willis et al. 2012). This is of course not entirely realistic - water is usually routed both vertically and horizontally on its way to the bed (Gulley et al. 2009). Horizontally rerouted drainage is probably more likely for the thicker parts of Hardangerjøkulen, where hydrofracturing may not be enough to create surface-to-bed pathways for water drainage. This problem is also noted by Clason et al (2014), although their concern is very thick ice associated with the Fennoscandian ice sheet during the last glacial.

The role of basal water in the sliding problem was introduced in Sect. 2.1.3, highlighting the importance of bed roughness and pressurized basal water. At Midtdalsbreen, recent studies (Vaksdal 2001; Willis et al. 2012) based on dye-tracing and water discharge measurements in proglacial streams suggest that the average water pressure is about 70% of ice overburden. The main subglacial drainage system was characterized as hydraulically efficient with broad, low channels (mean width/height ratio ≈ 75). The northwestern side of the ablation zone had a smaller, inefficient drainage system with very low channels (mean width/height ratio ≈ 350). The smallest drainage system at the center of Midtdalsbreen consists of very broad and extremely low channels (mean width/height ratio ≈ 450), and can be characterized as a linked cavity system, a result also indicated by Vaksdal (2001).

If the main subglacial drainage system is efficient channelized as suggested by Willis et al (2012), this strengthens the case for an elevation-dependent sliding formulation. This because any moderately anomalous meltwater inputs will be facilitated by the drainage system. As long as its efficient channelized structure remain unchanged, the effect on basal velocities should be small (Bartholomaus et al. 2008; Tedstone et al. 2013). Of course, this assumes that the drainage systems of the other outlet glaciers dominated by efficient drainage systems similar to that of Midtdalsbreen.

6.3.2 Should we let basal sliding parameterizations evolve with time?

A problem if we let sliding adapt to elevation changes is that we may be trying to capture the wrong processes. We initially assume sliding velocities inversely proportional to elevation, but additional factors also influence sliding. These include bed roughness and strength, in case of any sediment cover, as well as subglacial drainage and water availability. These are all lumped together in the ad hoc sliding formulation used. Bed properties are not likely to change much over time, while water availability indeed may do so. However, if subglacial drainage mainly consists of a network of tunnels

transporting water efficiently, as suggested for Midtdalsbreen by Willis et al (2012), further water supply will not particularly affect sliding speeds, as long as an efficient drainage is kept (Bartholomaus et al. 2008). Adjusting the sliding parameter to elevation changes in such a situation will therefore be a step away from actual glacier behaviour.

This leads us to a general problem with temporally evolving fields of parameterized processes. If an ad hoc sliding formulation is used, some of the processes lumped together in the parameterization will change over time (e.g. surface meltwater supply), while other factors (e.g. bed roughness and the type of drainage system) may not change. Adapting basal slipperiness in this study to elevation (or surface melt) changes may therefore be problematic. Indeed, Fig. 9.2-9.3 show that use of a time-adaptive sliding parameter increase the mismatch between observed and modelled ice volume and outlet lengths at Hardangerjøkulen. Considering these results, and the already physically incomplete assumption of an elevation dependent sliding, we choose to keep the basal sliding parameter $C(z)$ fixed in time to the linear relationship obtained from the steady-state calibration of the present-day ice cap. Better knowledge of the bed properties at Hardangerjøkulen (by means of, for example, Ground Penetrating Radar and/or seismics) as well as attempting to model the type of subglacial drainage system would be steps toward understanding the (transient) behaviour of basal slipperiness. Such a hydrologic model (Fleurian et al. 2014) has only just recently (May 2014) been implemented into ISSM. Applying this model to Hardangerjøkulen remain a task for future work.

6.4 The future of Hardangerjøkulen

By using the present-day ice cap as a starting point, and forcing with different mass balance scenarios while including a mass balance-altitude feedback, we show that Hardangerjøkulen is sensitive to climate warming (Fig. 6.2). In particular, Hardangerjøkulen is bound to disappear almost entirely for a mass balance anomaly around -0.15 m w.e., relative to the mean mass balance profile from 1963 to 2005. These results are consistent with those of Giesen (2009), who found that a mass balance anomaly of around -0.2 m w.e. probably will cause the ice cap to vanish. We can view these results in light of future climate change. The mean mass balance since 2000 is -0.3 m.w.e. While the mass balance at specific year is a direct result of prevailing meteorological conditions, it can also reflect geometric adjustment from earlier climatic forcing. However, Hardangerjøkulen was in approximately in balance during 1963-2013, so any dynamic adjustments are expected to be small. Thus if the mass balance stays like that experienced for the last decade or so, Hardangerjøkulen is bound to disappear within 750 years (Fig. 9.1). As evident from IPCC (2013), we expect a warming scenario for the future. Giesen and Oerlemans (2010) used an energy balance model to model the mass balance of Hardangerjøkulen for the next 100 years, using climate scenarios for southern Norway from the RegClim project (regclim.met.no). Modelled future mass loss largely exceeds that observed for the last decade. For example, for one of the "realistic" scenarios with a temperature rise of +3 °C and 10 % rise in precipitation relative to the normal period 1961-1990, the net

mass balance of Hardangerjøkulen as a whole was modelled to be -4.10 m w.e. in 2086. Given these predictions, and the modelled disappearance of all ice for a -0.3 to -0.5 m w.e., the time scale of future retreat will be much quicker than 750 years. Indeed, Giesen and Oerlemans (2010) coupled their mass balance model to a SIA model similar to that used in this study and suggested that Hardangerjøkulen will vanish almost completely before 2100.

A similar approach to that of Giesen (2009) has been used to investigate the response to future climate for ice caps and outlet glaciers in Iceland, namely Vatnajøkull (Adalgeirsdóttir et al. 2006), Langjøkull and Hofsjøkull (Gumundsson et al. 2009) and Hofellsjøkull (Adalgeirsdóttir et al. 2011). Given future climate warming, these studies conclude that the ice cap will last about 100-200 years into the future. Similarly, Le Meur et al. (2007) also applied a 2D SIA ice flow model found that Saint Sorlin Glacier (French Alps) is bound to disappear around 2070. Along these lines, the Great Aletschgletscher in Switzerland has been predicted to loose 90 % of its volume by 2100 by the use of a Full Stokes ice flow model (Jouvet et al. 2011). Except being a valley glacier and not an ice cap, this glacier share several characteristics with Hardangerjøkulen, being temperate ice masses with respective areas 83 km^2 (Bauder et al. 2007) and 73 km^2, ice volume $\sim$ 15 km^3 (Farinotti et al. 2009) and $\sim$10 km^3. Using a higher order model for Hardangerjøkulen to investigate future climate change remain a future task.

The large sensitivity to mass balance found here support changes inferred for the Holocene. Abrupt changes is evident from lake sediment records of glacial activity both at the northern (Dahl and Nesje 1994) and the southern (Nesje et al. 1994) sides of the ice cap. One example is the so called *Finse event*, when an advance to a maximum beyond that of present-day of the northern Blåisen outlet glacier around 7500 BP was followed by a complete melt-away of this glacier within less than a century. Since future warming is projected much larger than the changes associated during this period, a complete disappearance of Hardangerjøkulen as suggested by Giesen and Oerlemans (2010) does not sound unreasonable.

7 Conclusion

We have used a two-dimensional ice flow model forced with an optimized mass balance history since AD 1600 to model changes of Hardangerjøkulen ice cap in southern Norway since the Little Ice Age (LIA). We employed the Shallow Ice Approximation for ice flow and included a spatially variable sliding parameterization. Outlet glacier responses, ice cap extent and surface topography have been investigated. Additionally, sensitivity experiments regarding mass balance, sliding and ice rheology have been conducted. From this methodology, we conclude the following:

- The model successfully reproduces most of the LIA extent of Hardangerjøkulen, given temporal and spatial uncertainties in moraine evidence. Outlet glacier positions during the early 1900s are underestimated, while modelled ice extent after 1960 closely resembles observed margins. Surface topography in 1995 is very well represented, except for a too thick eastern ice cap.

- Hardangerjøkulen is found to be very sensitive to mass balance changes, consistent with previous studies of both the past and present. A shift by only -0.15 m w.e. relative to the reference mass balance 1963-2005 causes 90 % of the ice cap to melt away. At -0.3 to -0.5 m w.e., Hardangerjøkulen vanishes entirely within 500-750 years.

- The relationship between steady-state ice volume and mass balance perturbations is found to be strongly non-linear. The ice cap is much more sensitive to negative than positive mass balance changes.

- The model has problems in areas of steep bed and surface topography. These issues may be related to the neglect of longitudinal stresses by the SIA. Other explanations are possible in some areas, including the absence of a horizontal surface mass balance gradient (mass balance now is simply a function of altitude) and erroneous bed topography data. Testing the SIA results against a higher-order or Full Stokes model remain a priority for further studies. Insight in the relative importance of dynamics and mass balance for ice cap climatic responses would benefit from further studies of the surface velocity distribution and spatial variability in winter accumulation.

- A modified Weertman sliding formulation was used, where basal velocities are assumed proportional to the driving stress and a sliding parameter. Use of a spatially constant sliding parameter could not reproduce the surface topography of present-day outlet glaciers. When including a sliding parameter inversely proportional to elevation in a linear fashion, the match is considerably better. This *ad hoc* formulation aims to account for the effect of meltwater input to the bed. A more physically complete implementation, involving basal hydraulic potential or a fully coupled hydrological model will be considered for future work. Better knowledge about the physical, thermal and hydrological conditions of the glacier bed would facilitate successful application of such a model.

- Previous investigations (Giesen 2009; Giesen and Oerlemans 2010) have concluded that Hardangerjøkulen will disappear almost completely by 2100. We have not used our ice flow model to predict future ice cap evolution. However, the sensitivities to mass balance found in this study are consistent with those suggested by Giesen (2009). Moreover, the modelled mass balance by Giesen and Oerlemans (2010) for the most 'realistic' scenario for 2100 (+3°C and +10 % precipitation) is around 10 times larger than the mass balance causing a 90 % ice loss in this study, albeit on a longer timescale. We therefore support their conclusion that Hardangerjøkulen is unlikely to survive much longer than 100 years. There are nevertheless uncertainties regarding future changes, including mass balance distribution for a greatly altered geometry, ice albedo feedbacks and hydrological changes. Further work is needed to better constrain the timescale and the relative importance of these aspects.

8 Outlook

This thesis was carried out over the course of one year. During this time, some questions were answered, but new also arose. Suggestions for future research at Hardangerjøkulen are summarized here.

Ice flow apprixomation comparison. An assessment of SIA validity could be carried out by comparing with a Higher-Order and/or Full Stokes model. Hardangerjøkulen can serve as a test case for the applicability of the SIA for smaller ice masses.

Dynamics. Extension of existing velocity observations. Surface velocity measurements by means of differential GPSs would be one way to better constrain the modelled dynamics. Even better would be to use remote sensing platforms like InSAR to get a more complete picture of surface velocities. If a velocity distribution of the entire ice cap can be mapped, many new possibilities emerge, including inversions of basal friction and a more thorough validation of ice flow model performance when it comes to dynamics.

Mass balance. Implementation of a horizontal mass balance gradient. This thesis suggests that the outlet glaciers Rembesdalskåka and Midtdalsbreen are responding differently to climate forcing. The inability to accurately model both outlet glaciers may be related to the mass balance implementation. To better understand winter mass balance, additional field investigations focusing on the spatial distribution in winter accumulation are envisaged. Such data could also shed light on the role of snow redistribution by wind in modulating the mass balance at the high plateau. Use of a small-scale atmospheric model (e.g. a Weather Research and Forecast Model; WRF) as meteorological input for a mass balance model could also be worthwhile. Further, to constrain the unknown mass balance history during the 1800s, a simple mass balance model based on meteorological station data (e.g. from Bergen) could be applied.

Subglacial environment. In terms of subglacial properties, there are several things to consider. Use of new bedrock topography data (Melvold et al. 2011) can improve model results and provide a good basis for an ice flow model intercomparison. Investigating bed properties (for example, roughness and sediment cover) by combining GPR and seismics would also be very valuable. In addition, dye-tracing experiments and proglacial stream measurements at Rembesdalskåka, as already done for Midtdalsbreen (Willis et al. 2012), can be carried out to investigate subglacial drainage structure and efficiency. This knowledge could be used when developing a new, improved sliding formulation or when applying a hydrological model.

Basal sliding implementation. In this study, a modified Weertman sliding law is used to describe interaction between the glacier bed, water and basal ice. An alternative formulation involving basal hydraulic potential (Shreve 1972) could be used. The

hydraulic potential ϕ at the bed is given approximately by

$$\phi = f\rho_i g H + \rho_w g z_b \tag{8.1}$$

where ρ_i and ρ_w are the densities of ice and water, g is gravitational acceleration, H is ice thickness and z_b is bed elevation. The factor f, varying from 0 to 1, is the basal water pressure as a fraction of ice overburden pressure $p_i = \rho_i g H$. According to classical theory of temperate glacier hydrology (Shreve 1972), water flows down the gradient of hydraulic potential, that is, normal to the equipotential contours.

To a first approximation, we could set the fraction f to 0.7, which is the steady state, spatially and temporally averaged value obtained for Midtdalsbreen by Willis et al. (2012).

If we assume that f is spatially constant (as for example Elvehøy et al. 1997; Copland and Sharp 2000), we can use this parameterization to calculate basal sliding velocities by letting the sliding parameter C decrease with the hydrologic potential ϕ:

$$u_b = -C(\phi)\rho_i g H \nabla s, \tag{8.2}$$

where ∇s is the surface slope. This is still a physically incomplete description of basal motion, but could be justified as long as interest lie in ice cap and outlet glacier climatic responses, rather than to understand basal sliding and subglacial drainage. If the latter is of concern, the effective pressure would have to be included in a formulation for basal velocities (F. Ng, pers. comm.), for example by using the new ISSM hydrology model (Fleurian et al. 2014).

Thermal regime. Hardangerjøkulen is assumed isothermal in this study, which makes the modelling process much easier. However, this assumption is not entirely true. As noted by Reinardy et al. (2013), the lower ablation zone of Midtdalsbreen consists of cold ice, and this outlet glacier may be better described as polythermal. Most recently, field investigations in April 2014 suggest that the cold ice area at the terminus is still present. Further, there are also indications of cold ice nearby the nunatak separating Midtdalsbreen and Blåisen (Reinardy and Booth, unpubl. data). It would be interesting to extend this work further by mapping out the thermal properties at other places of the ice cap, especially for Rembesdalskåka. If extensive cold ice margins exist, this could affect ice flow by means of lateral drag. This would have implications for ice flow model assumptions, such as the neglect of lateral drag by the SIA.

Calving. Calving is not included in our model setup. However, the north-western part of the ice cap is presently terminating in a lake (Fig. 3.1). This lake has grown substantially in recent years. Due to the bed topography in this area, the ice cap margin will probably retreat another kilometre before the ice front is grounded (Melvold et al. 2011).

The time scale of such a retreat is uncertain, and also to what extent calving played a role in the past. Additionally, Rembesdalskåka terminated in lake Rembesdalsvatnet at the LIA-maximum. According to Liestøl (1962), this outlet glacier terminated at the

proximal side of the lake in AD 1928. The front position of Rembesdalskåka before the 20th century is not known, but given that the front was still there in 1928 and the lack of earlier terminal moraines, it would be reasonable to assume that it did terminate in the lake for large parts of this period. If we include a calving model, the bathymetry of the lake would have to be used, instead of the lake surface elevation used in this thesis.

Past activity. Knowledge of ice cap activity during centuries prior to the LIA maximum would be valuable. Additional lake sediment coring and/or and geomorphological work can be envisaged, for example along the eastern ice cap margin. If possible, putting a date on the suggested LIA-maximum moraine at Rembesdalskåka would enable a better assessment of the timing and importance of climatic forcing variables and outlet glacier responses during the LIA for the southwestern versus the northeastern ice cap.

For the Holocene, it would be possible to force the ice flow model with a mass balance scaled with reconstructed ELA-changes from lacustrine sediments. Other alternatives exist, like using a simplified energy balance model (an insolation-temperature model, e.g. Van Den Berg et al. 2008; Robinson and Goelzer 2014) to calculate the mass balance. Output from a paleo-Earth System Model could also be considered.

Future evolution. This thesis support previous studies (Giesen and Oerlemans 2010) suggesting that Hardangerjøkulen is bound to disappear in the future, perhaps as soon as in 100 years. By performing some of the improvements of model physics, mass balance, basal conditions and hydrology as outlined in previous points, we could further elucidate the timing and relevance of involved feedbacks for the future evolution of Hardangerjøkulen.

References

Abe-Ouchi, A, T Segawa, and F Saito (2007). Climatic Conditions for modelling the Northern Hemisphere ice sheets throughout the ice age cycle. *Climate of the Past* 3.3.

Adalgeirsdóttir, G et al. (2006). Response of Hofsjökull and southern Vatnajökull, Iceland, to climate change. *Journal of Geophysical Research: Earth Surface (2003–2012)* 111.F3.

Adalgeirsdóttir, G et al. (2011). Modelling the 20th and 21st century evolution of Hoffellsjökull glacier, SE-Vatnajökull, Iceland. *The Cryosphere* 5.4, pp. 961–975.

Adhikari, S and SJ Marshall (2013). Influence of high-order mechanics on simulation of glacier response to climate change: insights from Haig Glacier, Canadian Rocky Mountains. *Cryosphere* 7.5.

Alley, Richard B (1992). Flow-law hypotheses for ice-sheet modeling. *J. Glaciol* 38.129, pp. 245–256.

Andersen, JL and JL Sollid (1971). Glacial chronology and glacial geomorphology in the marginal zones of the glaciers, Midtdalsbreen and Nigardsbreen, south Norway.

Andreassen, L. M. and H. Elvehy. Volume change Hardangerjkulen. Glaciological investigations in Norway in 2000. Ed. by In B. Kjllmoen, 101102.

Andreassen, Liss M et al. (2005). Glacier mass-balance and length variation in Norway. *Annals of Glaciology* 42.1, pp. 317–325.

Andreassen, LM et al. (2012a). Inventory of Norwegian glaciers. *NVE, Oslo*.

Andreassen, LM, H Elvehøy, and B Kjøllmoen (2012b). "Laser scanning of Norwegian mass balance glaciers 2007-2011". In: *EGU General Assembly Conference Abstracts*. Vol. 14, p. 10941.

Askvik, Helge (2008). Berggrunnskart HARDANGERJØKULEN, 1416 II, M 1: 50 000 (printed). NGU.

Bakke, Jostein, Atle Nesje, Svein Olaf Dahl, et al. (2005). Utilizing physical sediment variability in glacier-fed lakes for continuous glacier reconstructions during the Holocene, northern Folgefonna, western Norway. *The Holocene* 15.2, pp. 161–176.

Bakke, Jostein et al. (2013). Numerical analyses of a multi-proxy data set from a distal glacier-fed lake, Sørsendalsvatn, western Norway. *Quaternary Science Reviews* 73, pp. 182–195.

Bamber, Jonathan L and Antony J Payne (2004). *Mass balance of the cryosphere*. Cambridge Univ. Press.

Bartholomaus, Timothy C, Robert S Anderson, and Suzanne P Anderson (2008). Response of glacier basal motion to transient water storage. *Nature Geoscience* 1.1, pp. 33–37.

Batchelor, G.K. (2000). *An introduction to fluid dynamics*. Cambridge university press.

Bauder, Andreas, Martin Funk, and Matthias Huss (2007). Ice-volume changes of selected glaciers in the Swiss Alps since the end of the 19th century. *Annals of Glaciology* 46.1, pp. 145–149.

Benn, Douglas I and David JA Evans (2010). *Glaciers and glaciation*. Hodder Education.

Blatter, Heinz (1995). Velocity and stress fields in grounded glaciers: a simple algorithm for including deviatoric stress gradients. *Journal of Glaciology* 41.138, pp. 333–344.

Bliss, Andrew, Regine Hock, and Valentina Radic (2014). Global response of glacier runoff to twenty-first century climate change. *Journal of Geophysical Research: Earth Surface*, n/a–n/a.

Blöschl, G, R Kirnbauer, and D Gutknecht (1991). Distributed snowmelt simulations in an alpine catchment: 1. Model evaluation on the basis of snow cover patterns. *Water Resources Research* 27.12, pp. 3171–3179.

Box, George EP and Norman R Draper (1987). Empirical model-building and response surfaces: Wiley Series in probability and mathematical statistics. *Empirical model-building and response surfaces: Willey series in probability and mathematical statistics*.

Briffa, Keith R et al. (1992). Fennoscandian summers from AD 500: temperature changes on short and long timescales. *Climate Dynamics* 7.3, pp. 111–119.

Budd, WF and TH Jacka (1989). A review of ice rheology for ice sheet modelling. *Cold Regions Science and Technology* 16.2, pp. 107–144.

Budd, WF and D Jenssen (1987). "Numerical modelling of the large-scale basal water flux under the West Antarctic Ice Sheet". In: *Dynamics of the West Antarctic ice sheet*. Springer, pp. 293–320.

Budd, WF, PL Keage, and NA Blundy (1979). Empirical studies of ice sliding. *J. Glaciol* 23.89, pp. 157–170.

Bueler, Ed, Jed Brown, and Craig Lingle (2007). Exact solutions to the thermomechanically coupled shallow-ice approximation: effective tools for verification. *Journal of Glaciology* 53.182, pp. 499–516.

Church, J.A. et al. (2013). Sea Level Change. In: ed. by T.F. Stocker et al. Cambridge University Press, Cambridge, United Kingdom and New York, NY, USA. Chap. Climate Change 2013: The Physical Science Basis. Contribution of Working Group I to the Fifth Assessment Report of the Intergovernmental Panel on Climate Change.

Clason, Caroline, Patrick Applegate, and Per Holmlund (2014). Modelling Late Weichselian evolution of the Eurasian ice sheets forced by surface meltwater-enhanced basal sliding. *Journal of Glaciology* 60.219, pp. 29–40.

Cogley, J Graham (2005). Mass and energy balances of glaciers and ice sheets. *Encyclopedia of hydrological sciences*.

Cogley, JG et al. (2011). *Glossary of glacier mass balance and related terms, IHP-VII technical documents in hydrology No. 86, IACS Contribution No. 2*.

Copland, Luke and Martin Sharp (2000). "Radio-echo sounding determination of polythermal glacier hydrology". In: *8th International Conference on Ground Penetrating Radar*. International Society for Optics and Photonics, pp. 59–64.

Crowley, Thomas J (2000). Causes of climate change over the past 1000 years. *Science* 289.5477, pp. 270–277.

Cuffey, Kurt M and William Stanley Bryce Paterson (2010). *The physics of glaciers*. Elsevier.

Dahl, Svein Olaf and Atle Nesje (1994). Holocene glacier fluctuations at Hardangerjøkulen, central-southern Norway: a high-resolution composite chronology from lacustrine and terrestrial deposits. *The Holocene* 4.3, pp. 269–277.

Dahl-Jensen, D and NS Gundestrup (1987). Constitutive properties of ice at Dye 3, Greenland. *The Physical Basis of Ice Sheet Modelling* 170, pp. 31–43.

De Woul, Mattias and Regine Hock (2005). Static mass-balance sensitivity of Arctic glaciers and ice caps using a degree-day approach. *Annals of Glaciology* 42.1, pp. 217–224.

Dhatt, Gouri, Emmanuel Lefrançois, and Gilbert Touzot (2012). *Finite element method*. John Wiley & Sons.

Dunse, Thorben (2011). "Glacier dynamics and subsurface classification of Austfonna, Svalbard: Inferences from observations and modelling". PhD thesis. University of Oslo.

Durand, Gaël et al. (2007). Change in ice rheology during climate variations–implications for ice flow modelling and dating of the EPICA Dome C core. *Climate of the Past* 3.1, pp. 155–167.

Elvehøy, H et al. (1997). Jøkullaup fra Demmevatn. *NVE Report* 17.

Etzelmüller, Bernd and Jon Ove Hagen (2005). Glacier-permafrost interaction in Arctic and alpine mountain environments with examples from southern Norway and Svalbard. *Geological Society, London, Special Publications* 242.1, pp. 11–27.

Farinotti, Daniel et al. (2009). An estimate of the glacier ice volume in the Swiss Alps. *Global and Planetary Change* 68.3, pp. 225–231.

Fischer, Robert et al. (2013). A system of conservative regridding for ice/atmosphere coupling in a GCM. *Geoscientific Model Development Discussions* 6, pp. 6493–6568.

Fleurian, B de et al. (2014). A double continuum hydrological model for glacier applications. *The Cryosphere* 8.1, pp. 137–153.

Flowers, Gwenn E et al. (2008). Holocene climate conditions and glacier variation in central Iceland from physical modelling and empirical evidence. *Quaternary Science Reviews* 27.7, pp. 797–813.

Fowler, AC (1987). Sliding with cavity formation. *J. Glaciol* 33.115, pp. 255–267.

Fowler, Andrew (2011). *Mathematical geoscience*. Vol. 36. Springer.

Gardner, Alex S et al. (2013). A reconciled estimate of glacier contributions to sea level rise: 2003 to 2009. *Science* 340.6134, pp. 852–857.

Giesen, RH (2009). "The ice cap Hardangerjøkulen in the past, present and future climate". PhD thesis. PhD thesis, IMAU, Utrecht University.

Giesen, RH and J Oerlemans (2010). Response of the ice cap Hardangerjøkulen in southern Norway to the 20th and 21st century climates. *The Cryosphere* 4, pp. 191–213.

Giesen, RH et al. (2008). Surface energy balance in the ablation zone of Midtdalsbreen, a glacier in southern Norway: Interannual variability and the effect of clouds. *Journal of Geophysical Research: Atmospheres (1984–2012)* 113.D21.

Giesen, RH et al. (2009). Comparison of the meteorology and surface energy balance at Storbreen and Midtdalsbreen, two glaciers in southern Norway. *The Cryosphere* 3.1, pp. 57–74.

Giesen, Rianne H and Johannes Oerlemans (2013). Climate-model induced differences in the 21st century global and regional glacier contributions to sea-level rise. *Climate dynamics* 41.11-12, pp. 3283–3300.

Glen, John W (1955). The creep of polycrystalline ice. *Proceedings of the Royal Society of London. Series A. Mathematical and Physical Sciences* 228.1175, pp. 519–538.

Glen, JW (1952). Experiments on the deformation of ice. *Journal of Glaciology* 2, pp. 111–114.

Gouirand, Isabelle, Anders Moberg, and Eduardo Zorita (2007). Climate variability in Scandinavia for the past millennium simulated by an atmosphere-ocean general circulation model. *Tellus A* 59.1, pp. 30–49.

Greve, Ralf and Heinz Blatter (2009). *Dynamics of ice sheets and glaciers*. Springer.

Greve, Ralf and Shoko Otsu (2007). The effect of the north-east ice stream on the Greenland ice sheet in changing climates. *The Cryosphere Discussions* 1.1, pp. 41–76.

Grove, Jean M (2001). "The initiation of the Little Ice Age in regions round the North Atlantic". In: *The Iceberg in the Mist: Northern Research in pursuit of a Little Ice Age*. Springer, pp. 53–82.

– (2004). *Little ice ages: ancient and modern*. Vol. 1. Taylor & Francis.

Gudmundsson, GH (2008). Analytical solutions for the surface response to small amplitude perturbations in boundary data in the shallow-ice-stream approximation. *The Cryosphere* 2.2, pp. 77–93.

Gulley, JD et al. (2009). Mechanisms of englacial conduit formation and their implications for subglacial recharge. *Quaternary Science Reviews* 28.19, pp. 1984–1999.

Gumundsson, S et al. (2009). Similarities and differences in the response to climate warming of two ice caps in Iceland. *Hydrology Research* 40.5.

Haeberli, Wilfried et al. (2007). Integrated monitoring of mountain glaciers as key indicators of global climate change: the European Alps. *Annals of Glaciology* 46.1, pp. 150–160.

Hagen, Jan O. (1978). "Brefrontprosesser ved Hardangerjkulen (Glacial terminus processes at Hardangerjkulen)." PhD thesis. Department of Geography. University of Oslo, Norway.

Hamby, DM (1994). A review of techniques for parameter sensitivity analysis of environmental models. *Environmental Monitoring and Assessment* 32.2, pp. 135–154.

Hanssen-Bauer, I (2005). Regional temperature and precipitation series for Norway: analyses of time series updated to 2004. *Met. no report* 15.2005, pp. 1–34.

Heimbach, Patrick and Veronique Bugnion (2009). Greenland ice-sheet volume sensitivity to basal, surface and initial conditions derived from an adjoint model. *Annals of Glaciology* 50.52, pp. 67–80.

Hindmarsh, RCA (2004). A numerical comparison of approximations to the Stokes equations used in ice sheet and glacier modeling. *Journal of Geophysical Research: Earth Surface (2003–2012)* 109.F1.

Hock, Regine (1999). A distributed temperature-index ice-and snowmelt model including potential direct solar radiation. *Journal of Glaciology* 45.149, pp. 101–111.

– (2005). Glacier melt: a review of processes and their modelling. *Progress in physical geography* 29.3, pp. 362–391.

Hooke, R LeB (1981). Flow law for polycrystalline ice in glaciers comparison of theoretical predictions, laboratory data, and field. *Rev. Geophys. Space Phys* 19.4, pp. 664–672.

Hooke, Roger LeB (2005). *Principles of glacier mechanics*. Cambridge university press.

Huss, Matthias et al. (2008). Determination of the seasonal mass balance of four Alpine glaciers since 1865. *Journal of Geophysical Research: Earth Surface (2003–2012)* 113.F1.

Hutter, Kolumban (1983). *Theoretical glaciology: material science of ice and the mechanics of glaciers and ice sheets*. Reidel.

Huybrechts, Philippe, Tony Payne, and Intercomparison EISMINT (1996). The EISMINT benchmarks for testing ice-sheet models. *Annals of Glaciology* 23, pp. 1–12.

Iken, Almut (1981). *The effect of the subglacial water pressure on the sliding velocity of a glacier in an idealized numerical model*. Versuchsanst. für Wasserbau, Hydrologie u. Glaziologie an d. Eidg. Techn. Hochsch.

Jansson, P, R Hock, and T Schneider (2003). The concept of glacier storage: a review. *Journal of Hydrology* 282.1–4, pp. 116 –129.

Johannesson, T, CF Raymond, and ED Waddington (1989). "A simple method for determining the response time of glaciers". In: *Glacier fluctuations and climatic change*. Springer, pp. 343–352.

Jouvet, Guillaume et al. (2011). Modelling the retreat of Grosser Aletschgletscher, Switzerland, in a changing climate. *Journal of Glaciology* 57.206, pp. 1033–1045.

Kamb, Barclay and K Echelmeyer (1986). Stress-gradient coupling in glacier flow. I: longitudinal averaging of the influence of ice thickness and surface slope. *Journal of Glaciology* 32.111, pp. 267–284.

Kaser, Georg, Andrew Fountain, Peter Jansson, et al. (2003). *A manual for monitoring the mass balance of mountain glaciers*. UNESCO.

Kjøllmoen, B. et al. (2011). Glaciological investigations in Norway in 2010, NVE Report No 3, 91 pp.

Konnestad, H. (1996). "Moreneformer i fronten av Midtdalsbreen en glasiologisk og geomorfologisk underskelse av dannelsesprosessene (Moraine formation at the terminus of Midtdalsbreen a glacial and geomorphological study of their creation). Master thesis unpublished." PhD thesis. Department of Geography. University of Oslo, Norway.

Krantz, K (2002). "Volume changes and traditional mass balance on two outlet glaciers at Hardangerjøkulen, Norway". PhD thesis. Masters thesis unpublished. Department of Geography. University of Oslo, Norway.

Lapidus, Leon and George F Pinder (2011). *Numerical solution of partial differential equations in science and engineering*. John Wiley & Sons.

Larour, E et al. (2012). Continental scale, high order, high spatial resolution, ice sheet modeling using the Ice Sheet System Model (ISSM). *Journal of Geophysical Research: Earth Surface (2003–2012)* 117.F1.

Larour, E. et al. (2014). Inferred basal friction and surface mass balance of North-East Greenland Ice Stream using data assimilation of ICESat-1 surface altimetry and ISSM. *The Cryosphere Discussions* 8.3, pp. 2331–2373.

Laumann, Tron and Atle Nesje (2014). Sprteggbreen, western Norway, in the past, present and future: Simulations with a two-dimensional dynamical glacier model. *The Holocene*. eprint: `http://hol.sagepub.com/content/early/2014/04/29/0959683614530446.full.pdf+html`.

Le Brocq, AM et al. (2009). A subglacial water-flow model for West Antarctica. *Journal of Glaciology* 55.193, pp. 879–888.

Le Meur, Emmanuel and Christian Vincent (2003). A two-dimensional shallow ice-flow model of Glacier de Saint-Sorlin, France. *Journal of Glaciology* 49.167, pp. 527–538.

Le Meur, Emmanuel et al. (2004). Glacier flow modelling: a comparison of the Shallow Ice Approximation and the full-Stokes solution. *Comptes Rendus Physique* 5.7, pp. 709–722.

Le Meur, Emmanuel et al. (2007). Disappearance of an Alpine glacier over the 21st Century simulated from modeling its future surface mass balance. *Earth and Planetary Science Letters* 261.3, pp. 367–374.

Lean, Judith, Andrew Skumanich, and Oran White (1992). Estimating the Sun's radiative output during the Maunder Minimum. *Geophysical Research Letters* 19.15, pp. 1591–1594.

Levermann, Anders et al. (2013). The multimillennial sea-level commitment of global warming. *Proceedings of the National Academy of Sciences* 110.34, pp. 13745–13750.

Leysinger-Vieli, GJ-MC and GH Gudmundsson (2004). On estimating length fluctuations of glaciers caused by changes in climatic forcing. *Journal of geophysical research* 109.F1, F01007.

Liestøl, Olav (1956). Glacier Dammed Lakes in Norway. *Norsk Geografisk Tidsskrift - Norwegian Journal of Geography* 15.3-4, pp. 122–149.

Lliboutry, Louis (1968). General theory of subglacial cavitation and sliding of temperate glaciers. *Journal of Glaciology* 7, pp. 21–58.

MacAyeal, Douglas R (1989). Large-scale ice flow over a viscous basal sediment: Theory and application to ice stream B, Antarctica. *Journal of Geophysical Research: Solid Earth (1978–2012)* 94.B4, pp. 4071–4087.

– (1993). A tutorial on the use of control methods in ice-sheet modeling. *J. Glaciol* 39.131, pp. 91–98.

Marzeion, Ben, AH Jarosch, and Marlis Hofer (2012). Past and future sea-level change from the surface mass balance of glaciers. *The Cryosphere Discussions* 6.4, pp. 3177–3241.

Matthews, John A and Keith R Briffa (2005). The Little Ice Age: Re-evaluation of an evolving concept. *Geografiska Annaler: Series A, Physical Geography* 87.1, pp. 17–36.

Meier, Mark F (1984). Contribution of small glaciers to global sea level. *Science* 226.4681, pp. 1418–1421.

Melvold, K., T. Laumann, and A. Nesje (2011). Kupert landskap under Hardangerjkulen. *GEO* 14.3, pp. 36–37.

Melvold, Kjetil and Thomas Schuler (2008). Mapping of subglacial topography using GPR for determining subglacial hydraulic conditions. In: ed. by C Hauck & C Kneisel. Applied Geophysics in periglacial environments. Cambridge University Press. Chap. 14.

Montagnat, Maurine and Paul Duval (2004). The viscoplastic behaviour of ice in polar ice sheets: experimental results and modelling. *Comptes Rendus Physique* 5.7, pp. 699–708.

Morland, LW (1984). Thermomechanical balances of ice sheet flows. *Geophysical & Astrophysical Fluid Dynamics* 29.1-4, pp. 237–266.

Morlighem, M et al. (2013). Inversion of basal friction in Antarctica using exact and incomplete adjoints of a higher-order model. *Journal of Geophysical Research: Earth Surface* 118.3, pp. 1746–1753.

Morlighem, Mathieu et al. (2010). Spatial patterns of basal drag inferred using control methods from a full-Stokes and simpler models for Pine Island Glacier, West Antarctica. *Geophysical Research Letters* 37.14.

Nesje, Atle and John A Matthews (2012). The Briksdalsbre Event: A winter precipitation-induced decadal-scale glacial advance in southern Norway in the ad 1990s and its implications. *The Holocene* 22.2, pp. 249–261.

Nesje, Atle et al. (1991). Holocene glacial and climate history of the Jostedalsbreen region, western Norway; evidence from lake sediments and terrestrial deposits. *Quaternary Science Reviews* 10.1, pp. 87–114.

Nesje, Atle et al. (1994). Holocene glacier activity at the southwestern part of Hardangerjøkulen, central-southern Norway: evidence from lacustrine sediments. *The Holocene* 4.4, pp. 377–382.

Nesje, Atle et al. (2008). Norwegian mountain glaciers in the past, present and future. *Global and Planetary Change* 60.1, pp. 10–27.

Nordli, PØ et al. (2003). Spring–summer temperature reconstruction in western Norway 1734–2003: a data-synthesis approach. *International Journal of Climatology* 23.15, pp. 1821–1841.

Nye, John F (1953). The flow law of ice from measurements in glacier tunnels, laboratory experiments and the Jungfraufirn borehole experiment. *Proceedings of the Royal Society of London. Series A. Mathematical and Physical Sciences* 219.1139, pp. 477–489.

Oerlemans, J (1980). Continental ice sheets and the planetary radiation budget. *Quaternary research* 14.3, pp. 349–359.

– (1992). Climate sensitivity of glaciers in southern Norway: application of an energy-balance model to Nigardsbreen, Hellstugubreen and Alfotbreen. *J. Glaciol* 38.129, pp. 223–232.

– (1997). A flowline model for Nigardsbreen, Norway: projection of future glacier length based on dynamic calibration with the historic record. *Journal of glaciology* 24, pp. 382–389.

Oerlemans, J and NC Hoogendoorn (1989). Mass-balance gradients and climatic change. *Journal 0/Glaciology* 35.121.

Oerlemans, Johannes (2001). *Glaciers and climate change*. CRC Press.

– (2005). Extracting a climate signal from 169 glacier records. *Science* 308.5722, pp. 675–677.

Oreskes, Naomi, Kristin Shrader-Frechette, and Kenneth Belitz (1994). Verification, validation, and confirmation of numerical models in the earth sciences. *Science* 263.5147, pp. 641–646.

Østrem, G and T Ziegler (1969). Atlas over breer i Sør-Norge [Atlas of glaciers in southern Norway]: Meddelelse No. 20 fra Hydrologisk avdeling. *Norges vassdrags-og Elektrisitetsvesen, Oslo*.

Otterå, Odd Helge et al. (2010). External forcing as a metronome for Atlantic multidecadal variability. *Nature Geoscience* 3.10, pp. 688–694.

Partridge, Dale (2013). "Numerical Modelling of Glaciers: Moving Meshes and Data Assimilation". PhD thesis. University of Reading.

Paterson, WSB (1994). *The physics of glaciers*. Butterworth-Heinemann.

Pattyn, F et al. (2008). Benchmark experiments for higher-order and full-Stokes ice sheet models (ISMIP–HOM). *The Cryosphere* 2, pp. 95–108.

Pattyn, Frank (2003). A new three-dimensional higher-order thermomechanical ice sheet model: Basic sensitivity, ice stream development, and ice flow across subglacial lakes. *Journal of Geophysical Research: Solid Earth (1978–2012)* 108.B8.

Payne, AJ (1995). Limit cycles in the basal thermal regime of ice sheets. *Journal of Geophysical Research: Solid Earth (1978–2012)* 100.B3, pp. 4249–4263.

– (1999). A thermomechanical model of ice flow in West Antarctica. *Climate Dynamics* 15.2, pp. 115–125.

Payne, AJ et al. (2000). Results from the EISMINT model intercomparison: the effects of thermomechanical coupling. *Journal of Glaciology* 46.153, pp. 227–238.

Radic, Valentina et al. (2013). Regional and global projections of twenty-first century glacier mass changes in response to climate scenarios from global climate models. *Climate Dynamics* 1, p. 107.

Rasmussen, LA and H Conway (2005). Influence of upper-air conditions on glaciers in Scandinavia. *Annals of Glaciology* 42.1, pp. 402–408.

Rasmussen, LA et al. (2010). Little Ice Ageprecipitation in Jotunheimen, southern Norway. *The Holocene* 20.7, pp. 1039–1045.

Raymond, CF (1980). Temperate valley glaciers. *Dynamics of snow and ice masses*, pp. 79–139.

Reinardy, Benedict TI, Iain Leighton, and Peter J Marx (2013). Glacier thermal regime linked to processes of annual moraine formation at Midtdalsbreen, southern Norway. *Boreas* 42.4, pp. 896–911.

Reist, Adrian, Jacques Rappaz, et al. (2005). Mathematical analysis and numerical simulation of the motion of a glacier.

Ritz, C., A. Fabre, and A. Letreguilly (1996). Sensitivity of a Greenland ice sheet model to ice flow and ablation parameters: consequences for the evolution through the last climatic cycle. English. *Climate Dynamics* 13.1, pp. 11–23.

Robinson, Alexander and Heiko Goelzer (2014). The importance of insolation changes for paleo ice sheet modeling. *The Cryosphere Discussions* 8, pp. 337–362.

Rutt, Ian C et al. (2009). The Glimmer community ice sheet model. *Journal of Geophysical Research: Earth Surface (2003–2012)* 114.F2.

Schoof, Christian (2005). The effect of cavitation on glacier sliding. *Proceedings of the Royal Society A: Mathematical, Physical and Engineering Science* 461.2055, pp. 609–627.

– (2010). Ice-sheet acceleration driven by melt supply variability. *Nature* 468.7325, pp. 803–806.

Sellevold, MA and KJELL Kloster (1964). Seismic measurements on the glacier Hardangerjokulen, Western Norway. *Norsk Polarinslitutt Arbok 1964*, pp. 87–91.

Shepherd, Andrew et al. (2012). A reconciled estimate of ice-sheet mass balance. *Science* 338.6111, pp. 1183–1189.

Shindell, Drew T et al. (2001). Solar forcing of regional climate change during the Maunder Minimum. *Science* 294.5549, pp. 2149–2152.

Shreve, RL (1972). Movement of water in glaciers. *J. Glaciol* 11.62, pp. 205–214.

Sollid, J.L. and A Bjørkenes (1978). Genesis of moraines at Midtdalsbreen, southern Norway. *Norsk Geografisk Tidskrift*, Bd 32.

Stokes, G (1845). On the theories of internal friction of fluids in motion. *Transactions of the Cambridge Philosophical Society* 8, p. 287.

Sundal, Aud Venke et al. (2011). Melt-induced speed-up of Greenland ice sheet offset by efficient subglacial drainage. *Nature* 469.7331, pp. 521–524.

Tedstone, Andrew J et al. (2013). Greenland ice sheet motion insensitive to exceptional meltwater forcing. *Proceedings of the National Academy of Sciences* 110.49, pp. 19719–19724.

Vaksdal, MB. (2001). "Sammenligning av to dreneringssytemer i Midtdalsbreen, Hardangerjkulen, Sr-Norge (Comparison of two drainage systems at Midtdalsbreen, Hardangerjkulen, South Norway). Masters thesis unpublished." MA thesis. Department of Geography. University of Oslo, Norway.

Van Den Berg, Jojanneke, Roderik van de Wal, and Hans Oerlemans (2008). A mass balance model for the Eurasian Ice Sheet for the last 120,000 years. *Global and Planetary Change* 61.3, pp. 194–208.

Van Der Veen, CJ (1989). A numerical scheme for calculating stresses and strain rates in glaciers. *Mathematical geology* 21.3, pp. 363–377.

– (1999). Evaluating the performance of cryospheric models 1. *Polar Geography* 23.2, pp. 83–96.

– (2013). *Fundamentals of glacier dynamics*. CRC Press.

Vasskog, Kristian et al. (2012). A new approach for reconstructing glacier variability based on lake sediments recording input from more than one glacier. *Quaternary Research* 77.1, pp. 192–204.

Vaughan, D.G. et al. (2013). Observations: Cryosphere. *In: Climate Change 2013: The Physical Science Basis. Contribution of Working Group I to the Fifth Assessment Report of the Intergovernmental Panel on Climate Change. [Stocker, T.F., D. Qin, G.-K. Plattner, M. Tignor, S.K. Allen, J. Boschung, A. Nauels, Y. Xia, V. Bex and P.M. Midgley (eds.)]. Cambridge University Press, Cambridge, United Kingdom and New York, NY, USA*.

Vincent, C et al. (2000). Dynamic behaviour analysis of glacier de Saint Sorlin, France, from 40 years of observations, 1957–97. *Journal of Glaciology* 46.154, pp. 499–506.

Walder, Joseph S (1986). Hydraulics of subglacial cavities. *J. Glaciol* 32.112, pp. 439–445.

Weertman, J (1973). Creep of ice. *Physics and chemistry of ice*, pp. 320–337.

Weertman, Johannes (1957). On the sliding of glaciers. *J. Glaciol* 3.21, pp. 33–38.

Willis, Ian C (1995). Intra-annual variations in glacier motion: a review. *Progress in Physical Geography* 19.1, pp. 61–106.

Willis, Ian C. et al. (2012). Structure, morphology and water flux of a subglacial drainage system, Midtdalsbreen, Norway. *Hydrological Processes* 26.25, pp. 3810–3829.
Winkelmann, R et al. (2011). The Potsdam parallel ice sheet model (PISM-PIK)–Part 1: Model description. *The Cryosphere* 5.3, pp. 715–726.

9 Appendix

Here follows some additional figures thought to add extra value for the interested reader, as referenced in the main text.

Ice volume response to mass balance perturbations

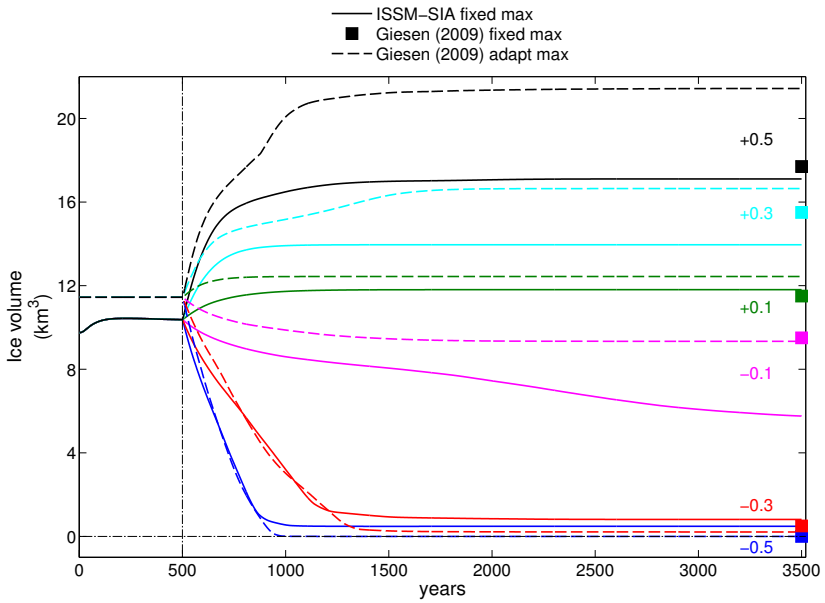

Figure 9.1: Time series of ice volume responses to selected mass balance anomalies using a fixed maximum in the mass balance profile, corresponding to Fig. 6.2. Shown are also time series for a temporally fixed and adaptive maximum in the mass balance profile from Giesen (2009).

.

Effects of time-dependent basal slipperiness

To test the effect of a temporally evolving field of basal slipperiness, we let the sliding parameter vary in time, that is $C = C(z, t)$. This means that for every time step, the sliding parameter is calculated in a linear fashion according to the updated elevation z. Fig. (9.2) show the effect on velocities and ice volume for a temporally evolving sliding parameter field, for the historic run from AD 1600 to present. Ice volumes at the LIA maximum are almost identical, pointing towards a dominating mass balance signal. However for the remaining part of the record, the imposed mass balance changes are small and modelled ice volume for the temporally adaptive sliding diverges from the fixed sliding parameter run. Modelled ice volumes during the 1900s are further from observed ice volumes for the temporally evolving field (+20 % overestimation) than for the run with a fixed sliding parameter (+10 % overestimation).

Additionally, velocities in the adaptive run vary less than those from the fixed run, for example during the LIA, despite the similarity in total ice volume. This way, the

adapted sliding acts a negative feedback, dampening the effect of changed topography. Moreover, using the temporally evolving sliding, modelled outlet glacier lengths show greater mismatches compared to the observed length record before the 1900s. For the last 100 years, outlet lengths are similar (Fig. 9.3). At the end of the record, the adaptive sliding parameter captures the advance of Rembesdalskåka during the 1990s, while the temporally fixed parameter does not. Noteworthy though is that these changes are similar to or smaller than the spatial resolution of the model.

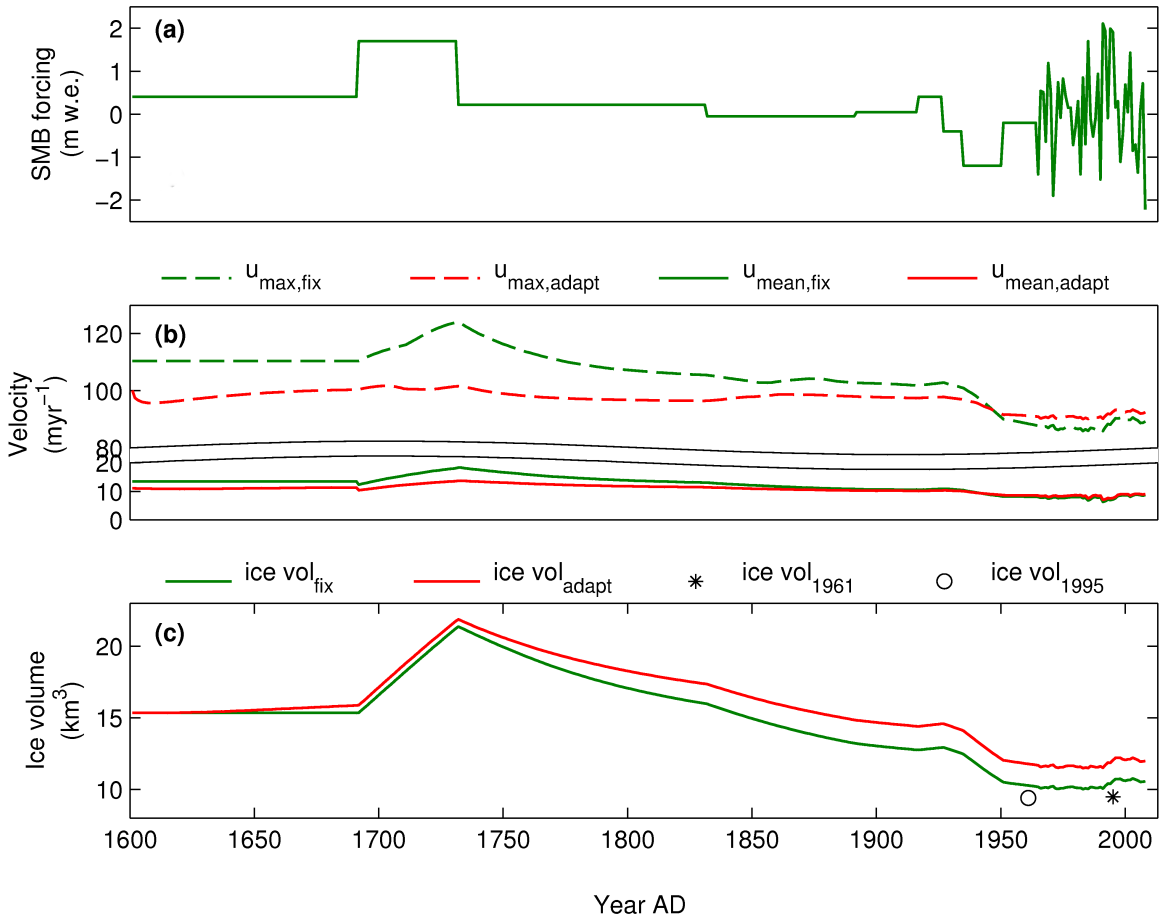

Figure 9.2: Comparison of a temporally fixed and adaptive field of basal slipperiness for the velocity and ice volume evolution of Hardangerjøkulen since the Little Ice Age. Note the break in the y-axis. For details of the sliding formulation, see text.

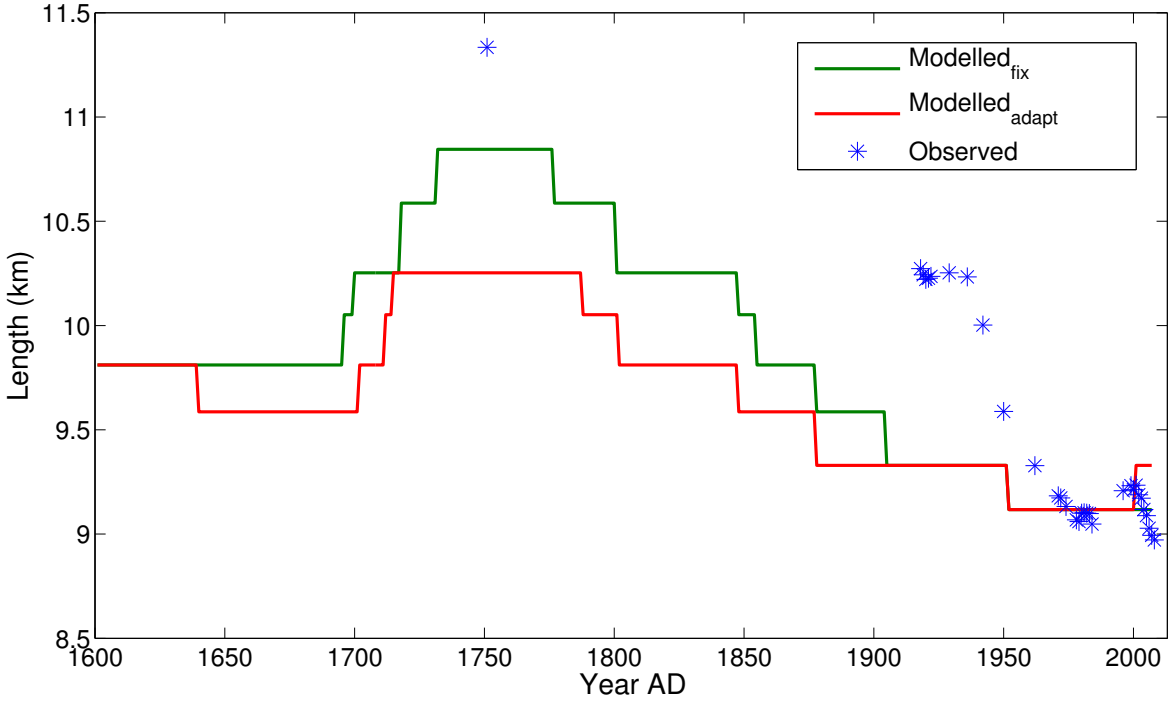

(a)

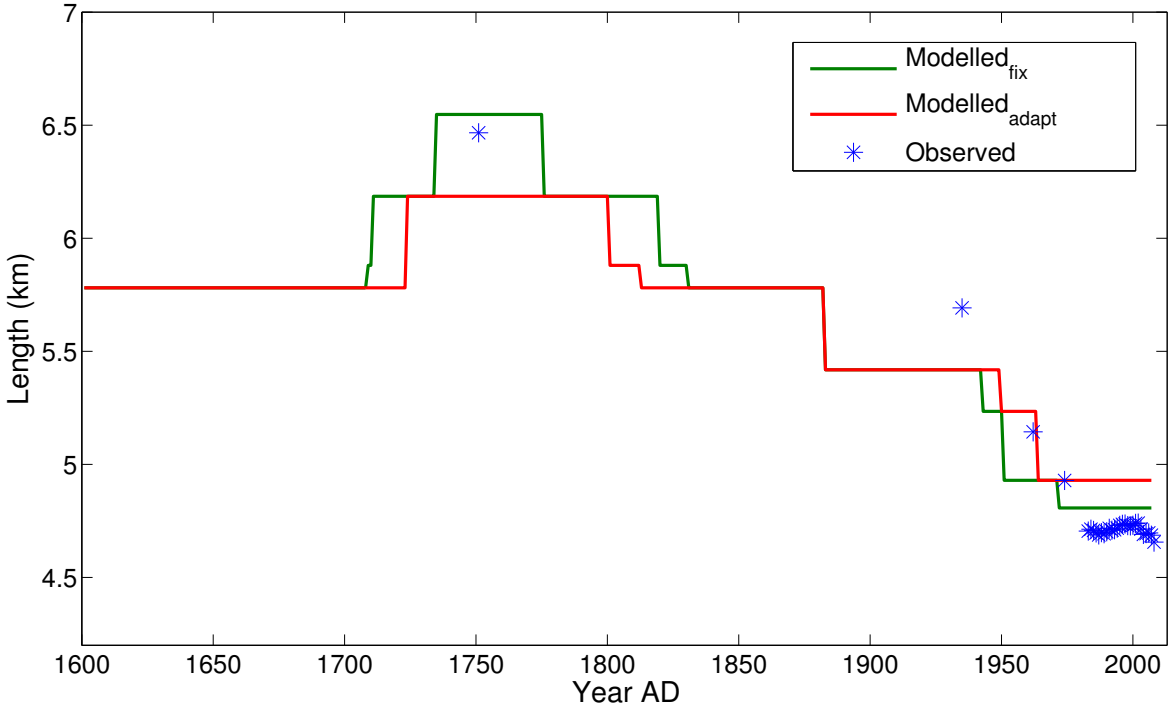

(b)

Figure 9.3: Modelled and observed length of the outlet glaciers (a) Rembesdalskåka and (b) Midtdalsbreen, using a fixed and adaptive field of basal slipperiness.